Università degli Studi di Napoli *Federico II*

in consorzio con

Seconda Università di Napoli

Università degli Studi di Napoli *Parthenope*

in convenzione con

Istituto per l'Ambiente Marino Costiero - C.N.R.

Stazione zoologica *Anton Dohrn*

Dottorato di Ricerca in Scienze e Ingegneria del Mare - Ciclo XIX

Tesi di Dottorato di Ricerca

The role of the interfacial layer in exchange and hydraulics in the Strait of Gibraltar: a 3D numerical modeling study.

Dott. Gianmaria Sannino
Candidato

Prof. Stefano Pierini
Tutor

Dott. Vincenzo Artale
Tutor

Prof. Bruno D'Argenio
Coordinatore del Dottorato

Anno Accademico
2006/2007

Abstract

A three-dimensional sigma coordinate free-surface parallel model is used to investigate the semidiurnal tidal exchange through the Strait of Gibraltar. The model makes use of a coastal-following, curvilinear orthogonal grid, that includes the Gulf of Cadiz and the Alboran Sea, with very high resolution in the Strait (less than 500 m). A lock-exchange initial condition is used: the western part of the model domain is filled with Atlantic water, whereas the eastern part with Mediterranean water. The model is forced at the open boundaries through the specification of the semidiurnal (M_2 and S_2) tidal surface elevation. The model is run over a spring-neap cycle (fortnightly period), and the results are compared with most of the available observed data. Simulated cotidal maps of the M_2 and S_2 tidal elevation components are in quantitative and qualitative good agreement with observed data as well as the simulated major and minor axis of tidal ellipse. The model reproduces the generation and the subsequent propagation of internal bores both eastward and westward, showing that they are always generated during the fortnightly period.

However, the principal aim of this work is to study the effect of the intermediate layer (a layer in between the Atlantic and Mediterranean layers) both on the exchanged transports and hydraulics. To this aim, first the ability of the model in reproducing the interfacial layer between the Atlantic and Mediterranean waters in the Strait of Gibraltar is verified. Model results show that the model is able to reproduce a thick interfacial layer that carries a substantial fraction of the total volume transport. The interfacial thickness is strongly modulated by tidal forcing that enhances the vertical exchanges between layers.

In order to take into account the thick interfacial layer, a three-layer approximation is used to study the hydraulics. Results show that the exchange regime is intermittently maximal due to cyclically controlled regions over Camarinal Sill and within Tarifa Narrows. The analysis has been repeated in a two-layer framework to evaluate the impact of the introduction of an interfacial layer on the calculation of hydraulics. In the two-layer approximation, there is not any controlled region extending on the whole cross section, so the exchange is always submaximal. Concluding, the two-layer approximation underestimates hydraulic controls in the strait respect to the three-layer approach.

Abstract in Italian

Lo stretto di Gibilterra costituisce l'unica connessione dinamicamente significativa tra il mar Mediterraneo e l'oceano Atlantico (Figura 1.2). Attraverso lo stretto di Gibilterra, infatti, il Mediterraneo scambia acqua, sale e calore con l'oceano Atlantico.

Lo stretto di Gibilterra è un canale stretto e poco profondo, caratterizzato da una batimetria complessa. Si estende in longitudine per circa 60 Km, mentre in latitudine si estende, in media, per circa 20 Km. L'estremità orientale dello stretto, chiamata *Tarifa Narrows*, è caratterizzata dalla presenza di un canale profondo 800 m e largo (in latitudine) circa 18 Km (Figura 1.3). Muovendoci verso ovest, il canale si restringe fino a raggiungere una larghezza di soli 12 Km in prossimità di Punta Tarifa. 8 Km ad ovest di tale punta, la batimetria diminuisce rapidamente da 800 m fino a 284 m (sell di Camarinal). L'estremità occidentale dello stretto è caratterizzata dalla presenza di un'altra sella sottomarina, chiamata sella Espartel. Qui la batimetria raggiunge una profondità di 360 m. Il fondo compreso tra queste due selle sottomarine si presenta fondamentalmente piatto e ad una profondità media di 400 m.

La circolazione marina media nello stretto di Gibilterra è caratterizzata da un flusso a due strati sovrapposti: uno superficiale, diretto verso il Mediterraneo, ed uno profondo, diretto verso l'oceano Atlantico. Questa circolazione, tradizionalmente chiamata estuarina inversa, è causata dall'eccesso di evaporazione nel bacino del Mediterraneo. Diversi processi, su differenti scale temporali, modificano la circolazione media. L'ampiezza di queste fluttuazioni può essere dello

stesso ordine di grandezza, o perfino maggiore (come nel caso delle maree), del valore medio.

Obiettivo di questo lavoro è lo studio della circolazione marina presente nello stretto di Gibilterra, in termini sia di trasporto di volume che di controllo idraulico, mediante l'utilizzo di un modello numerico tridimensionale.

Il modello numerico tridimensionale utilizzato in questo lavoro è il CEPOM, una versione modificata del *Princeton Ocean Model* (**POM**, Blumberg & Mellor (1987)). CEPOM, a differenza di POM, è scritto in **FORTRAN90**, è parallelo, ed utilizza come schema di avvezione dei traccianti l'algoritmo MPDATA (*Multidimensional Positive Definite Advection Transport Algorithm*), sviluppato da Smolarkiewicz (1984), nella versione implementata da Sannino *et al.* (2002). La parallelizzazione di CEPOM è stata ottenuta mediante **SMS** (*Scalable Modeling System*), una libreria software sviluppata da Govett *et al.* (2003) presso l'*Advanced Computing Branch of the Forecast Systems Laboratory* della NOAA (vedi Sannino *et al.* (2005), per ulteriori dettagli sulla parallelizzazione).

Il dominio computazionale del modello include oltre allo stretto di Gibilterra anche il golfo di Cadice ad est, ed il mare di Alboran ad ovest. La griglia computazionale ha una risoluzione variabile; in particolare, nello stretto di Gibilterra la griglia raggiunge la massima risoluzione di circa 500 m, mentre nel mare di Alboran e nel Golfo di Cadiz la risoluzione si riduce a circa 15 Km.

Il modello è stato inizializzato con temperature e salinità tipiche della stagione primaverile; in particolare il golfo di Cadice è stato inizializzato con i dati forniti dal *dataset* Levitus, mentre il mar di Alboran con dati provenienti dal *dataset* MODB.

Il dominio computazionale del modello è caratterizzato da due lati aperti. Questi sono localizzati rispettivamente alla estremità occidentale ed orientale del dominio. Su questi due lati il modello è forzato

attraverso l'imposizione delle componenti semidiurne (componente M_2 ed S_2) dell'elevazione superficiale. Il modello è stato girato in modo da simulare un intero periodo di marea semidiurna (14.79 giorni). I risultati ottenuti sono stati confrontati con il maggior numero di dati sperimentali disponibili per lo stretto di Gibilterra. Dal confronto è emerso che il modello simula le caratteristiche principali della circolazione nello stretto con una buona aprrossimazione. Questo è particolarmente evidente confrontando le mappe cotidali dell'elevazione superficiale simulata dal modello, con quelle calcolate con dati osservati, come pure confrontando i semiassi maggiori e minori delle ellissi di marea simulate ed osservate. Il modello è anche in grado di riprodurre la generazione e la successiva propagazione delle due onde interne (*internal bore*) che si generano sulla sella di Camarinal e si propagano in direzione opposta verso le due estremità dello stretto.

Uno dei principali scopi di questo lavoro è stato lo studio degli effetti prodotti dallo strato intermedio di acqua che separa quello puramente mediterraneo da quello atlantico, sul trasporto di volume e sul controllo idraulico nello stretto di Gibilterra.

Dall'analisi della simulazione è emerso che questo strato intermedio non è uno strato stagnante, ma anzi, è uno strato attivo capace di trasportare volumi di acqua considerevoli. È emerso inoltre che il suo spessore è fortemente condizionato dal forzante mareale. Per l'analisi del controllo idraulico nello stretto è stata applicata, per la prima volta, la teoria idraulica a tre strati rispetto alla classica teoria a due strati generalmente utilizzata per analizzare il controllo idraulico nello stretto di Gibilterra. I risultati hanno evidenziato che il regime idraulico nello stretto varia, in maniera intermittente, tra *sub-maximal* e *maximal*.

Contents

List of Figures

List of Tables

Chapter 1

Introduction

1.1 History and Geography

Since ancient times the *Fretum Gaditanum* (the Roman name of the Strait of Gibraltar) has fascinated and captured mankind's imagination: for long time the Hercules' pillars, the two promontories of *Calpe* (now Gibraltar) on the European side, and *Abila Mons* (now Monte Hacho in the Spanish enclave of Ceuta) on the African side, were thought to be the extreme edges of the Earth (Figure 1.1).

About five million years ago, during the Miocene, the strait was topographically blocked. This triggered the desiccation of the Mediterranean, inducing the so-called Messinian Salinity Crisis (Hsü *et al.* (1973)) characterized by a dramatic sealevel drop that has been estimated up to 1500 m below the current sea-level. The opening of the Strait of Gibraltar in the Early Pliocene allowed restoring the water exchange between the Atlantic and Mediterranean waters. About the opening of the Strait of Gibraltar the most recent theory proposes that it is the result of the regressive erosion of a stream that was flowing from the Atlantic toward the desiccated Mediterranean basin.

Most probably the first definition of the Strait of Gibraltar from an oceanographic point of view is to ascribe to Quintus Horatius Flaccus [1] who wrote:

[1] Quintus Horatius Flaccus, (December 8, 65 BC - November 27, 8 BC), known in the English-speaking world as Horace, was the leading Roman lyric poet during the time of Augustus.

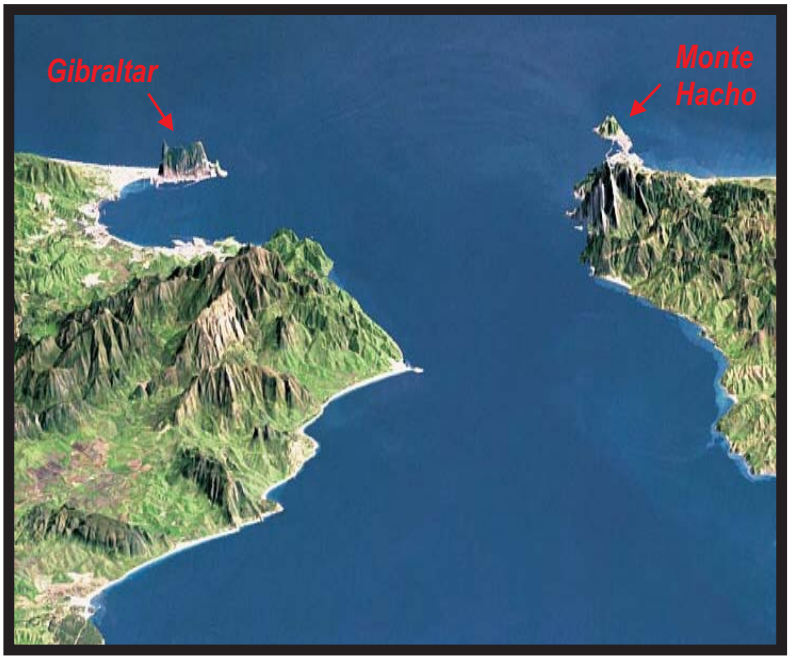

Figure 1.1: Three dimensional perspective view of the Strait of Gibraltar. Europe (Spain) is on the left, Africa (Morocco) is on the right. (Image from SRTM (Shuttle Radar Topography Mission) Team, NASA JPL).

(Roma) Horrenda late nomen in ultimas extendat oras, qua medius liquor secernit Europem ab Afro, qua tumidus rigat arva Nilus...[1] Horatius (23 B.C.). In this *Ode* Horatius describes the Strait of Gibraltar as the place where the midway water separates Europe from Africa.

The Strait of Gibraltar represents the only dynamically significant connection between the Mediterranean Sea and the World Ocean (Figure 1.2). Through the Strait of Gibraltar the Mediterranean Sea exchanges water, salt and heat with the North Atlantic. Accurate observations of the mass, salt, and heat transports in the strait can provide important integral information about the processes in the interior of the Mediterranean basin. Time variability in these transports may be indicative of changes in the strait dynamics or in the basin interior balances as well. Consequential the Strait represents a key point for the general thermohaline circulation of the whole Mediterranean basin[2].

The Strait of Gibraltar is a narrow and shallow channel, 60 km long and 20 km wide, characterized by a complex system of contractions and sills. At the eastern end, which it will be referred in this work as Gibraltar-Ceuta section, the deep channel, called Tarifa Narrows, is about 18 Km wide and more than 800 m deep (Figure 1.3). Going toward west the channel narrows to about 12 Km at Pt. Tarifa while, 8 Km west of Tarifa, the bottom rises steeply at Camarinal Sill where it reaches the minimum depth of the whole strait (284 m). The western entrance of the strait is characterized by the presence of another sill, called Espartel Sill, where the bottom reaches a minimum depth of about 360 m. In between these two sills there is a quite flat basin, 400 m deep, called Tangier basin.

[1] *(Rome) Feared everywhere, let her extend her name to the uttermost shores, where the midway water separates Europe from Africa, where the swollen Nile irrigates the fields...*

[2] The thermohaline circulation is that part of the ocean circulation which is driven by density differences. Sea water density depends on temperature and salinity, hence the name thermohaline. The salinity and temperature differences arise from heating/cooling at the sea surface and from the surface freshwater fluxes (evaporation and sea ice formation enhance salinity; precipitation, runoff and ice-melt decrease salinity).

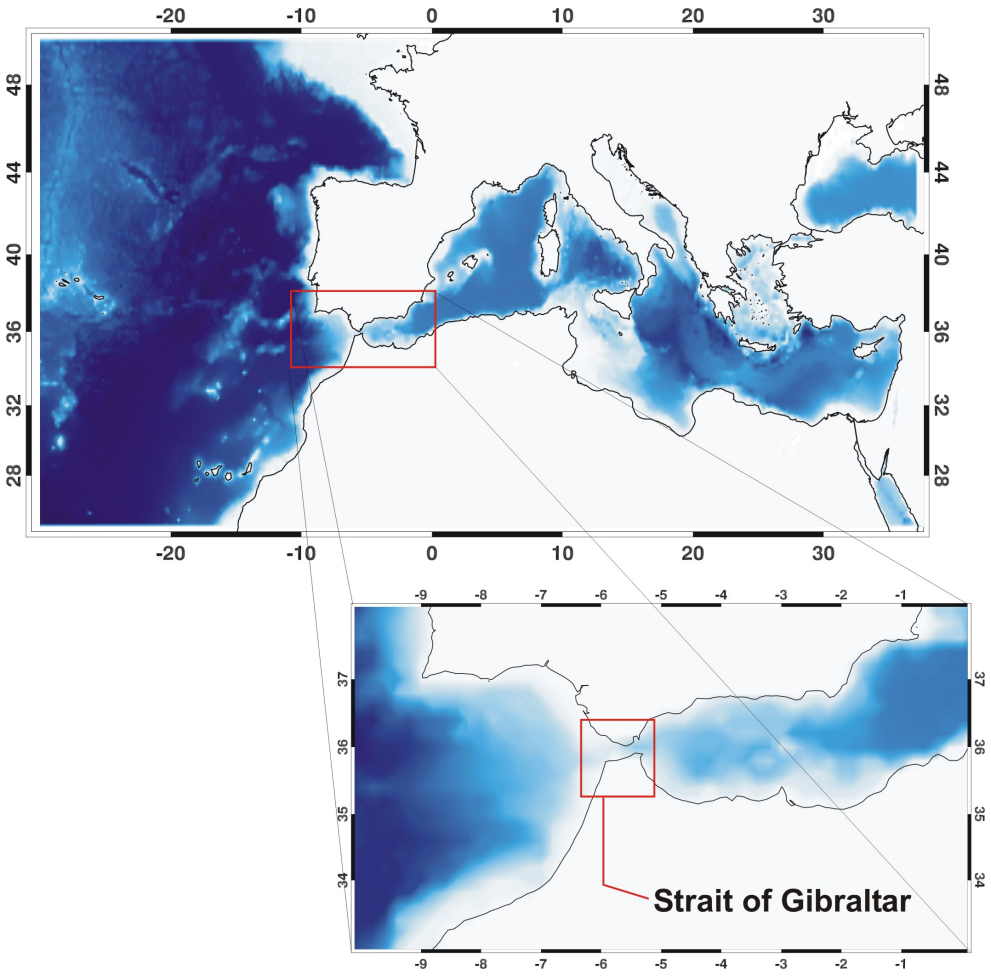

Figure 1.2: Maps showing the geographical location of the Strait of Gibraltar.

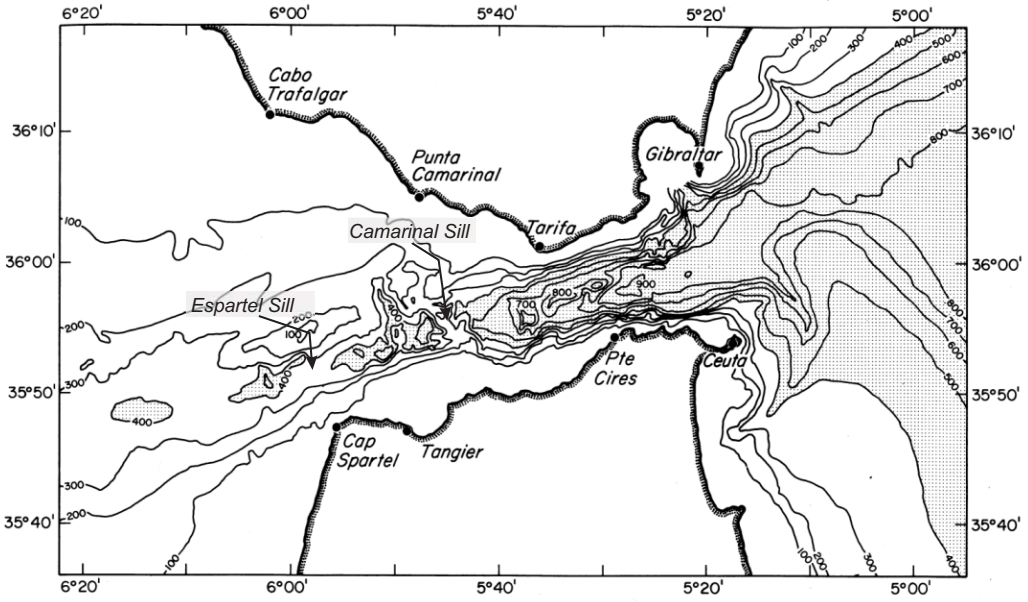

Figure 1.3: Chart of the Strait of Gibraltar, adapted from Armi & Farmer (1988), showing the principal geographic features referred to in the text. Areas deeper than 400 m are shaded.

1.2 Background

1.2.1 Exchange flow description

1.2.1.1 Mean Exchange

The excess of evaporation (E) over precipitation (P) and river runoff (R) over the Mediterranean basin represents, together with the conservation of mass and salt for the Mediterranean Sea, the main driver of the mean circulation through the strait.

This circulation, generally called *inverse estuarine* (Stommel & Farmer (1953)), has been traditionally modeled as a two-layer system: in the upper layer a flow (Q_1) of fresh ($S_1 \simeq 36.2$) and warm Atlantic water spreads in the Mediterranean basin, while in the lower layer a compensating flow (Q_2) of colder and saltier water ($S_2 \simeq 38.4$) exits from the Mediterranean toward the Atlantic (Figure 1.4).

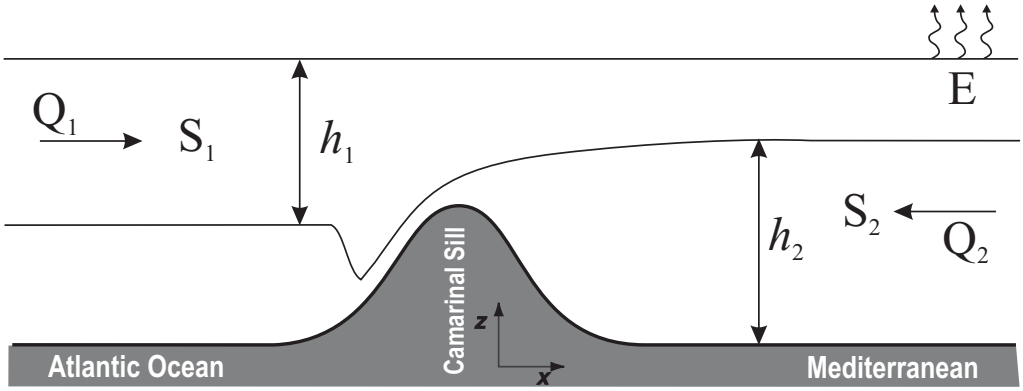

Figure 1.4: Simplified sketch showing the two-layer system.

Mathematically this model can be written as:

$$\begin{cases} Q_1 + Q_2 = E - P - R \\ \\ Q_1 S_1 + Q_2 S_2 = 0 \end{cases} \tag{1.1}$$

where equations 1.1 represent mass and salt conservation respectively. From these equations it is easy to derive two expressions for the mass transports as

Table 1.1: Different estimations of the mean Atlantic (Q_1) and Mediterranean (Q_2) transports, net evaporation over the Mediterranean basin (E_{net}), and salinity difference (ΔS) between Atlantic and Mediterranean water in Gibraltar. Data corresponding to Nielsen (1912), Lacombe & Richez (1982) and Bryden *et al.* (1994) have been adapted from Table 1 in Bryden *et al.* (1994) as in Vargas (2004).

Source	$Q_1(Sv)$	$Q_2(Sv)$	$E_{net}(my^{-1})$	ΔS
Nielsen (1912)	1.87	1.78	1.17	1.91
Lacombe & Richez (1982)	1.21	1.15	0.75	1.75
Bryden & Stommel (1984)	1.67	1.59	0.95	1.72
Bryden *et al.* (1994)	0.72	0.68	0.52	0.12
García-Lafuente *et al.* (2000)	0.92	0.87	0.63	-
Candela (2001)	1.01	0.97	0.45	-
Tsimplis & Bryden (2000)	0.66	0.57	1.12	-
Baschek *et al.* (2001)	0.81	0.76	0.63	-

function of the net evaporation term ($E_{net} = E - P - R$) and salinity difference between the Atlantic and Mediterranean waters:

$$\begin{cases} Q_1 = \frac{S_2 E_{net}}{S_2 - S_1} \\ \\ Q_2 = -\left[\frac{S_1 E_{net}}{S_2 - S_1}\right]. \end{cases} \tag{1.2}$$

These equations are known as the Knudsen (1899) equations. Even if these relations appear very simple, their direct application is not so easy. This is due to the fact that none of S_1, S_2 and E_{net} is very well known. However from both direct and derived measurements it emerges that the values of the exchanged flows, averaged on a sufficiently long time-scale, is of the order of $1Sv$ ($Sverdrup$, $1Sv = 10^6 m^3 s^{-1}$). In Table 1.1 are shown the estimated transports in the last 89 years.

1.2.1.2 Time dependent Exchange

Various processes at different timescales modify the mean exchange flow through the Strait of Gibraltar. The amplitude of these fluctuations can be of the same

order of magnitude, or even greater, than the above mentioned mean value of about $1Sv$ (Candela *et al.* (1990), Bryden *et al.* (1994)). In general these fluctuations are divided in four main frequency bands: low, subinertial, tidal and short. The low frequency is related to the seasonal and interannual variability of the hydrological properties of both the western Mediterranean Sea and the north Atlantic Ocean (Garrett *et al.* (1990)). The subinertial frequency, characterized by a period of some days up to few months, is mainly related to the wind blowing over the Alboran Sea and the Gulf of Cadiz, and the atmospheric pressure differences between the Atlantic and Mediterranean Sea (Candela *et al.* (1989), García-Lafuente *et al.* (2002b) and García-Lafuente *et al.* (2002a)). The tidal frequency is mainly semidiurnal [1] (Candela *et al.* (1990) and Tsimplis & Bryden (2000)), while the short frequency is due to the propagation through the strait of internal waves reaching amplitudes of up to 150 m called *bore* (Richez (1994)).

Among these time-dependent forcing the most energetic one is the barotropic tidal forcing. Analyzing data collected during the *Gibraltar Experiment*, [2] (Kinder & Bryden (1987), Kinder & Bryden (1988)) Candela *et al.* (1990) showed that about 90% of the total kinetic energy present in the strait is due to the semidiurnal components M_2 and S_2; in particular 75% is due to the M_2 and about 12% is due to the S_2. Currents induced by tidal forcing are very strong especially over Camarinal Sill (Bruno *et al.* (2000)). Here tidal currents are so strong to reverse periodically, during each semidiurnal cycle, the direction of both the Mediterranean and Atlantic flow (Bryden *et al.* (1994)). In other words the entire water column over Camarinal Sill can flow in the same direction twice per day.

Recently, others studies have been carried out analyzing data based on direct observations collected during the CANIGO [3] project (1995-1996) (Parrilla *et al.* (2002)). García-Lafuente *et al.* (2000) have analyzed in detail the tide at the eastern section of the Strait. They showed that tides have a marked semidiurnal character; moreover they showed that while the lower layer flow periodically is reversed, the upper layer flow is always directed toward the Mediterranean basin.

[1] A tidal variation consisting of two high and two low tides per lunar day (24.84 hrs.).

[2] The *Gibraltar Experiment*(GIBEX) was carried out by a group of American, Spanish, Moroccan, Canadian and French scientists during the period from October 1985 to May 1986.

[3] Canary Islands Azores Gibraltar Observations

They argued that this different behavior is due to the smallness of the mean flow and the strong amplitude of the semidiurnal tidal currents in the lower layer and vice versa for the upper layer. Using an acoustic doppler current profiler (ADCP) Tsimplis (2000) has described the vertical structure of tidal currents at Camarinal Sill. He showed that the semidiurnal tidal components are the most energetic, they are characterized by an along-strait velocity up to 120 cm s^{-1} for M_2 and 48 cm s^{-1} for S_2. Using the same data Tsimplis & Bryden (2000) have estimated the water transports over Camarinal Sill. They defined as interface between the Atlantic and the Mediterranean water the time-dependent depth where velocity exhibits the maximum vertical shear. Using the derived time series of the depth of the interface and the currents they estimated a transport of about 0.78 Sv for the Atlantic inflow and 0.67 Sv for the Mediterranean outflow.

The volume transport was also estimated at the eastern entrance of the strait by Baschek *et al.* (2001). In order to describe the two-dimensional structure of the tidal flow at the Gibraltar-Ceuta section as well as the depth of the interface between Mediterranean and Atlantic water, they used a tidal inverse model to merge currents data recorded both by current meter moorings and intensive shipboard measurements. The volume transport was estimated to be 0.81 ± 0.07 Sv for the upper layer and 0.76 ± 0.07 Sv for the lower layer.

1.2.2 Hydraulic Control

It is important to note that the Knudsen (1899) equations (equations 1.2) do not determine the salinity difference $(S_1 - S_2)$ between the Atlantic and Mediterranean. In other words these equations are not able to explain why the observed salinity difference between the Atlantic and Mediterranean is about 2 psu. There are, in fact, infinite possible solutions for equations 1.2: we can have large flows corresponding to small salinity differences, or weak flows corresponding to large salinity differences. Thus, in order to explain the observed salinity difference further constrains must be considered.

As initially suggested by Bryden & Stommel (1984) one constraint is the hydraulic control [1] at Camarinal Sill. For a steady two-layer flow through a rect-

[1] The beginning of hydraulic control theory in physical oceanography is due to Stommel

angular cross-section and a sill, both Armi (1986) and Lawrence (1990) showed that the hydraulic control occurs over the sill when

$$G^2 \equiv F_1^2 + F_2^2 = 1 \tag{1.3}$$

with

$$F_i^2 = \frac{u_i^2}{g' h_i}, \tag{1.4}$$

where G is the composite Froude number, F_i, u_i and h_i represent respectively the layer Froude number, velocity and thickness of the upper ($i = 1$) and lower ($i = 2$) layers, and $g' = g\Delta\rho/\rho_2$ is the reduced gravity ($\Delta\rho = \rho_2 - \rho_1$). At the hydraulic control locations the flow undergoes a transition from subcritical ($G^2 < 1$) to supercritical ($G^2 > 1$). A hydraulic jump occurs instead when the flow undergoes a transition from supercritical to subcritical. Hydraulic jump is characterized by turbulent dissipation of energy.

Subsequently, Dalziel (1990) demonstrated that the condition for critical flow can be restated as:

$$G^2 \equiv 1 + \frac{C_1 C_2}{h_1 h_2}, \tag{1.5}$$

where C_1 and C_2 are the phase velocities of the first internal waves mode (long wave propagating at the interface between the two layers), normalized by $\sqrt{g'D}/2$, where D represents the water depth $h_1 + h_2$ (see Figure 1.4). At a control, where the flow is critical and $G^2 = 1$, C_1 or C_2 must be zero, i.e. long waves at the interface cannot propagate upstream against the flow. Where the flow is subcritical they have opposite signs and can propagate in both directions. Where the flow is supercritical C_1 and C_2 have the same sign, and both waves propagate away from the control into a basin. Consequently, changes within that basin cannot propagate back to affect the controls or the other basin.

Armi & Farmer (1986, 1987) introduced another element in the hydraulic theory applied to the Strait of Gibraltar: the concept of *maximal* and *submaximal* exchange. In these works they stated that the flow through the strait can exhibit

& Farmer (1953) who applied the hydraulic theory to study the processes that determine the salinity of an estuary.

two distinct regimes: the first, called maximal exchange, occurs when the flow is hydraulically controlled both at Camarinal Sill and Tarifa Narrow, while the second, called submaximal exchange, characterizes flows that are only controlled at Camarinal Sill. In the first regime, the flow exchange between the Atlantic and the Mediterranean Sea is maximal, and it is only determined by processes occurring in the region in between the two controls. A physical explanation is that the subcritical region between the two controls cannot exchange information with either basin because internal long waves are unable to propagate upstream past either control location.

In order to improve the steady hydraulic theory developed by Bryden & Stommel (1984) and Armi (1986) other features, such as Earth's rotation, friction, time dependence, and nonrectangular cross sections for the configuration of the strait, have been added in literature. Assuming potential vorticity conservation Bormans & Garrett (1989b) estimated the influence of the Earth's rotation on the flow. They found that the main effect of the Earth's rotation is to produce a tilt across the strait of the interface between the two layers, which is minimum at Camarinal Sill section, while is enhanced to the east of Tarifa Narrows. Also Dalziel (1990) estimated the influence of the Earth's rotation on the flow predicting a decrease in the exchange up to one-third with respect to the non rotating case. Including friction in the model of Farmer & Armi (1986), Bormans & Garrett (1989a) estimated the effect of both interfacial and bottom friction. They concluded that, using reasonable drag coefficients (compatible with dissipation measurements carried out by Wesson & Gregg (1988) during the *Gibraltar Experiment*), the interfacial friction has a smaller influence on the exchange than the bottom friction. They also found that, by including the bottom friction on the sloping sides of the strait, the maximal and submaximal solutions tend to come closer than in the inviscid model. Using a more realistic bathymetry, modeled via triangular or parabolic cross-strait sections, Bormans & Garrett (1989a) showed that the exchange is reduced and the interface between the two layers is raised compared with a simple rectangular cross-section bathymetry. In order to take in to account the time dependent tidal forcing in the two-layer hydraulic theory, Farmer & Armi (1986) proposed the so called quasi-steady approximation in which the steady solution is applied at each time of a tidal cycle. However Helfrich (1995) demonstrated that

this quasi-steady approach is not valid for dynamically long straits, i.e. straits having a length greater than the distance traveled by an internal wave during a tidal cycle, which is precisely the situation that occurs in the Strait of Gibraltar. However both theories assert that the exchanged flows increase with the strength of the barotropic tidal forcing, but the quasi-steady theory always predicts more flow than the time-dependent theory. Helfrich (1995) showed that the exchange flow is a function of two non-dimensional parameters: the dynamic length of the strait and the tidal forcing strength (q_{b_0}). He showed that for the Strait of Gibraltar, with a $q_{b_0} = 0.6$ (corresponding to a barotropic velocity over Camarinal Sill of about 1.5 ms^{-1}), transport increases of 1.2 respect to the unforced case, but he also suggested that this increment should be reduced by 20% because of the increased diffusion caused by the tidal mixing. Farmer & Armi (1986), instead, predicted, with their quasi-steady theory, a larger increment of about 1.6 respect to the steady case. Moreover, applying their quasi-steady theory Armi & Farmer (1988) provided a detailed analysis of the control locations in the strait. They observed four controls within the strait, two permanent and two episodic. The first permanent control is located to the west of Espartel Sill while the second is sited within the Tarifa Narrow, moving cyclically toward east in accordance with the eastward-traveling internal bore released at Camarinal Sill. The two episodic controls are located over the two sills: Spartel and Camarinal; the control over Spartel Sill is lost during high water at Tarifa and recovered just one hour before low water; the control over Camarinal Sill is lost at the end of each half-tidal cycle. The presence of the two permanent controls makes the exchange maximal, independently from the others two episodic controls.

It is important to underline that both the time dependent and the quasi-steady theory are based on the assumption that the flow is 1-dimensional, i.e. the flow does not have any across-strait dependency. This assumption is not valid for the Strait of Gibraltar as demonstrated by two of the most recent numerical modeling studies (Izquierdo *et al.* (2001) and Sannino *et al.* (2002)). Thus, results from time-dependent as well as quasi-steady two layer hydraulic theory should be interpreted with care.

1.2.3 Two-way Exchange

Observational data presented by Wesson & Gregg (1994) indicate that there is considerable entrainment and mixing at the interface between Mediterranean and Atlantic water. As initially observed by Bray *et al.* (1995), the flow exchange through the Strait of Gibraltar is strongly affected by both entrainment and mixing. This entrainment and mixing leads to the formation of a thick interfacial layer where density and velocity change gradually in vertical. They suggested that a three-layer model, i.e. a two-layer model with the inclusion of an interfacial (between the two layers) nonuniform layer of considerable thickness and intermediate density, is more appropriate to describe the flow exchange through the strait respect to the two-layer model.

Extending the traditional Knudsen model of exchange (equations 1.1) to three layers, they found that the interfacial layer is capable of carrying a significant fraction of the horizontal mass transport in both directions (Figure 1.5). They found also that the horizontal transport within the interfacial layer changes dramatically with distance along the strait, implying substantial vertical exchange between the interface and the Atlantic and Mediterranean layers. At the eastern end of the strait, roughly half of the transport into the Mediterranean is found in the interface layer, while at the west end an equivalent outflowing transport occurs in the interface layer.

It appears clear that it should be better to define the exchange flow through the Strait of Gibraltar as a two-way exchange rather than a simple two-layer exchange.

1.2.4 Numerical Models

In the last 15 years the Strait of Gibraltar has been studied also by means of numerical models. Different hydrodynamic models have been developed: one-dimensional models were developed by Longo *et al.* (1992), Brandt *et al.* (1996b) and Castro *et al.* (2004), two-dimensional models by Tejedor *et al.* (1999), Izquierdo *et al.* (2001), Morozov *et al.* (2002), and three-dimensional model were developed by Wang (1989, 1993) and Sannino *et al.* (2002, 2004, 2006).

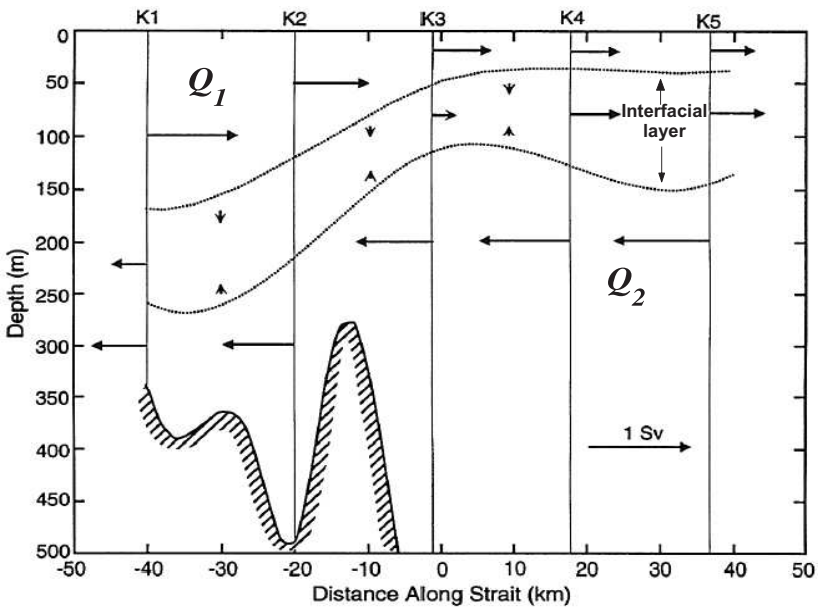

Figure 1.5: Summary of along-strait variations in transports and interface structure. Dotted contours outline the average interface layer along the strait. Arrows are scaled to indicate the magnitude of horizontal transports in each layer at the various sections along the strait. Vertical arrows indicate the vertical transport between the upper and interfacial layer and between the lower and interfacial layer (adapted from Figure 21 in Bray *et al.* (1995)).

One of the first one-dimensional models developed to study the generation of nonlinear internal tides in the Strait of Gibraltar is the one-dimensional, two-layer, rigid-lid[1], hydrostatic model implemented by Longo *et al.* (1992). Although this model was able to describe sufficiently well the generation of internal waves, by the interaction of the semidiurnal tidal flow with the Camarinal Sill, it was not able to describe the subsequent evolution and propagation of these internal waves. This is due to the fact that unlike the generation of the internal tides, their propagation has to be described by a nonhydrostatic model (Pierini (1989)).

Brandt *et al.* (1996b) developed a weakly nonhydrostatic, two-layer model that was capable of describing both the generation and propagation of nonlinear internal waves in the Strait of Gibraltar, as well as their subsequent disintegration into trains of internal solitary wave[2].

The most recent one-dimensional two-layer model has been developed by Castro *et al.* (2004) who, however, focused their work on the development of a new numerical discretization of the two layer shallow water equations, rather than on the dynamics of the strait.

Using a two-dimensional, nonlinear, boundary-fitted coordinate, barotropic model, with a nominal resolution of 0.5 km, Tejedor *et al.* (1999) simulated the M_2 and S_2 surface tides. The resulting cotidal maps were in good agreement with the same maps proposed by Candela *et al.* (1990) that analyzed data collected during the *Gibraltar Experiment*.

A detailed description of the generation and the subsequent propagation and evolution of the internal tides in the Strait of Gibraltar can be found in a paper by Morozov *et al.* (2002). In their study they developed a two-dimensional (in the x-z plane), fully nonhydrostatic model with continuous stratification, and forced both by semidiurnal and diurnal tidal components. Model results showed

[1]The rigid lid approximation assumes that the surface elevation of the sea water is static. Doing so filters out fluctuations of the sea associated with motions of the sea surface (i.e. surface gravity waves such as tides and tsunamis.)

[2]Solitary waves are non-linear waves that propagate without change of shape. The first soliton was discovered by John Scott Russell (1808 - 1882), who followed a solitary wave generated by a boat in Edinburghs Union Canal in 1834. The properties of a solitary waves result from an exact balance between dispersion which tends to spread the solitary wave into a train of waves, and non-linear effects which tend to shorten and steepen the wave.

the strong influence played by the density stratification on the propagation of the internal wave. In other words they underlined that reducing the internal wave motion only to the displacement of the interface (like in a two-layer model) is not enough to describe the evolution of the internal tides.

The first two-dimensional - two-layer - hydrostatic model applied to study the timespace variability of hydraulic controls in the Strait of Gibraltar is the model implemented by Izquierdo *et al.* (2001). Ther model domain is characterized by a very high-resolution horizontal grid, with a nominal resolution, inside the strait, of only 125 m. The model is forced at the open boundaries by the four major semidiurnal (M_2, S_2) and diurnal (O_1, K_1) tidal components. This model predicts the occurrence of four controls located to the west of the Espartel Sill, at the Espartel and Camarinal Sills and in the Tarifa Narrows. The last of these controls is apparent in the sense that it consists of discrete fragments alternating with subcritical flow regions. The only control which extends over the whole width of the strait is the control at the Camarinal Sill, but it breaks down during neap tide, too.

Surprisingly only two three-dimensional models have been developed and applied, in the last 15 years, to the Strait of Gibraltar. Using a three-dimensional general ocean circulation model, Wang (1989, 1993) was able to describe some of the aspect of the mean and tidally forced circulation of the Strait of Gibraltar. However, because of the relatively low horizontal and vertical resolutions ($\sim$ 5 Km and 50 m respectively), the model did not reproduce the hydraulic control over Camarinal Sill. He found in fact that while the surface flow is supercritical, i.e. hydraulically controlled on the eastern entrance the bottom flow is subcritical, i.e. not controlled on the western entrance, over Camarinal Sill.

Considering the occurrence of the interfacial layer between Atlantic and Mediterranean waters, that is, the existence of a three-layer system, where the interfacial layer is an active participant in the process of exchange, Sannino *et al.* (2002) added further complexity to the simulated exchange flow through the Strait of Gibraltar. Thanks to the relatively high resolution of the model (less than 500 m in the strait region) they were able to describe in detail, for the first time, the mean exchange through the Strait of Gibraltar. Moreover, applying a three-layer hydraulic theory to the model results, they found only one permanent control

located over Camarinal Sill. Subsequently, in order to improve this model, they included also the tidal forcing in the model (Sannino *et al.* (2004, 2006)). Implementation of this tidal model and results obtained, in term of exchange flow and hydraulics, represent part of this Thesis work and will be described in details in the next chapters.

1.3 Novel aspects of the Thesis

From the previuos background section, it emerges that recent studies indicate that the 2-layer model is a reasonable approximation for the flow exchange through the Strait of Gibraltar, but, if one is interested in realistic values, it is necessary to include to the 2-layer model a third interfacial layer. However, although it is believed that this interfacial layer is important in determining the correct two-way exchange and hydraulics within the Strait of Gibraltar, there is still a tendency to consider the actual two-way exchange as a two-layer exchange. Also recently, in some numerical studies, two-layer numerical models have been used to study the Strait of Gibraltar (Izquierdo *et al.* (2001); Brandt *et al.* (2004)). Except for the numerical study by Sannino *et al.* (2002) (that however did not consider the tidal forcing) at the best of my knowledge, there are none numerical models that take into account the presence of this interfacial layer.

Despite the large number of studies that have dealt with the applicability of the two-layer hydraulic control theory to the Strait of Gibraltar, there is still an uncertainty about the flow regime through the strait; in particular it is not clear if the regime is maximal or submaximal.

In order to fill the gap between the observational study carried out by Bray *et al.* (1995) and the numerical modeling studies of the Strait of Gibraltar, the first goal of this Thesis is to test the ability of a three-dimensional high-resolution model, forced by the two principal semidiurnal tide components, to simulate the interfacial layer between the Atlantic and Mediterranean water. In this Thesis will be also explored the effect of tides on the hydrological and physical properties of this layer.

However, the principal aim of this Thesis is the investigation of the effects induced by the presence of the interfacial layer on both hydraulics and exchange

flow through the strait. In order to better understand these effects, a comparison between the classical two-layer, and the relatively new three-layer approximation will be performed.

1.4 Thesis organization

The Thesis is organized as follows. Chapter 2 starts with a description, from a numerical point of view, of the model used. Then it continues showing the strategy used to parallelize the model, while details on the boundary conditions and experiment set up conclude this chapter. The model validation has been carried out in Chapter 3. Here model results are compared with most of the available experimental data. Chapter 4 is devoted to evaluate both volume transports and hydraulic regimes in the 'classical' two-layer approximation. The ability of the model in reproducing the interfacial layer between the Atlantic and the Mediterranean layers will be tested in Chapter 5. Always in this chapter the simulated volume transports and hydraulics, computed in the three-layer framework, are presented together with a comparison between the two-layer and the three-layer approximations. Conclusions and discussions complete the Thesis.

Chapter 2

Numerical Model

2.1 Model Description

2.1.1 POM model

The circulation tidal model developed for this study is based on the *Princeton Ocean Model* (hereinafter **POM**), the ocean circulation numerical model designed in the late 1970's by Blumberg & Mellor (1987) to study both coastal and open ocean circulation. POM is one of the most popular community models of the ocean circulation; it is used by a large number of research and academic institutes all over the world. It is a public domain model (URL: POM (2006)) which, thanks to its ability to simulate both shallow water and deep ocean dynamics, has been used for a variety of applications, ranging from small scale coastal management problems to general circulation studies of the Atlantic Ocean (see URL: POM papers (2006) for a complete and updated list of related papers). POM is a σ-coordinates, free surface, primitive equation ocean model, which includes a turbulence sub-model. The prognostic variables of the Princeton Ocean Model are the three components of the velocity field, temperature, salinity, turbulent kinetic energy, turbulent macroscale and sea water level. POM numerically solves, in finite difference form, the momentum equation, the continuity equation and the tracer (temperature and salinity) equations along with a non-linear equation of state $\rho = \rho(\theta, S, P)$ (**UNESCO** equation of state adapted by Mellor (1991)) which couples the two active tracers to the fluid velocity. Two more prognostic

equations are used to calculate turbulent kinetic energy and turbulent macroscale. These equations are part of the *Mellor - Yamada 2.5* (Mellor & Yamada (1982)) turbulence closure scheme used to parameterize the vertical turbulent mixing processes (vertical diffusivity). This numerical scheme, as recently demonstrated by Ezer (2005), is able to take into account also the effect of entrainment. The horizontal momentum, heat and salt small scale mixing processes are parameterized as horizontal diffusion (along sigma surfaces), depending on the horizontal velocity shear and on the grid spacing via the Smagorinsky diffusion scheme (Smagorinsky (1963)):

$$A_H\left(x,y,t\right) \;=\; A_M\left(x,y,t\right) \;=\; C\,\Delta x\,\Delta y\,\left[N^2\left(x,y,t\right)+S^2\left(x,y,t\right)\right]^{\frac{1}{2}} \tag{2.1}$$

where Δx, and Δy, are the grid sizes, C is a constant taken to be 0.2 in this study, and S and N are the mean shear and the normal stress respectively:

$$N\left(x,y,t\right) \;=\; \frac{\partial}{\partial x}u\left(x,y,t\right) \;-\; \frac{\partial}{\partial y}v\left(x,y,t\right) \tag{2.2}$$

$$S\left(x,y,t\right) = \frac{\partial}{\partial x}v\left(x,y,t\right) - \frac{\partial}{\partial y}u\left(x,y,t\right). \tag{2.3}$$

The model uses an explicit leapfrog scheme for time stepping, except for the vertical diffusion terms, which are treated with a forward implicit scheme. To provide explicitly the free surface variations the model also solves, with a small time step, the related barotropic equations, which is a set of vertically integrated equations of continuity and motion, usually called *external mode*. For computer time economy the 3D-equations, usually called *internal mode*, are solved with a larger time step, limited by the *Courant-Friedrichs-Lewy* (CFL) stability condition for the internal gravity wave speed, using a time splitting technique.

The model specifies the values of all variables at the nodes of a curvilinear orthogonal grid (which are very useful in applications with complex coastline), staggered as in *Arakawa-C* scheme (Arakawa & Lamb (1977)), conserving linear and quadratic quantities like mass and energy (Figure 2.1). As pointed out before in this paragraph, the model as vertical grid uses the σ-coordinates system [1] which

[1] Known also as *terrain following* coordinate system.

is the most appropriate for areas with significant topographic variability like the Strait of Gibraltar (Figure 2.2).

Details on the transformed equations on a horizontal curvilinear orthogonal framework in a σ-coordinate system and the numerical algorithm can be found on the POM's user guide (Mellor (2006)).

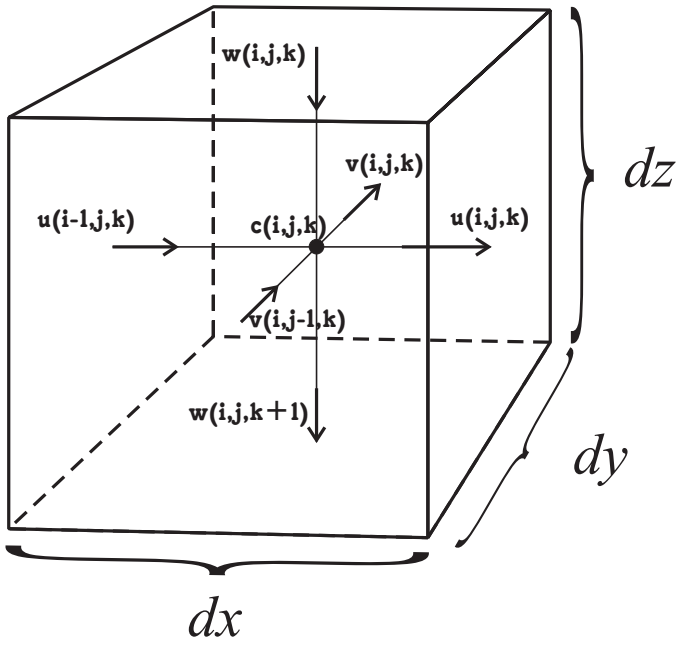

Figure 2.1: In the *Arakawa-C* grid the velocity components u, v, and w are staggered by half a grid spacing. c represents any other grid variable in the model, like salinity S or temperature T.

2.1.2 Modified POM model (CEPOM)

The version of POM used in this study has been extensively rewritten in **FORTRAN90** and a modular parallel version of the model, called **CEPOM**, has been developed. The basic structure of the numerical schemes of POM are not modified in CEPOM except for the advection scheme for tracers, which is completely different.

As advection scheme for tracers POM uses a second order centred (both spatially and temporally) scheme. It is well-known that such a scheme is dispersive.

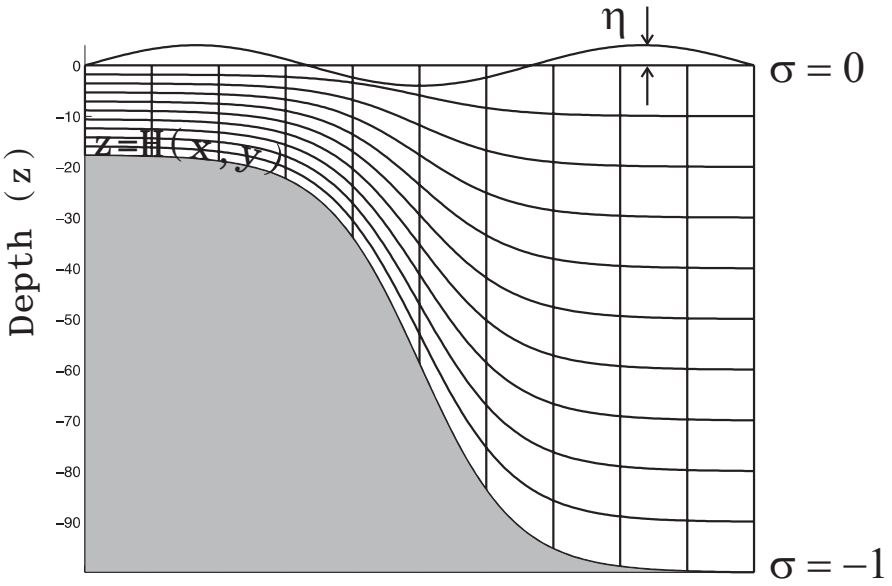

Figure 2.2: Schematic representation of a σ-coordinates system.

Dispersion is more evident in presence of strong density gradients where it creates spurious temperature and salinity values. Thus, the presence of density gradients within the Strait of Gibraltar makes the centred scheme unable to simulate correctly the water exchange. For this reason in CEPOM the Multidimensional Positive Definite Advection Transport Algorithm (MPDATA), as developed by Smolarkiewicz (1984), has been implemented. MPDATA is a flux corrected upstream scheme, i.e. an upstream scheme characterized by a small implicit diffusion. It is reduced by means of an iterative method based on the antidiffusive velocities which is applied to correct the excessive numerical diffusion of standard upstream scheme. The number of iterations is optional; each additional iteration increases the solution accuracy as well as the computing time: the number of iterations chosen for this study is three, which gives sufficient accuracy for our purposes. MPDATA, which is second-order accurate on space and time, has been already used in other ocean models applied to the Strait of Gibraltar giving satisfactory results (see for example Wang (1989, 1993)).

In order to develop a parallel version of the POM model, both efficient and portable, the *Scalable Modeling System* (**SMS**) tool has been used. SMS has been

recently developed by Govett *et al.* (2003) of the Advanced Computing Branch of the Forecast Systems Laboratory at NOAA (National Oceanic and Atmospheric Administration). In this section we recall only the principal SMS features used to parallelize our POM implementation, while a complete overview of SMS can be found at the URL: SMS (2006).

SMS makes use of a set of directives (about 20) that users have to add to their code in form of comments. SMS translates the code and directives into a parallel version which runs efficiently on both shared and distributed memory high performance computing platforms; in particular it uses a source-to-source translation technique to generate different parallel target codes from a single source code. The advantage of the SMS approach is that no complicated compiler-generated communication statements have to be included in the code, moreover SMS contains a number of features to speed up the debugging process and to support incremental parallelization. Further, no code changes are required when porting the SMS serial version to other shared and distributed memory machines. As in Sannino *et al.* (2001) the parallelization strategy used for POM follows the well known domain decomposition technique, applied to the two horizontal coordinates, which is automatically achieved by SMS.

The resulting SMS version of POM includes only 3% more code lines respect to the original serial code, while the speed-up obtained for our implementation of POM is about 21 using 32 IBM Power4 CPUs (1.3 Ghz clock and 64 Gb). In Table 2.1 speed-up details for the principal routines are shown (see Sannino *et al.* (2005) for more details).

2.2 Model Configuration

2.2.1 Grid and Bathymetry

The region covered by the tidal model includes, in addition to the Strait of Gibraltar, also the two sub-basins connected to it: the eastern part of the Gulf of Cadiz and the Alboran Sea. The horizontal model domain extends longitudinally from 8 $^\circ$ W to 5 $^\circ$ E and meridionally from 33 $^\circ$ N to 39 $^\circ$ N. The horizontal grid, that is

Table 2.1: Time (in milliseconds) and speed-up of the full code and for the principal routines referred to a single time step.

	Time(ms)	**Speed-up**							
CPUs	1	4	8	12	16	20	24	28	32
full code	14900	4.1	7.7	10.8	13.3	15.1	17.5	19.5	21.2
profq	1610	4.3	8.4	12	15.5	17.9	20.9	23	23.7
proft	720	4.2	8.8	13	17.1	21.2	24.8	26.6	31.3
advct	717	4.5	7.9	11.4	13.8	16.3	19.4	21.7	22.4
dens	632	4.3	11.1	18	23.4	28.7	35.1	39.5	45.1
denst	511	4.5	12.8	21.3	28.4	35.7	42.5	51.1	53.8
advq	428	5.1	9.9	14.3	17.5	20.4	21.9	23.1	26.7
profs	248	4.3	8.5	11.8	16.5	17.7	20.7	22.5	24.8
profu	242	4.2	7.8	11.5	15.1	18.6	22	26.9	28.5
profv	240	4.4	8.3	11.5	15.5	20.2	22	26.3	26.4
baropg	175	4.2	7.6	12.1	12.1	12.5	15.1	15.3	16.1
vertvl	146	4.7	9.1	11.7	14.6	14.7	15.4	15.5	15.7
advave	128	4.3	8.3	12.2	16	19.4	21.7	27.3	28.4

made by 306×53 grid points, is characterized by a non-uniform spacing; resolution is maximum in the strait, where it is less than $500m$, while at the eastern and western ends it reaches $10-20$ km and $8-15$ km, respectively (Figure 2.3).

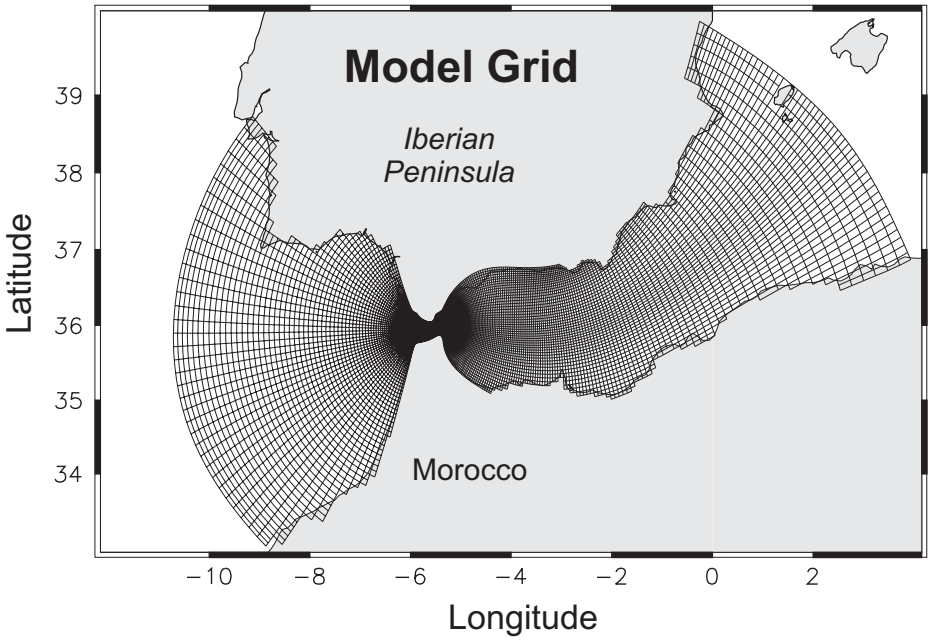

Figure 2.3: Orthogonal curvilinear model grid; the calculated maximum departure of the grid cells from a rectangular shape is less than 10^{-12}.

The portion of the horizontal grid representing the strait is rotated anticlockwise of about 17° so that the along-strait velocity is quite well represented by the model u component (Figure 2.4).

The vertical grid is made of 32 sigma levels, logarithmically distributed at the surface and at the bottom, and uniformly distributed in the rest of the water column.

The model topography was constructed by bilinear interpolation of the depth data onto each grid point of the horizontal model grid. The depth data were obtained by merging the high resolution (<1 Km) topographic data set of the Strait of Gibraltar, provided by the LODYC laboratory, with the relatively low resolution ($5'$) DBDB5 data set provided by the U.S. Navy for the Alboran Sea and the Gulf of Cadiz.

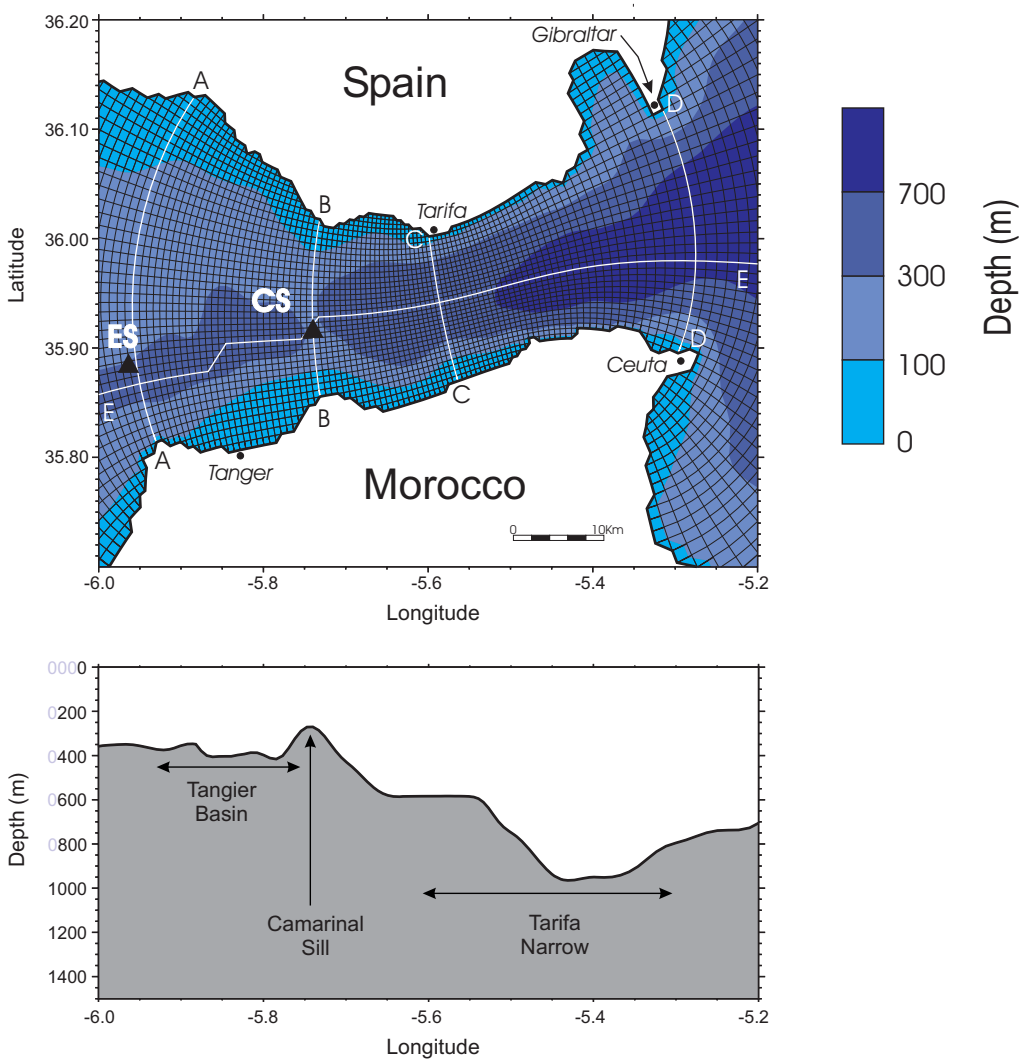

Figure 2.4: (top) Model bathymetry, computational grid, and transects for the presentation of model results within the Strait of Gibraltar. The blue levels indicate the water depths. The points **CS** and **ES** mark the points where Espartel Sill and Camarinal Sill, respectively, are located. (bottom) Bathymetry along the longitudinal section **E**.

In an attempt to reduce the well-know pressure gradient error produced by sigma coordinate grids in regions of steep topography (Haney (1991)) an additional smoothing was applied where the slope ($\delta H/H$) was greater than 0.2, as suggested by Mellor *et al.* (1994). In order to estimate the residual pressure gradient error, the model was integrated for one year without initial horizontal density gradient, i.e., with salinity and temperature fields varying only with depth, with no open boundary applied, i.e. closed domain, and without any other external forcing. The maximum intensity of erroneous currents introduced by the σ-coordinates was of 2 cm s^{-1}. Since the expected baroclinic velocities are up to 1 $m\ s^{-1}$ this error seems to be tolerable.

The resulting model topography, with the minimum depth of the shelf set to 25 m, is illustrated in (Figure 2.5); in particular, the bottom topography and the computational grid in the region of the strait is shown in Figure 2.4. Here are clearly recognizable the dominant topographic features of the strait (from west to east): Spartel Sill (ES), Tangier basin, Camarinal Sill (CS) with a depth of 284 m and Tarifa Narrows.

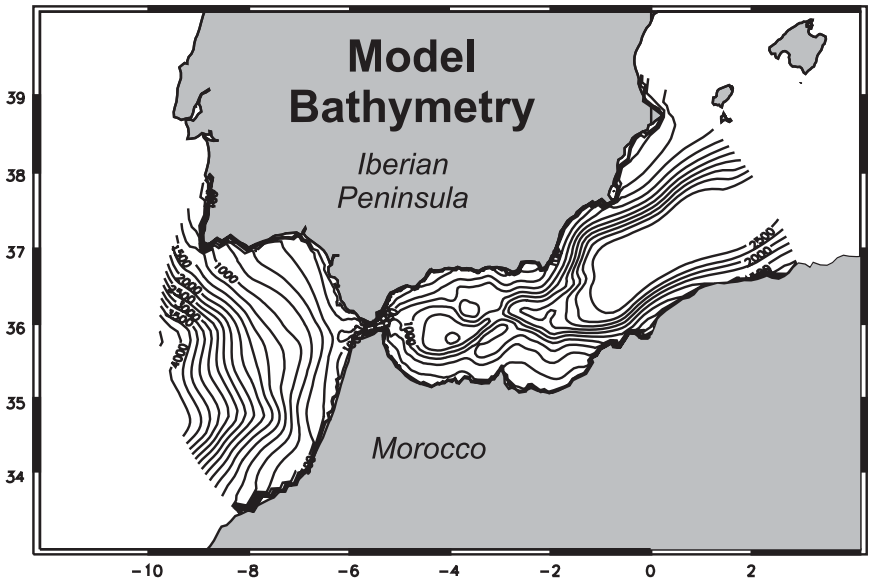

Figure 2.5: Model bathymetry; contour interval is 250 m.

2.2.2 Initial and Boundary Conditions

Model domain is characterized by two open boundaries. They are located at the eastern and western ends of the model domain respectively. On these boundaries values of velocity, temperature, salinity and surface elevation must be specified.

Several kinds of combinations of open boundary conditions have been tested. In the following is described in details only the set of open boundary conditions that performed the best model results. For the depth-dependent velocity an Orlanski radiation condition (Orlanski (1976)) is used at both boundaries. This boundary condition has been used because it minimizes the contamination of the interior model solution due to wave reflection at the boundaries. A zero gradient condition is used for the depth-integrated velocity while a forced-Orlanski radiation condition (Bills & Noye (1987)) is used for the surface elevation at the western and eastern boundaries:

$$\zeta_i^{n+\frac{1}{2}} = \frac{(\zeta_{Ti}^{n-\frac{1}{2}} + \zeta_{Mi}) - (Cr/2)\zeta_i^{n-\frac{1}{2}} + Cr\zeta_{i-1}^{n}}{1 + Cr/2} \tag{2.4}$$

where ζ_i^n represents the surface elevation at the "i" grid point of the open boundary at time step "n", $Cr = c\Delta t/(2\Delta x)$ is a Courant number defined in the $x-$direction, ζ_{Ti}^{n-1} is the forcing tide elevation at the grid point "i" and time step $n-1$, and ζ_{Mi} is the time independent mean elevation at the grid point "i", which is set to about 12 cm at the western open boundary and to 0 cm at the eastern open boundary. Equation 2.4 incorporates a radiation mechanism that allows the undesired transients to pass through the open boundaries, going out of the model basin, without contaminating the desired forced solution. The time independent mean elevation (ζ_{Mi}) value used at the open boundaries is obtained running the model in barotropic mode. This model, as the baroclinic version, has at the eastern and western ends of the computational domain two open boundaries where values of barotropic velocity and surface elevation must be specified. For the surface elevation an Orlansky radiation condition (Orlanski (1976)) was used at the western boundary while a clamped to zero condition was used for the eastern end. For the barotropic velocity a zero gradient condition

was used at both ends. In this way the barotropic model was able to freely adjust the western surface elevation, after 180 days of simulation, to about 12 cm.

Temperature and salinity are specified on the open boundaries by using an upwind advection scheme that allows the advection of temperatures and salinities into the model domain under inflow conditions. Normal velocities are set to zero along coastal boundaries, at the bottom, adiabatic boundary conditions are applied to temperature and salinity and a quadratic bottom friction, with a prescribed drag coefficient, is applied to the momentum flux. This is calculated by combining the velocity profile with the logarithmic law of the wall:

$$C_D = \max\left[2.5 \times 10^{-3}, k^2 \ln(\Delta z_b / z_0)\right] \tag{2.5}$$

where k is the Von Karman constant, z_0 is the roughness length, set to 1 cm, and Δz_b is the distance from the bottom of the deepest velocity grid point.

The so-called *lock-exchange* initial condition has been used in this work. It consists in "filling" the model domain with two different water masses separated by an imaginary dam; in particular in this case the imaginary dam is located in the middle of the strait, while the two water masses are obtained horizontally averaging the spring MODB data (URL: MODB (2006)) for the Alboran basin, and the spring Levitus data (Levitus (1982)) for the Gulf of Cadiz. Vertical profiles of temperature and salinity of the two water masses are shown in Figure 2.6.

The model is forced at the open boundaries through the specification of the two major semidiurnal surface tidal elevation components: M_2 with a period of 12.42 h, and S_2 with a period of 12.00 h. This choice does not represent a limitation; in fact, as already seen in the Introduction of this thesis, more than 90% of the total kinetic energy present in the strait is due to the semidiurnal components M_2 and S_2. The resulting semidiurnal tidal elevation forcing applied at the open boundaries of the model is defined as:

$$\zeta_T(y,t) = \sum_{n=1}^{2} A_n(y) \cos(\sigma_n t - \varphi_n(y)) \tag{2.6}$$

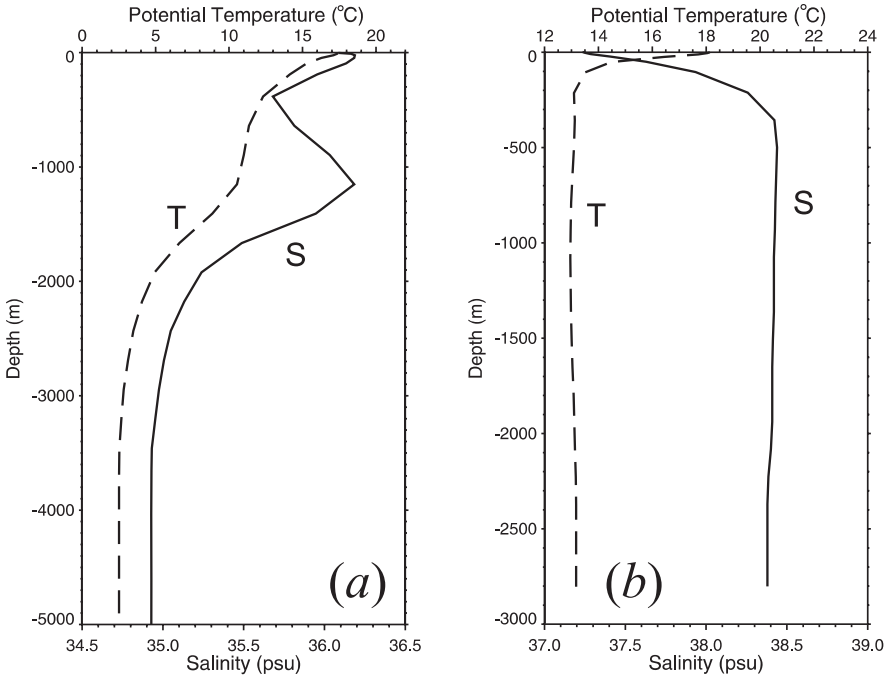

Figure 2.6: Initial conditions; (a) vertical profiles of salinity (solid line) and temperature (dashed line) for the Gulf of Cadiz; (b) vertical profiles of salinity (solid line) and temperature (dashed line) for the Alboran Sea.

where $A_n(y)$ and $\varphi_n(y)$ are the prescribed surface elevation amplitude and phase of the n-th tidal constituent, and σ_n is its frequency. The M_2 and S_2 surface tidal elevation amplitudes and phases have been obtained from the global tidal model of Kantha (1995) and Kantha *et al.* (1995). The resulting $\zeta_T(y_m^w, t)$ applied at the middle point of the western open boundary (y_m^w) during the neap tide ranges from –48 to +75 centimeters, while during the spring tide it ranges from –128 to +140 centimeters (Figure 2.7).

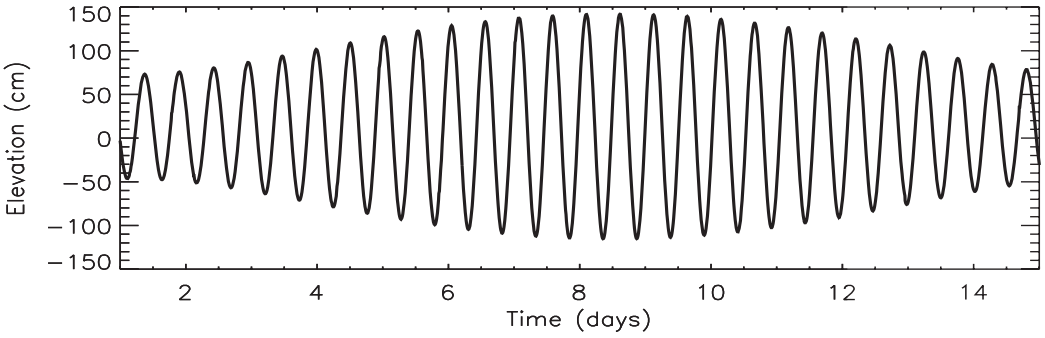

Figure 2.7: Semidiurnal tidal elevation forcing $\zeta_T(y_m^w, t)$ applied at the middle point of the western open boundary.

Due to the strong velocities generated by the tidal forcing, very short external and internal time steps, of 0.1 and 6 seconds respectively, are used to perform the numerical simulation.

2.3 Model Experiments

The model was initially run for 360 days without tidal forcing, in order to achieve a steady two-way circulation that represents the non-tidal experiment. Then the model simulation was extended for another 29 days, forced only by the M_2 and S_2 semidiurnal tidal components, in order to achieve a stable time-periodic solution, and finally the model was run for a further fortnight period (14.79 days) that represents the tidal experiment.

Chapter 3

Model Validation

3.1 Armonic Analysis

In order to validate the tidal model a least squares harmonic analysis was performed for both the sea surface elevation and currents for the tidal experiment.

3.1.1 Tidal Elevation

In Tables 3.1 and 3.2 the observed amplitudes (A) and phases (P) of the two semidiurnal tidal components of the surface elevation are compared with the simulated amplitudes (A) and phases (P) of the same components. A general good agreement between observed and predicted values is found; the maximum differences do not exceed 6.2 cm in amplitude (with a maximum error of about 15%) and 13 $^\circ$ in phase. The maximum differences are confined to coastal points as Ceuta (CE), Algesiras (AL), Tarifa and Pta. Cires, since the model grid is not coastal-fitted.

In Figure 3.1 are also shown the computed cotidal charts for the Strait region, for the simulated M_2 and S_2 surface tidal waves. The M_2 chart is in good qualitative agreement with the empirical cotidal chart presented by Candela *et al.* (1990). The only difference is in the Camarinal Sill area, where the cotidal lines (lines of constant phase) undergo a deviation toward North. The principal features to be noted on this chart are the reduction (more than 50%) of the amplitude in the

Table 3.1: Comparison between Observed and Predicted Amplitudes A and Phases P of M_2 tidal elevation.

			Observed M_2		Predicted M_2		Prediceted - Observed		
Location	Latitude	Longitude	A,cm	P,deg	A,cm	P,deg	A,cm	A,%	P,deg
			Tsimplis *et al.* (1995)						
Gibraltar	36 ° 08′	05 ° 21′	29.8	46.0	29.7	46.0	-0.1	0.3	+0.0[a]
			García-Lafuente (1986)						
Pta. Gracia	36 ° 05.4′	05 ° 48.6′	64.9 ± 0.2	49.0 ± 0.5	64.9	51.0	+0.0	0.0	+1.5
Tarifa	36 ° 00.2′	05 ° 36.4′	41.5 ± 0.2	57.0 ± 0.5	40.5	46.3	-0.8	1.9	+10.2
Pta. Cires	35 ° 54.7′	05 ° 28.8′	36.4 ± 0.2	46.5 ± 0.5	33.6	50.1	-2.6	7.1	+3.1
Pta. Carnero	36 ° 04.3′	05 ° 25.7′	31.1 ± 0.2	47.5 ± 0.5	29.1	43.8	-1.8	5.8	-3.2
			Candela *et al.* (1990)						
DN	35 ° 58′	05 ° 46′	60.1	51.8	56.2	53.9	!3.9	6.4	+2.1
DS	35 ° 54′	05 ° 44′	54.0	61.8	51.4	61.6	-2.6	4.8	-0.2
SN	36 ° 03′	05 ° 43′	52.3	47.6	50.1	48.2	-2.2	4.2	+0.6
SS	35 ° 50′	05 ° 43′	57.1	66.8	58.0	65.3	+0.9	1.5	-1.5
DW	35 ° 53′	05 ° 58′	78.5	56.1	73.3	58.4	-5.2	6.6	+2.3
TA	36 ° 01′	05 ° 36′	41.2	41.2	41.0	47.3	-0.2	0.4	+6.1
AL	36 ° 08′	05 ° 26′	31.0	48.0	28.6	46.0	-2.4	7.7	-2.0
CE	35 ° 53′	05 ° 18′	29.7	50.3	27.5	47.3	-2.2	7.4	-3.0
DP5	36 ° 00′	05 ° 34′	44.4	47.6	38.2	43.9	-6.2	13.9	-3.8

[a]Calibration.

Table 3.2: Comparison between Observed and Predicted Amplitudes A and Phases P of S_2 tidal elevation.

			Observed S_2		Predicted S_2		Prediceted - Observed		
Location	Latitude	Longitude	A,cm	P,deg	A,cm	P,deg	A,cm	A,%	P,deg
			Tsimplis *et al.* (1995)						
Gibraltar	36 ° 08′	05 ° 21′	10.7	72.0	10.5	72.0	-0.2	1.8	+0.0[a]
			García-Lafuente (1986)						
Pta. Gracia	36 ° 05.4′	05 ° 48.6′	22.3 ± 0.2	74.0 ± 1.0	20.3	77.9	-1.8	8.1	+2.9
Tarifa	36 ° 00.2′	05 ° 36.4′	14.2 ± 0.2	85.0 ± 1.5	14.7	69.8	-0.3	2.0	-13.7
Pta. Cires	35 ° 54.7′	05 ° 28.8′	14.1 ± 0.2	74.0 ± 1.	13.1	76.7	-0.8	5.7	+1.7
Pta. Carnero	36 ° 04.3′	05 ° 25.7′	11.5 ± 0.2	71.0 ± 1.0	10.6	68.6	-0.7	6.9	-1.4
			Candela *et al.* (1990)						
DN	35 ° 58′	05 ° 46′	22.5	73.8	20.3	77.9	-2.2	9.7	+4.1
DS	35 ° 54′	05 ° 44′	21.1	83.3	18.3	87.3	-2.8	13.2	+4.0
SN	36 ° 03′	05 ° 43′	18.5	73.4	18.1	74.2	-0.4	2.1	+0.8
SS	35 ° 50′	05 ° 43′	20.6	92.3	21.0	90.0	+0.4	1.9	-2.3
DW	35 ° 53′	05 ° 58′	29.0	82.2	26.6	81.8	-2.4	8.2	-0.4
TA	36 ° 01′	05 ° 36′	14.7	67.9	15.1	70.7	+0.4	2.7	+2.8
AL	36 ° 08′	05 ° 26′	11.1	73.9	10.2	71.2	-0.9	8.1	-2.7
CE	35 ° 53′	05 ° 18′	11.4	75.6	9.6	74.8	-1.8	15.7	-0.8
DP5	36 ° 00′	05 ° 34′	16.1	73.9	14.0	69.1	-2.1	13.0	-4.8

[a]Calibration.

along-strait direction, the invariability of the amplitude in the cross-strait direction (except for the eastern part of Tarifa narrow), and the southwestward phase propagation, more evident east of Camarinal Sill as far as the eastern entrance of the Strait. The same features are also present on the S_2 cotidal chart even if the cotidal lines exibit a greater deviation toward North over the Camarinal Sill. In agreement with Candela *et al.* (1990), the ratios and phase differences between the M_2 and S_2 components remain quite constant throughout the Strait; the amplitude ratio is confined between 2.6 and 2.8 and the phase difference decreases from west to east of only 2 degrees between –24 ° to –26 °.

3.1.2 Tidal Ellipse

A direct comparison between the predicted fields of major and minor axes of tidal ellipse and data are difficult because of the lack of data in most part of the Strait, with the exception of Camarinal Sill (see Candela *et al.* (1990)) and of the eastern entrance of the Strait (see García-Lafuente *et al.* (2000)). Thus, in order to quantitatively compare the model results with observed data, a linear regression between predicted and observed semimajor axis, in only ten different locations, was performed (Figure 3.2). The mean errors and the root mean square errors are shown in Table 3.3. The errors are limited to 4.0 cm s^{-1} and 7.5 cm s^{-1} for the S_2 and 5.9 cm s^{-1} and 7.9 cm s^{-1} for the M_2, except for the stations M3 and F3 where the mean error reaches the value of 24.7 cm $s^{-1}$and the root mean square reaches 31.9 cm s^{-1}. These differences are mainly due to an overestimation of the simulated lower layer currents.

3.2 Tidal Currents

Figures 3.3 and 3.4 show a complete semidiurnal tidal cycle simulated by the model during spring tide at the Gibraltar-Ceuta and Camarinal Sill sections respectively. It is clear from Figures 3.3 that the lower layer flow, at the eastern section (sec. D in Figure 2.4), is periodically reversed by tidal currents toward the Mediterranean Sea (also during neap tide, not showed). The typical currents range from –60 to 30 cm s^{-1} during spring tide and from –40 to 30 cm s^{-1} during

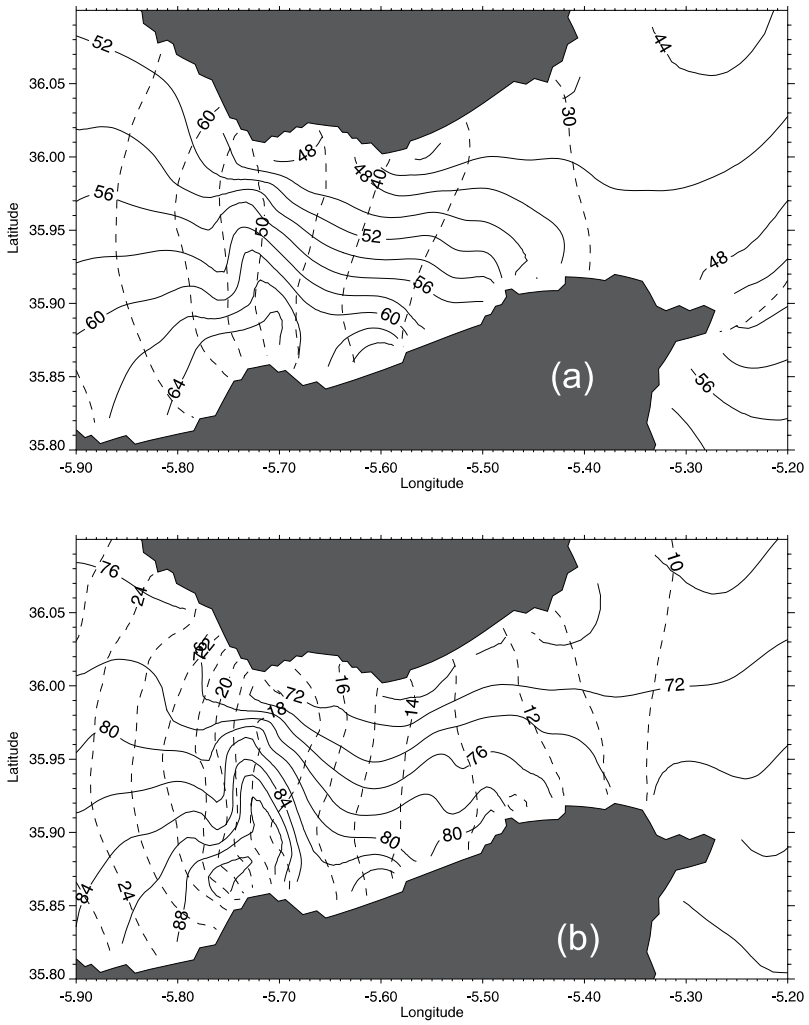

Figure 3.1: Cotidal charts of the (a) M_2 and (b) S_2 surface tides. Solid lines are phase contours, in degrees; dashed lines are amplitude contours, in centimeters.

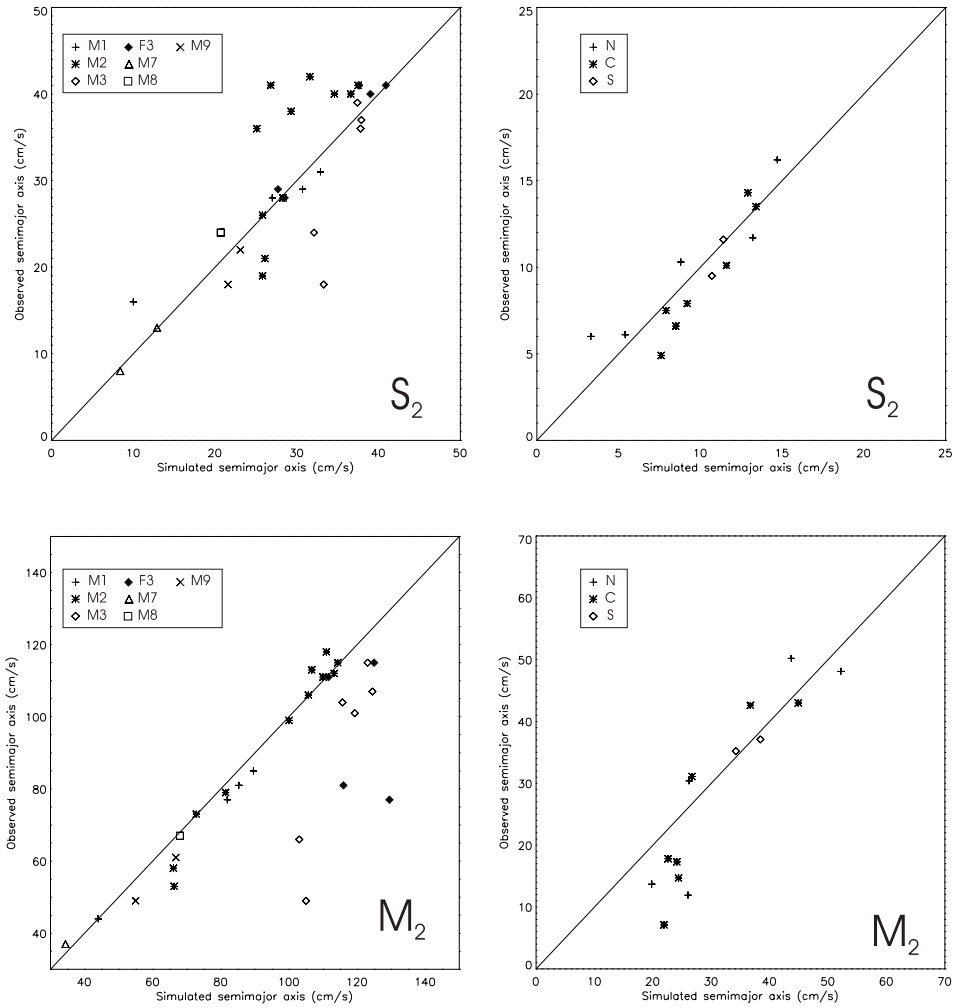

Figure 3.2: Comparison between observed and simulated semimajor axis component of tidal ellipses. Observed data M1, M2, M3, M7, M8, M9, and F3 are from Candela *et al.* (1990) and N, C, and S are from García-Lafuente *et al.* (2000).

Table 3.3: Mean and Root Mean Square (RMS) error of the simulated semimajor axis. Station locations are shown in Figure 2.4.

	M_2		S_2	
Station	Mean Error	RMS Error	Mean Error	RMS Error
		Candela *et al.* (1990)		
M1	3.4	3.9	-0.8	3.3
M2	0.9	5.5	-4.0	7.5
M3	24.7	29.8	3.5	7.2
M7	-0.8	1.9	0.1	0.3
M8	1.0	1.0	-3.3	3.3
M9	5.9	5.9	2.3	2.6
F3	24.5	31.9	-0.4	0.8
		García-Lafuente (1986)		
N	2.7	7.9	-0.9	1.7
C	3.9	7.9	0.9	1.5
S	0.1	1.1	0.5	0.8

neap tide. On the contrary, the upper layer is always directed toward the Mediterranean Sea, indicating a clear weakness of the tidal amplitude in comparison with the mean upper layer flow, that is too strong to be reversed. For the upper layer, the currents range from 80 to 140 cm s^{-1} during spring tide and from 60 to 110 cm s^{-1} during neap tide. These results are in good agreement with Baschek *et al.* (2001), who showed very similar results for the M_2 component, computed with an inverse model at the eastern entrance of the Strait.

At Camarinal Sill, the tidal signal is so strong to always reverse the currents, both in the upper and lower layers, for a part of each semidiurnal tidal cycle, except for the neap tide where the Mediterranean layer is not reversed completely (for the spring tidal cycle see Figure 3.4). To discriminate between upper and lower layer velocities we superimposed to the velocity contours the depth of the 37.25 isohaline, that, as suggested by Sannino *et al.* (2002), can be considered as an interface between the two layers. Using this method, it is possible to see that velocity in the upper layer ranges from –130 to 200 cm s^{-1}during spring tide and from –100 to 130 cm s^{-1} during neap tide. For the lower layer, velocity ranges from –230 to 150 cm s^{-1} during spring tide and from –190 to 70 cm s^{-1} during neap tide.

Figures 3.5, 3.6, 3.7, and 3.8 show the simulated M_2 and S_2 tidal amplitude and phase of the along-strait velocity at Camarinal Sill and Gibraltar-Ceuta cross-strait sections. Looking at Figures 3.5a and 3.6a it is clear that there is a drastic decrease in the M_2 amplitude (more then 70%) going from Camarinal Sill to the eastern entrance of the Strait. At Camarinal Sill the amplitude constantly increases from 100 cm s^{-1} at the surface up to 140 cm s^{-1} at a depth of about 220 m and then decreases in the vicinity of the bottom due to the influence of friction. On the other hand, in good agreement with Baschek *et al.* (2001), at the eastern entrance of the Strait the amplitude increases from 8 cm s^{-1} at the surface to 42 cm s^{-1} in the lower layer. The main increase is in the upper layer: amplitude reaches the value of 34 cm s^{-1} in the first 200 m, and remains rather constant in the rest of the water column. A meridional variation of the amplitude from the southern part (40 cm s^{-1}) to the northern part (18 cm s^{-1}) of the Strait is also evident. Another point to highlight is that the phase at Camarinal Sill (Figure 3.6b) is quite constant from the upper layer to the lower layer; there is

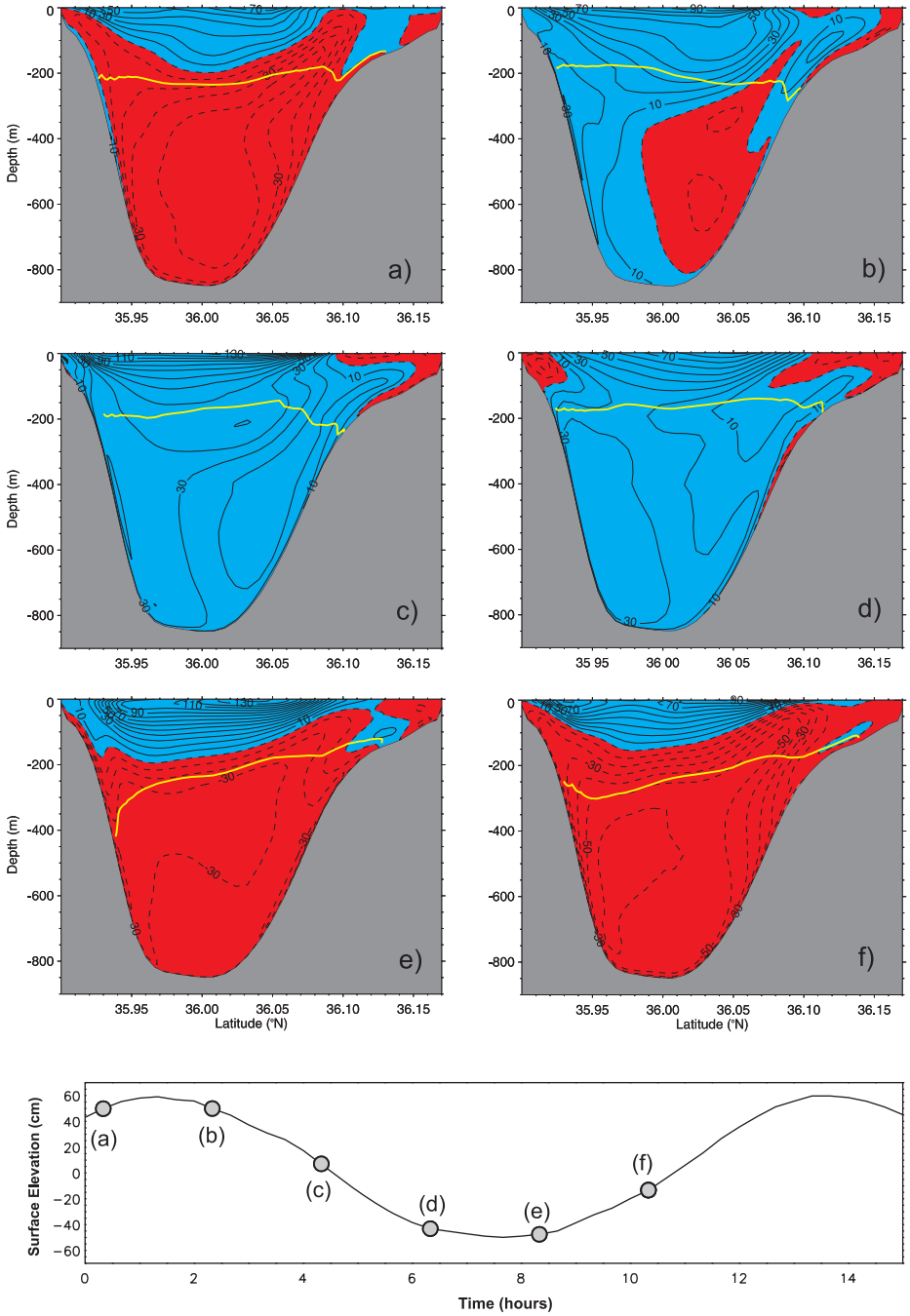

Figure 3.3: (a-f) Simulated sections of the along-strait current (cm s^{-1}) showing several phases of a semidiurnal ($M_2 + S_2$) tidal cycle during spring tide at Gibraltar-Ceuta section(sec. D in Figure 2.4). The time difference between the single sections is 2 hours. The time moments are referred to the surface elevation at Tarifa (lower panel). Contour interval is 10 cm s^{-1}. Red and blue shadows highlight outflow and inflow currents respectively. Yellow line represents the depth of the 38.1 isohaline.

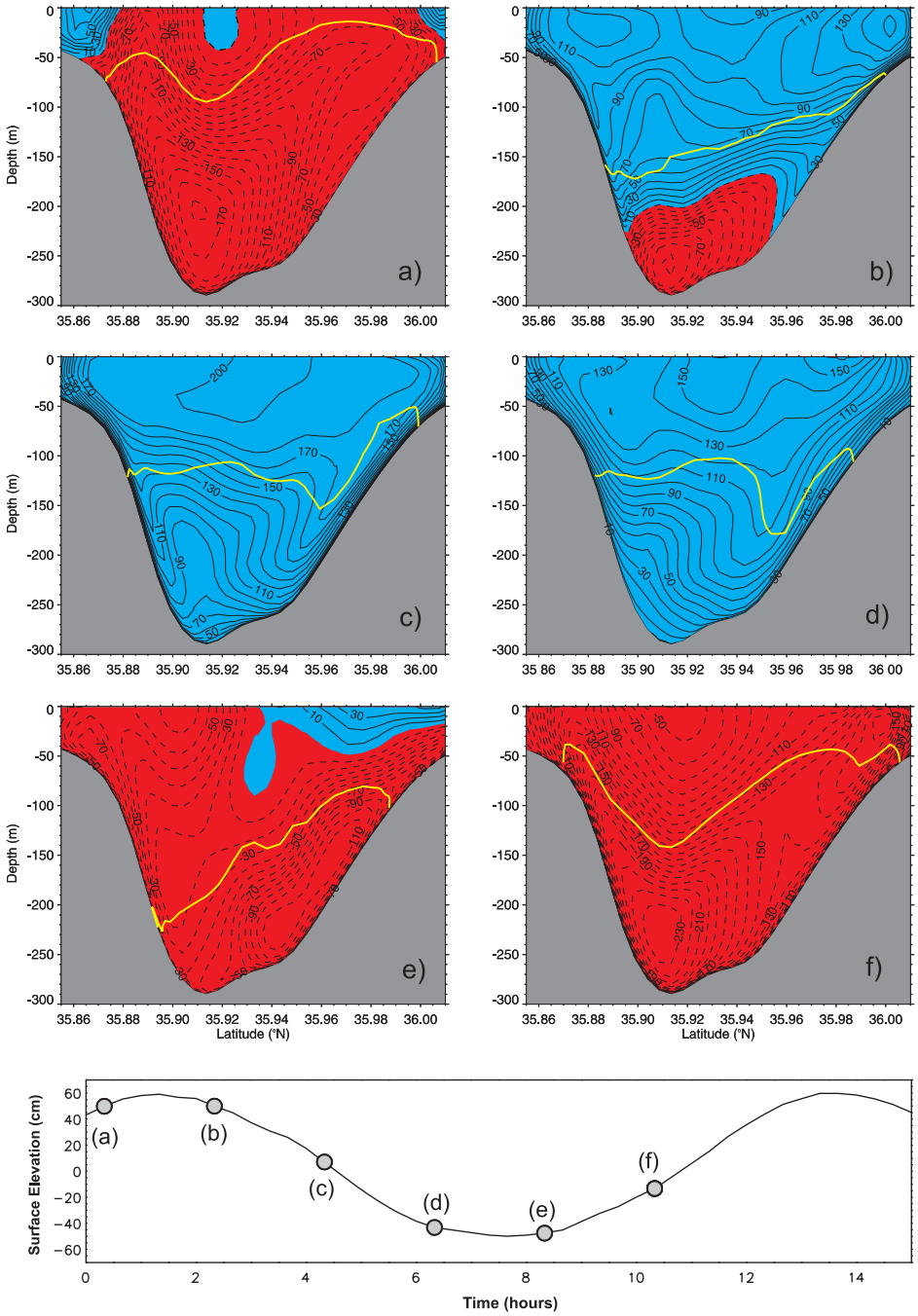

Figure 3.4: (a-f) Simulated sections of the along-strait current (cm s^{-1}) showing several phases of a semidiurnal (M_2 + S_2) tidal cycle during spring tide at the Camarinal Sill section (sec. B in Figure 2.4). The time difference between the single sections is 2 hours. The time moments are referred to the surface elevation at Tarifa (lower panel). Contour interval is 10 cm s^{-1}. Red and blue shadows highlight outflow and inflow currents respectively. Yellow line represents the depth of the 37.25 isohaline.

only a difference of 20 °, i.e. a difference of 40 minutes between the appearing of the maximum velocity in the upper layer and the appearing of the maximum velocity in the lower layer. This difference goes up to 60 ° (2^h) at the eastern entrance (Figure 3.5b), where the phase decreases from about 210 ° in the upper layer to 150 ° in the lower layer.

The S_2 tidal current amplitude also decreases of more than 70% from Camarinal Sill to the eastern entrance (Figures 3.8a and 3.7a respectively). At the eastern entrance the amplitude increases with depth, from the surface to about 250 m, of only 2 cm s^{-1}, remaining constant at 11 cm s $^{-1}$as far as the bottom on the southern side. S_2 tidal current phase (Figure 9b) decreases from 170 ° to 130 ° in the first 200 m and increasing up to 150 ° at about 350 m, remaining constant below 350 m to the bottom. At Camarinal Sill the S_2 tidal current amplitude increases from surface to 90 m of about 14 cm s $^{-1}$, with an increment that is not uniform along the cross section (maximum values of about 42 cm s $^{-1}$ are concentrated on the south and north sides), while below 150 m the amplitude decreases going toward the bottom. Phase (Figure 3.8b) is constant (150 °) from the surface to the bottom for nearly the whole section.

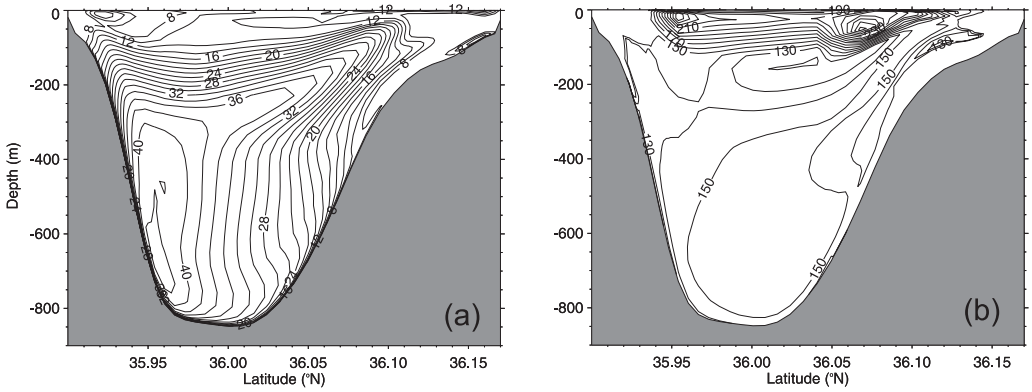

Figure 3.5: M_2 tidal constituent of the along-strait velocity at the eastern section (sec. D in Figure 2.4). (a) Amplitude in cm $^{-1}$, contour interval is 2.0 cm $^{-1}$. (b) Phase relative to the moon transit at Greenwich in degrees, contour interval is 10 °.

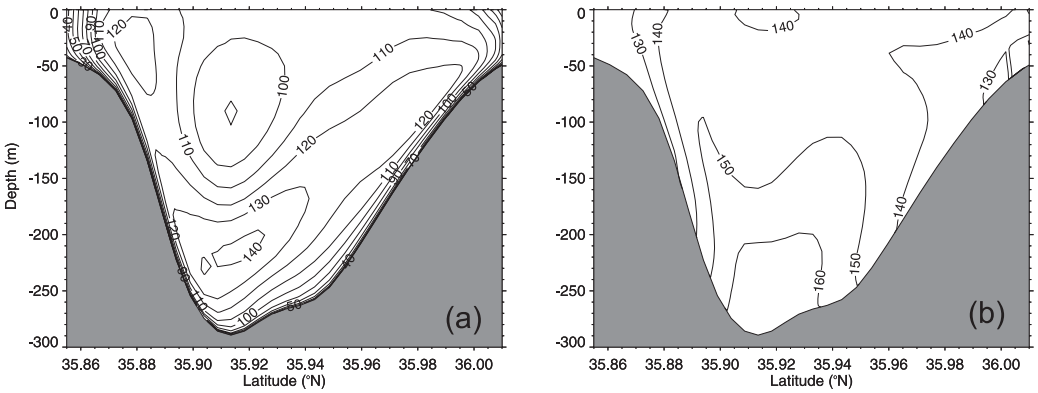

Figure 3.6: M_2 tidal constituent of the along-strait velocity at the Camarinal Sill section (sec. B in Figure 2.4). (a) Amplitude in cm $^{-1}$, contour interval is 2.0 cm $^{-1}$. (b) Phase relative to the moon transit at Greenwich in degrees, contour interval is 10 $^{\circ}$.

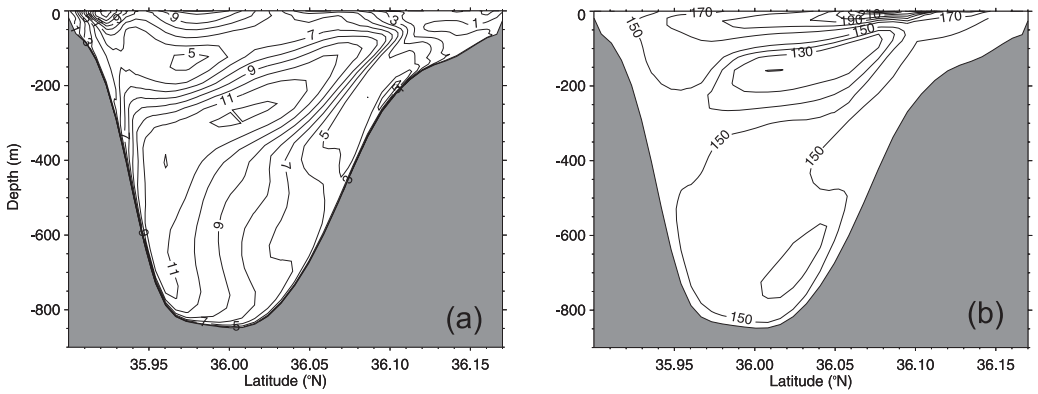

Figure 3.7: S_2 tidal constituent of the along-strait velocity at the eastern section (sec. D in Figure 2.4). (a) Amplitude in cm $^{-1}$, contour interval is 2.0 cm $^{-1}$. (b) Phase relative to the moon transit at Greenwich in degrees, contour interval is 10 $^{\circ}$.

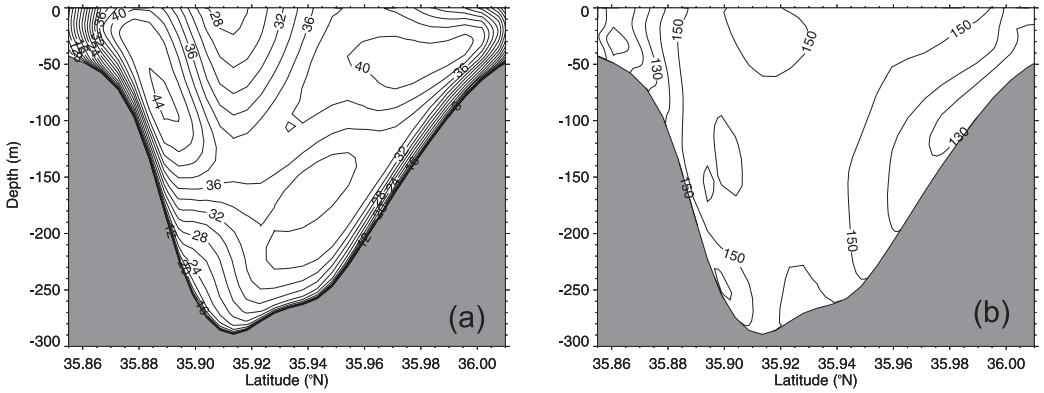

Figure 3.8: S_2 tidal constituent of the along-strait velocity at the Camarinal Sill section (sec. B in Figure 2.4). (a) Amplitude in cm $^{-1}$, contour interval is 2.0 cm $^{-1}$. (b) Phase relative to the moon transit at Greenwich in degrees, contour interval is 10 $^{\circ}$.

3.3 Internal Bore

One of the most important features of the dynamics in the Strait is the presence of internal bores which are generated over Camarinal Sill and propagate both eastward and westward (Armi & Farmer (1988)). In Figure 3.9 six sequential snapshots, representing a longitudinal salinity section during the spring tidal period, are shown. Here one can see that, in good agreement with the two-dimensional, two-layer, hydrostatic model of Izquierdo *et al.* (2001), the generation of the eastward propagating internal bore begins with the formation of an interfacial depression over the western edge of Camarinal Sill, approximately 1.5 hours before high tide at Tarifa, i.e. as soon as the westward barotropic forcing over Camarinal Sill starts weakening and the interface located upstream of Camarinal Sill is not sustained any more. Subsequently, about 30 minutes before high tide at Tarifa, the internal bore is released from Camarinal Sill and starts to travel eastward. The bore is released when the upper layer starts to move toward east while the lower layer continues to move westward. Its initial length scale, in the along-strait direction, is about 3 Km and its travel times from Camarinal Sill to Tarifa, Pta. Cires and Gibraltar sections are 2, 4 and 6 hours, respectively. It follows that, always in agreement with the two dimensional model of Izquierdo

et al. (2001), the speed of the bore is about 1.7 m s^{-1} between Camarinal Sill and Tarifa sections, 2.5 m s^{-1} between Tarifa and Pta. Cires sections, and 1.5 m s^{-1} between Pta. Cires and Gibraltar sections.

In agreement with Armi & Farmer (1988), a much weaker westward propagating internal bore is also released from Camarinal Sill, just 30 minutes before the eastward propagating bore reaches Gibraltar-Ceuta section, i.e. 40 minutes before the low tide at Tarifa.

The amplitude of the eastward propagating bore decreases progressively from about 100 m on the western edge of Camarinal Sill to about 50 m at the Gibraltar section. Initially the bore is characterized by two large and steep internal waves that during the eastward propagation seem to be subject to an amplitude dispersion. What actually happens is that the bore, during its eastward propagation, disintegrates into a train of internal solitary waves (Pierini (1989), Artale & Levi (1990), Artale *et al.* (1990), Brandt *et al.* (1996a)).

The model is not able to reproduce these internal solitary waves since nonhydrostatic effects are neglected and the horizontal model resolution is lower in the eastern part of the domain; however the final effect is the same, since the bore is in any case dispersed.

The model shows also that the bores are always released from Camarinal Sill in the course of the fortnight period, even during neap tides.

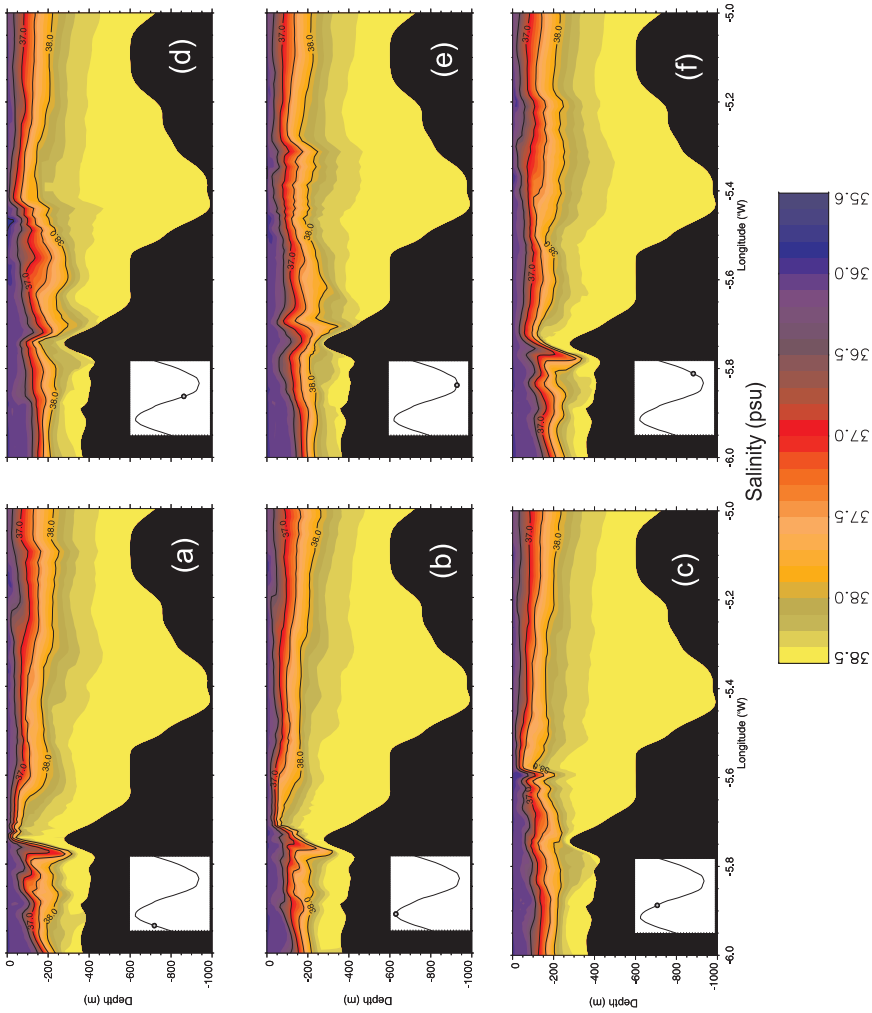

Figure 3.9: Evolution of salinity perturbations during a tidal period. Contours are shown with an interval of 0.5 psu. The snapshots are plotted at an interval of 2 h. The time moments are referred to the surface elevation at Tarifa (left-down panel).

Chapter 4

The two-layer approximation

4.1 Interface definition

The most intuitive definition of interface between the Atlantic and Mediterranean water, in the Strait of Gibraltar, is the one that considers the interface as the internal surface where velocity changes sign, in other words where the velocity reduces to zero. Applying this definition to the non-tidal experiment it has been possible to compute a volume exchange (Figure 4.1) characterized by an inflow (toward the Mediterranean) and an outflow (toward the Atlantic Ocean) of 0.62 and –0.51 Sv at the Camarinal Sill section (sec. B in Figure 2.4), and of 0.69 and –0.58 Sv at the Gibraltar-Ceuta section (sec. D in Figure 2.4). Transports were computed integrating the along-strait velocity first vertically, from the bottom up to the depth where the along-strait reverts its direction for the outflow, and from this depth up to the surface for the inflow, and then meridionally, from the south to north side of the strait:

$$IN(x) = \int_{y=south}^{y=north} \int_{z=h(x,y)}^{z=0} u(x,y,z)dzdy \tag{4.1}$$

$$OUT(x) = \int_{y=south}^{y=north} \int_{z=bottom}^{z=h(x,y)} u(x,y,z)dzdy, \tag{4.2}$$

where u is the along strait velocity, h is the depth of the interface, and x is the longitude.

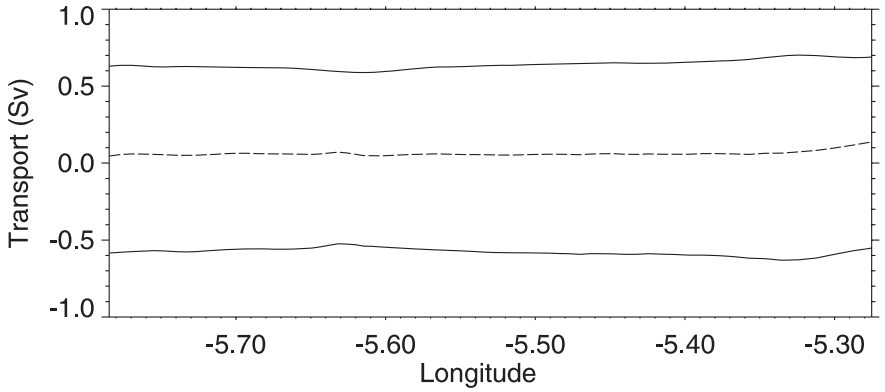

Figure 4.1: Variation of the eastward (positive values) and westward (negative values) transports along the strait computed for the cases without tidal forcing for the two-layer case.

It appears clear that this simple and intuitive method of computation of inflow and outflow volume transport, is strictly related to the existence of an internal surface of zero along strait velocity. For this reason this method cannot be used to determine the volume transport when tidal forcing is included, since, as described in Section 3.2, the semidiurnal tidal signal is so strong to reverse the inflow or the outflow during part of each tidal cycle, obscuring the two-layer character of the mean flow.

Another way of defining the interface between upper and lower layer is by using an isohaline. For example, Bryden *et al.* (1994) and Candela *et al.* (1989) used respectively the 37.0 and 37.5 isohaline to define the exchange interface over Camarinal Sill, while Baschek *et al.* (2001) used the 38.1 isohaline at the eastern entrance of the strait. The choice of different values for the separating isohaline has to be ascribed, as it will be discussed in the next Chapter, to the strong entrainment developing along the strait.

Thus, it emerges that it is incorrect to use a single isohaline as an interface for the whole strait. For this reason, an alternative definition is used in this Thesis. Here, the interface is defined as the fortnightly averaged salinity surface corresponding with the internal surface where the fortnightly averaged along-strait velocity is zero (Sannino *et al.* (2004)). The resulting internal salinity surface obtained in this way is shown in Figure 4.2a. Here it is possible to note

that the salinity interface changes from ∼37.25 psu at Camarinal Sill up to ∼38.1 at the eastern entrance of the strait, in good agreement with value used by Bryden *et al.* (1994), Candela *et al.* (1989) and Baschek *et al.* (2001).

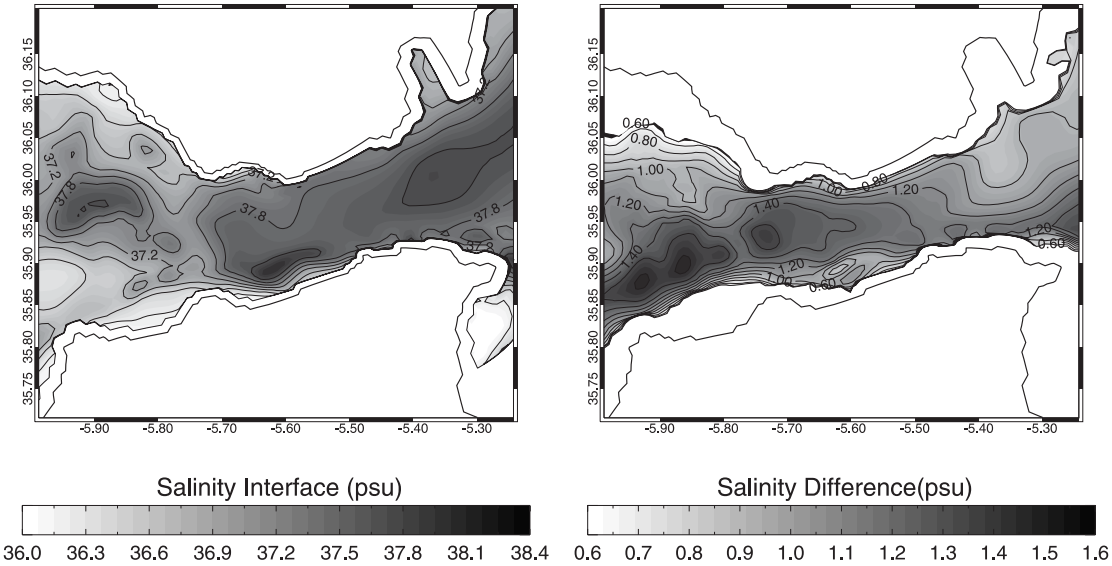

Figure 4.2: Internal surface salinity interface between the Atlantic and Mediterranean waters and time-averaged salinity difference between upper-layer and lower-layer for the two-layer case.

4.2 Transports

The salinity interface defined in the previous section can be used to find the time dependent depth of the internal surface interface between the two layers. Thus, it is possible to compute the instantaneous upper (ULT) and lower layer transport (LLT) in the whole strait by using the following equations:

$$ULT(x,t) = \int_{z=south}^{z=north} \int_{z=h(x,y,t)}^{z=0} u(x,y,z,t)dzdy \tag{4.3}$$

$$LLT(x,t) = \int_{z=south}^{z=north} \int_{z=bottom}^{z=0} h(x,y,t)dzdy, \tag{4.4}$$

where u is the along-strait velocity and h is the time dependent depth of the interface.

In Figure 4.3, the computed upper and lower layer transports are shown for a complete fortnight cycle at three different cross-strait sections: over Camarinal Sill, Tarifa, and at the eastern entrance of the strait. In agreement with Candela *et al.* (1990), the largest amplitude of the instantaneous transport occurs in the upper layer at the sill, and in the lower layer at the eastern section. The behaviour of tidal currents noted in Section 3.2 is apparent in the transports: it is clear that the upper currents have decreasing amplitudes going eastward and reverse their directions only as far as Tarifa, while the lower currents increase eastward and reverse their direction everywhere in the strait.

Figure 4.4 show the mean along strait transports, obtained averaging over the fortnight period the ULT and LLT. From west to east the upper layer transport ranges from 0.68 Sv to 0.9 Sv, while lower layer transport ranges between –0.5 Sv to –0.75 Sv. At Camarinal Sill the transports are 0.85 Sv and –0.70 Sv for the upper and lower layer respectively, while at the east entrance they are 0.9 Sv and –0.75 Sv.

At Camarinal Sill the most accurate estimates of transports from direct measurements are the ones given by Bryden *et al.* (1994) and, more recently, by Tsimplis & Bryden (2000). In their computation they considered the vertical movement of the interface and determined the transport of the upper layer to be 0.72±0.16 Sv and 0.78 Sv respectively, and the transport of the lower layer to be –0.68±0.15 Sv and –0.67 Sv respectively. At the eastern entrance of the strait the last most accurate estimates of transports are from Baschek *et al.* (2001). They calculated the transports using an inverse model to predict for every instant the depth of the isohaline 38.1 obtaining an upper layer transport of 0.81±0.07 Sv and a lower layer transport of –0.76±0.07 Sv. Results of the present study are in reasonable agreement with all these transport estimates since they lie within the error bars.

Comparing these transports with the transports computed for the experiment without tidal forcing (equation 4.1) it emerges that the tidal forcing increases transport, both in the upper and in the lower layer. It is also interesting to note that the increment is different between upper and lower layer; in particular, at

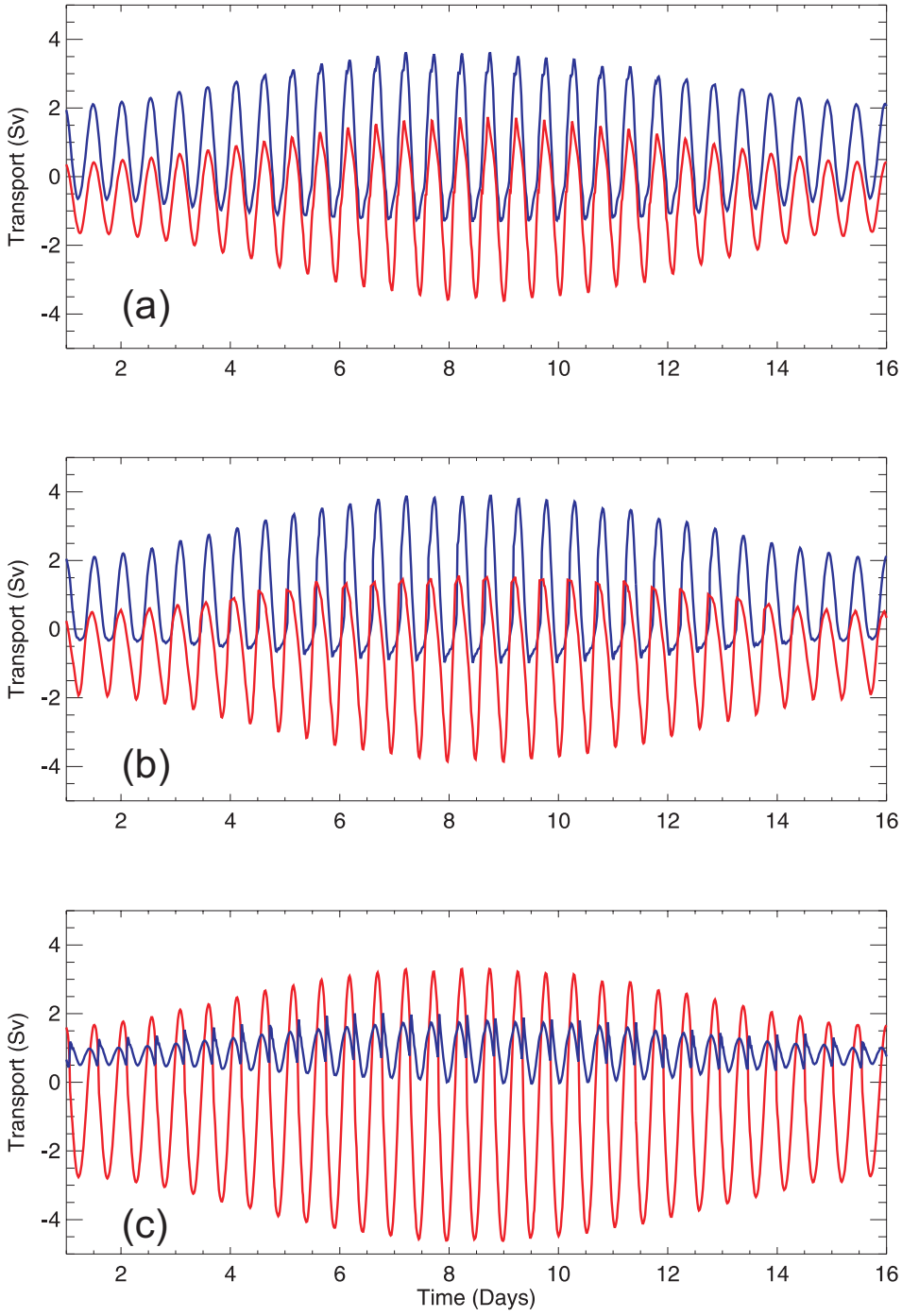

Figure 4.3: Sixteen days of computed upper (blue) and lower (red) layer transport at three different cross-strait section: over Camarinal sill (a), at Tarifa (b) and at the eastern entrance of the strait (c), for the two-layer case. Sections (a), (b) and (c) are marked as: B, C and D in Figure 2.4.

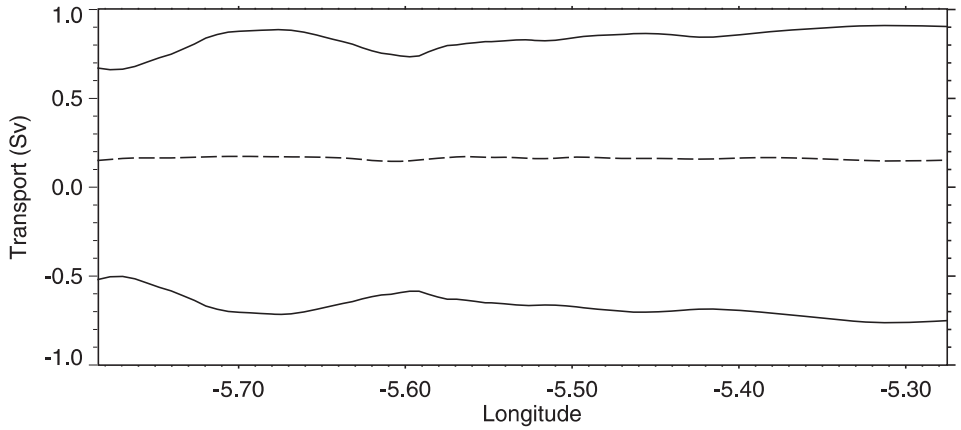

Figure 4.4: Variation of the eastward (positive values) and westward (negative values) transports along the strait computed for the cases with tidal forcing for the two-layer case.

Camarinal Sill is 37% for the upper layer and 34% for the lower layer, while at the eastern entrance the increment is 28% and 29% for the upper and lower layer respectively.

4.3 Hydraulic Control

As already presented in the introduction, for a two-layer flow the hydraulic control occurs when:

$$G^2 \equiv F_1^2 + F_2^2 = 1, \tag{4.5}$$

with

$$F_i^2 = \frac{u_i^2}{g' h_i}, \tag{4.6}$$

where G^2 is the composite Froude number, F_i^2 represents the internal Froude number for the i-th layer with $i = 1, 2$ (1 for the upper layer and 2 for the lower layer), whose velocity and thickness are u_i and h_i respectively, $g' = g(\rho_2 - \rho_1)/\rho_2$ is the reduced gravity, and ρ_i is the layer density.

In order to identify regions where the flow is hydraulically controlled in the two-layer approximation, the instantaneous internal Froude numbers for the upper and lower layer, as well as the composite Froude number is evaluated. In

particular layer velocities and densities, necessary to compute the internal Froude numbers, are computed by averaging the along-strait velocity and density from the surface to the internal interface depth for the upper layer, and from the interface depth down to the bottom for the lower layer. The resulting maps, showing the frequency of occurrence, over the fortnight period, of supercritical Froude numbers for the upper layer ($F_1^2 \geqslant 1$), for the lower layer ($F_2^2 \geqslant 1$) and the composite Froude number ($G^2 \geqslant 1$) are shown in Figure 4.5. Looking at G^2 the flow is supercritical over Camarinal Sill and along the north and south coast both west and east of the Sill; in particular both internal Froude numbers contribute to reach the supercritical regime in those regions. The flow is supercritical also on the northern boundary of Tangier basin, but in this case it is only the Froude number of the lower layer that contributes to the criticality. None of the previously described supercritical regions is permanent, in fact the maximum frequency of about 70% is reached only on the northern and southern side of Camarinal Sill. The above described supercritical composite Froude number pattern is in good agreement with that computed by Izquierdo *et al.* (2001) and Brandt *et al.* (2004) by means of a two dimensional two-layer model.

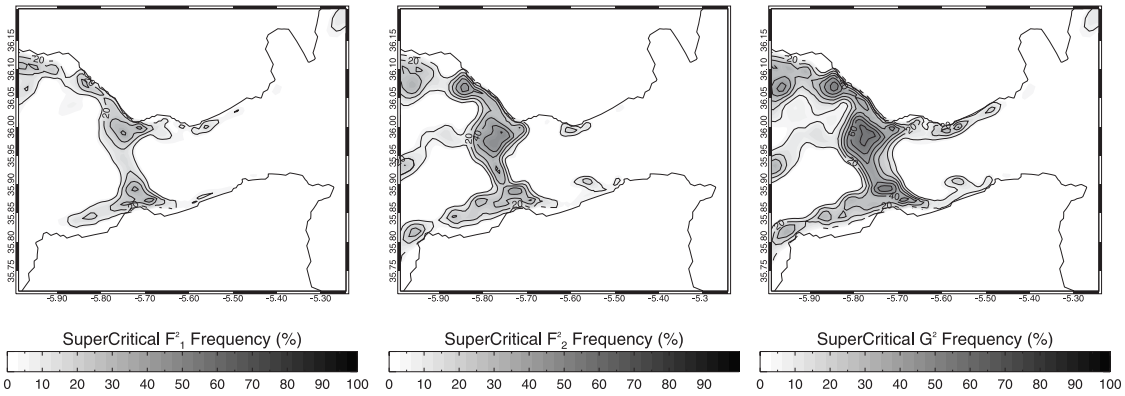

Figure 4.5: Maps of the frequency of occurrence of supercritical internal Froude numbers for the (a) upper-layer, (b) lower-layer and (c) Composite Froude number for the two-layer case.

Over Camarinal Sill the control is achieved two times for each semidiurnal period: the flow is controlled during the rising water at Tarifa then the control is lost

and recovered again during the subsequent descending tidal phase (Figure 4.6).

It is interesting to note the complete absence of a supercritical region extending over any entire cross-section within Tarifa Narrow for the two-layer case. This is the clear indication that, in this case, the exchange regime through the strait is always predicted to be submaximal.

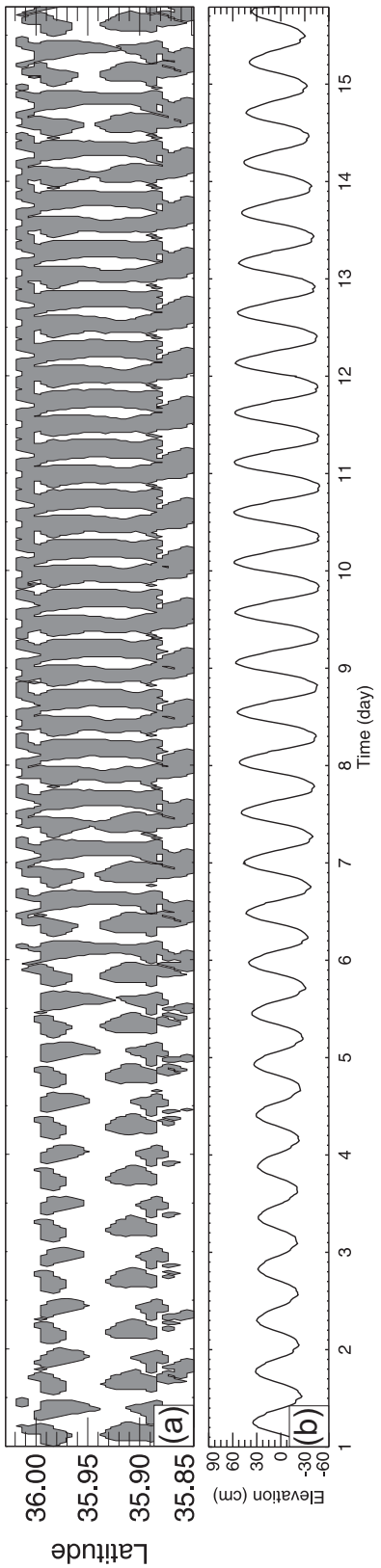

Figure 4.6: (a) Variation of the supercritical region over a fortnight period in the cross-strait direction at Camarinal Sill for the two-layer case, regions where the flow is supercritical are shaded. (b) Tidal elevation at Tarifa.

Chapter 5

The three-layer approximation

5.1 Interfacial layer definition and characteristics

As suggested by Bray *et al.* (1995), we use the upper and lower limit of the halocline to define the interfacial layer. However a different quantitative method for dividing all salinity profiles into Atlantic layer, interfacial layer, and Mediterranean layer has been used. In this work salinity profiles are fitted with an hyperbolic tangent. The upper and lower bounds of the interfacial layer are identified as the intersections of the tangent at the flex of the hyperbolic tangent with two vertical lines passing respectively through the simulated salinity at surface and at the deepest salinity (defined as the arithmetic mean between the deepest simulated salinity, and the deepest fitted salinity). In order to quantitatively measure the fit quality of all salinity profiles, the amount of variance that is explained by the hyperbolic tangent fitting was computed as:

$$fq \equiv \left(1 - \frac{\sum_k \left(S_k - \hat{S}_k \right)^2}{\sum_k \left(S_k - \bar{S}_k \right)^2} \right) \times 100 \tag{5.1}$$

where k represents the model vertical levels, S_k is the simulated salinity, $\hat{S}_k$ is the fitted salinity and $\bar{S}$ is the arithmetic mean of the profiles. Only salinity profiles with a fit quality $> 98\%$ are retained; that however represent more than

80% of the available salinity profiles (about 3000). The mean fit quality value obtained averaging over the entire set of retained salinity profiles is about 99.5%. As example, four different salinity profiles, and the respective fitted curves are shown in Figure 5.1.

Figure 5.2 shows the time-averaged thickness of the three layers together with the depth of the midpoint of the interfacial layer. The thickness of the Atlantic layer is characterized by a positive north-south gradient, more intense in the region to the west of Camarinal Sill, where the thickness ranges from 30 m up to 120 m. Along Tarifa Narrow the thickness presents a value of about 40 m, decreasing to 20 m at the eastern end of the strait. It is evident that the Atlantic layer is strongly influenced by Camarinal Sill, in fact the thickness almost halves its value crossing the sill. In accordance with the bathymetric gradient, the thickness of the Mediterranean layer is characterized by a negative along-strait gradient going from the eastern end of the strait towards Camarinal Sill, with a decrease of the thickness along Tarifa Narrow from 800 m to about 80 m. On the western side of the strait, instead, the Mediterranean layer is very shallow with a thickness of about 100 m along the Tangier basin. The interfacial layer thickness has a relative minimum of about 120 m over Camarinal Sill and a maximum of 180 m just west of it along Tangier Basin; a north-south gradient is evident both to the west and to the east of the sill. This pattern is reflected in the depth of the midpoint of the interfacial layer which presents a north-south gradient throughout the entire strait that is more intense east of Camarinal Sill. Here the values range from about 180 m in Tangier Basin to 40 m on the north coast, while in Tarifa Narrow the values range from about 120 m on the south to 40 m on the north.

Comparison with the results of Bray *et al.* (1995) shows a general agreement for the midpoint depth of the interfacial layer, while differences are evident both in the magnitude and pattern of the interfacial layer thickness. Bray *et al.* (1995) shows a thickness that is everywhere lower than the simulated one, with an along-strait gradient to the east of Camarinal Sill that is not present in our simulation, and lower values on the western side of Camarinal Sill, along the Tangier Basin. These discrepancies can be mainly attributed to the fact that the analysis of Bray *et al.* (1995) does not take tidal variability into account explicitly, while in this

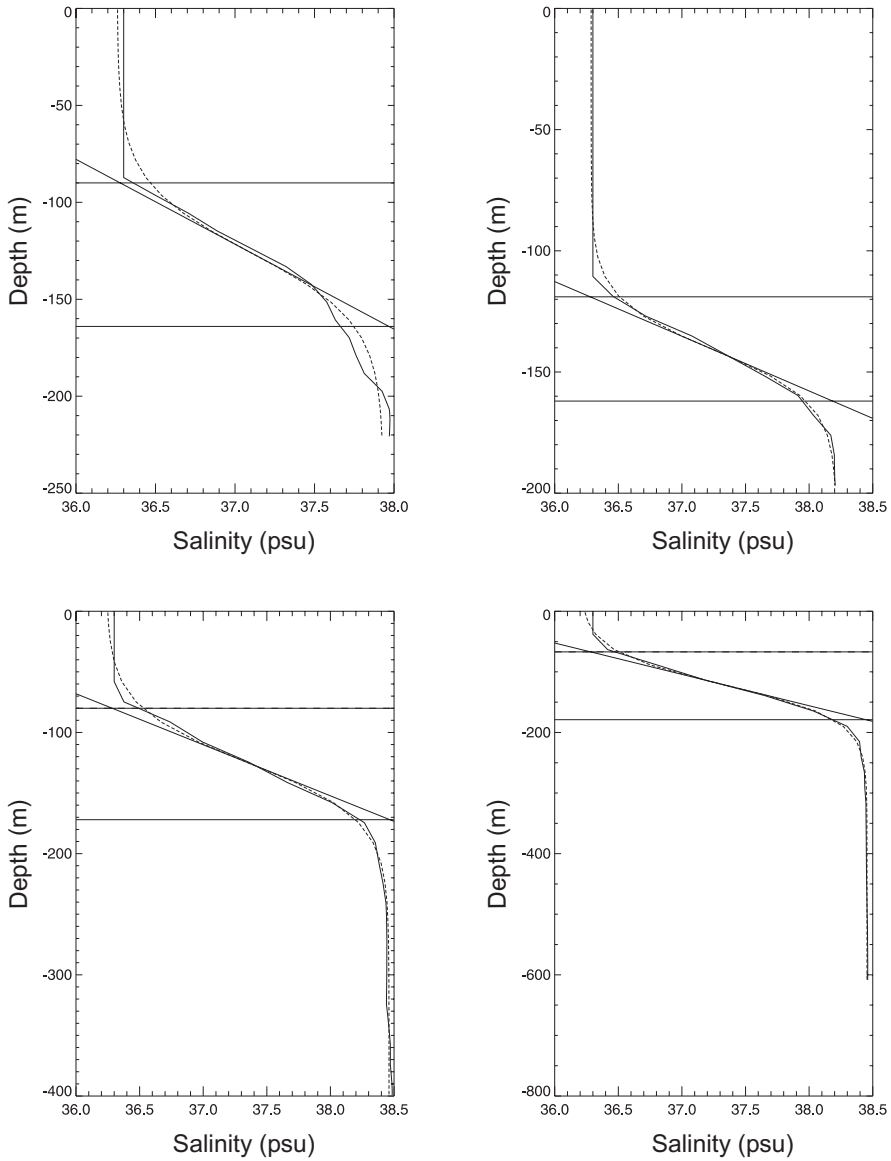

Figure 5.1: Comparison of the simulated (solid lines) with fitted (dashed lines) salinity profiles. The tangent to the flex of the hyperbolic tangent and the two horizontal lines indicating the upper and lower bound of the interfacial layer are also plotted.

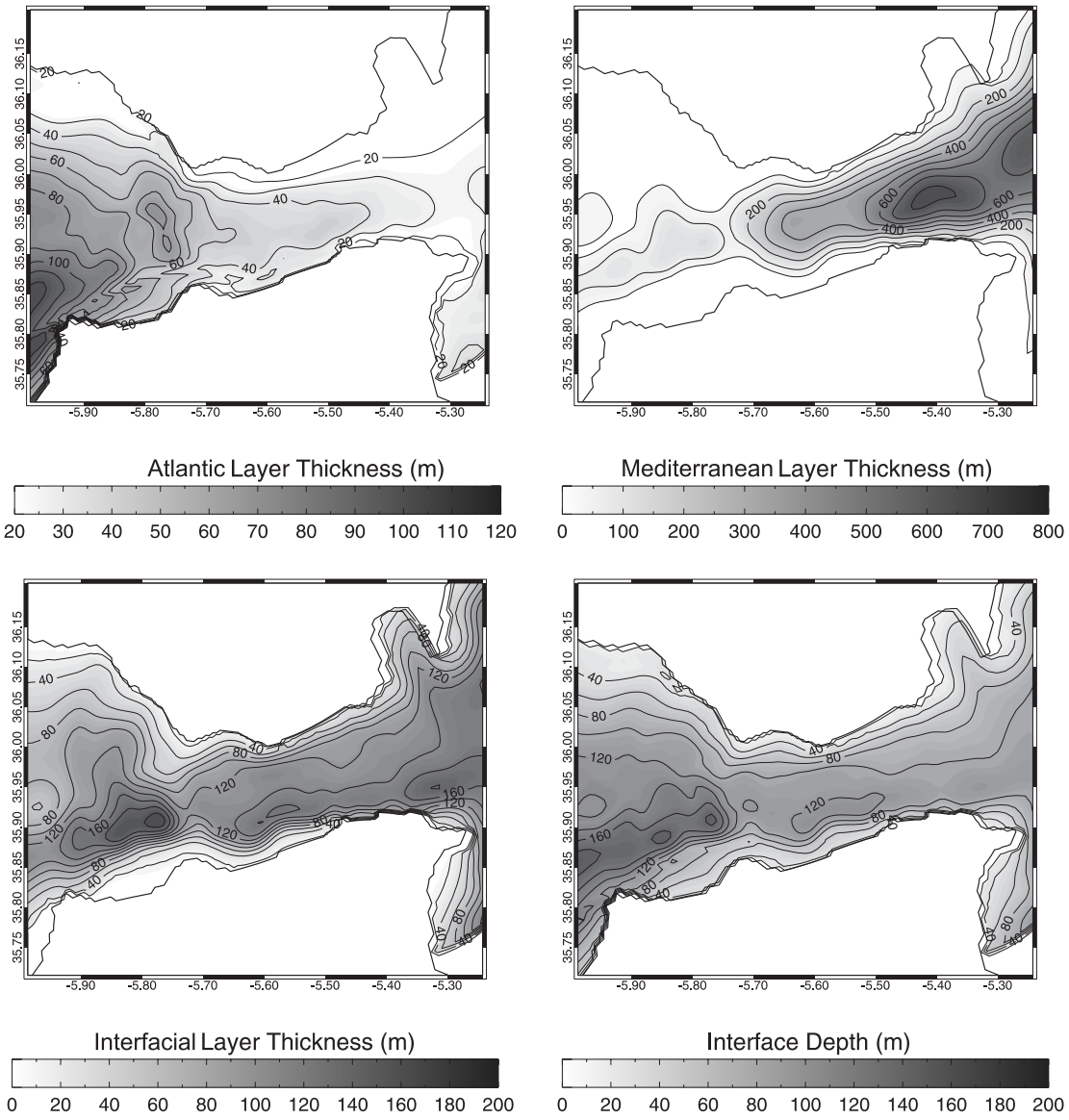

Figure 5.2: Time-averaged Atlantic-layer, interfacial-layer and Mediterranean-layer thickness, and depth of the midpoint of the interfacial layer as simulated by the numerical model.

Thesis simulated data from an entire fortnight tidal cycle are used, and secondly to the fact that here it is used a different method to define the upper and lower bounds of the interfacial layer.

That tidal forcing strongly affects the interfacial layer thickness may be clearly observed comparing Figure 5.2 and Figure 5.3a where the interfacial layer thickness, computed for the non-tidal experiment, is plotted. It appears evident that for the tidal experiment a general increase in thickness of about 50 m is present throughout all the strait. On the contrary no differences are present in the midpoint depth of the interfacial layer for the non-tidal (Figure 5.3b) and tidal experiments.

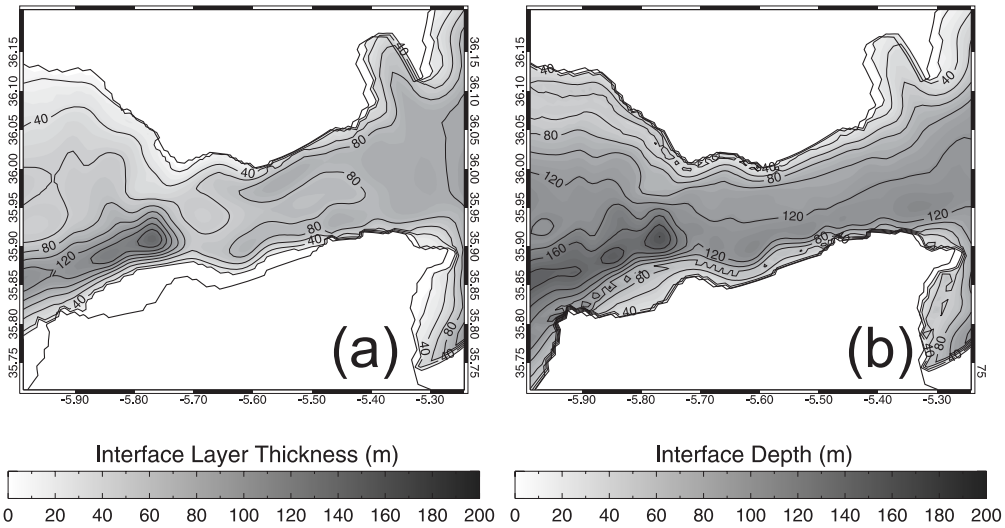

Figure 5.3: (a) Interfacial-layer thickness, (b) and depth of the midpoint of the interfacial layer as simulated by the numerical model for the non-tidal simulation.

Temporal variation of the interfacial layer thickness for the main experiment may be observed in Figure 5.4, where the interfacial layer thickness is plotted as a function of longitude and time. Values are referred to section E (see Figure 2) and cover an entire day during neap tide (Figure 5.4a) and during spring tide (Figure 5.4b). Figure 5.4b shows that the maximum variability is confined in Tarifa Narrow, where a maximum of about 200 m starting from Camarinal Sill, propagates towards east, in accordance with the eastward propagating bore.

On the contrary, on the western side of the strait the interfacial layer thickness remains almost constant. It is noteworthy that during neap tide (Figure 5.4a), while the thickness on the western side of the strait is almost equal to that obtained for spring tide, the interfacial layer thickness variability in Tarifa Narrow is clearly reduced and maximum values does not exceed 150 m.

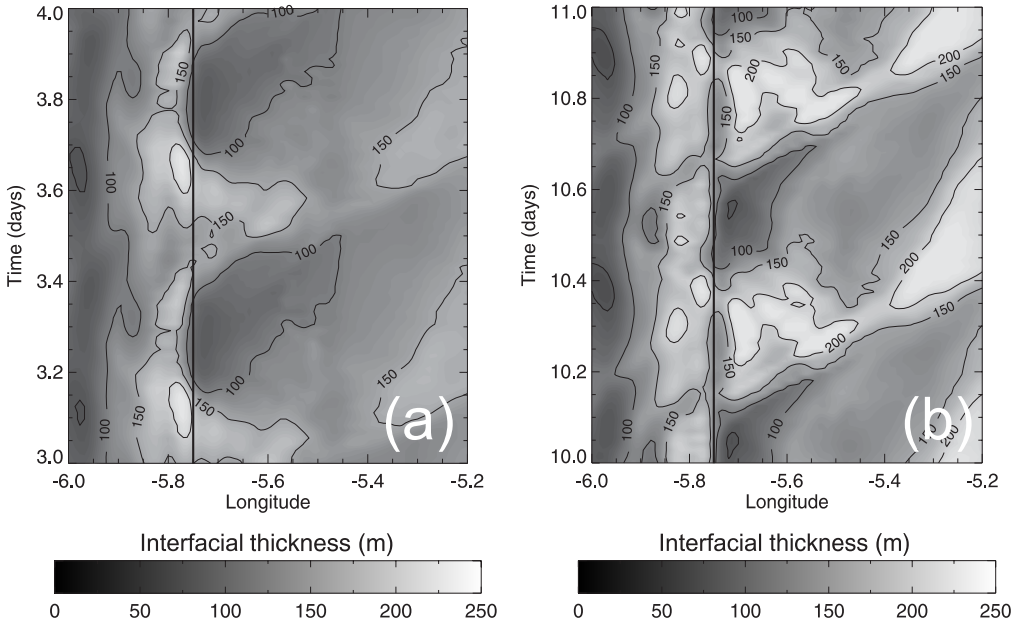

Figure 5.4: Frequency of occurrence of supercritical first mode, second mode, and simultaneous first and second internal modes over the fortnight period.

The time-averaged salinity of the three layers together with the time-averaged salinity difference between Atlantic layer and Mediterranean layer are shown in Figure 5.5. In the Atlantic layer the salinity slowly increases from 36.3 at the western end of the strait up to 36.4 at the eastern end of the strait. This is an indication of entrainment of saltier water coming from the underlying Mediterranean water. Conversely in the Mediterranean layer salinity decreases from the eastern end of the strait toward the western end indicating in this case entrainment from the above Atlantic water. The time-averaged salinity of the interfacial layer is characterized by values between 37.3 and 37.4 along the strait, with a minimum of less than 37.2 at Camarinal Sill. Moreover, the time-averaged salinity difference between Atlantic layer and Mediterranean layer is found to have

an almost constant value between 1.9 and 2.0 throughout the strait, except over Camarinal Sill where a local minimum of about 1.8 is reached. This is the clear indication that the time-averaged mixing in that region is stronger than in the other regions of the strait in agreement with Wesson & Gregg (1994).

Finally, the time averaged along-strait Atlantic layer, interfacial layer and Mediterranean layer velocities are depicted in Figure 5.6. The Atlantic layer velocity is always positive, with an absolute maximum of about 1 m s^{-1}, reached in the eastern part of the strait, and a relative maximum, higher than 0.5 m s^{-1}, just west of Camarinal Sill. The Mediterranean layer only shows negative values with the largest velocities of about 1.0 m s^{-1} along the Tangier Basin, just to the west of Camarinal Sill. It is interesting to note that only the interfacial layer is characterized by both positive and negative velocities, that can reach 0.5 m s^{-1}. The velocity pattern is divided in two parts by Camarinal Sill: a western side where velocities are toward west and an eastern part where they are everywhere directed toward east.

5.2 Transports

The instantaneous Atlantic layer transport (ALT), interfacial layer transport (ILT) and Mediterranean layer transport (MLT) for each model cross-section within the strait, have been computed by using the following equations:

$$ALT(x,t) = \int_{z=south}^{z=north} \int_{z=H_U(x,y,t)}^{z=0} u(x,y,z,t)dzdy \tag{5.2}$$

$$ILT(x,t) = \int_{z=south}^{z=north} \int_{z=H_L(x,y,t)}^{z=H_U(x,y,t)} u(x,y,z,t)dzdy \tag{5.3}$$

$$MLT(x,t) = \int_{z=south}^{z=north} \int_{z=0}^{z=H_L(x,y,t)} u(x,y,z,t)dzdy, \tag{5.4}$$

where u is the along-strait velocity component, and H_U, H_L represent the instantaneous depths of the upper and lower bounds of the interfacial layer respectively. The resulting transports, over the fortnight period, are shown in Figure 5.7, for three different cross-strait sections located at Gibraltar, Tarifa and

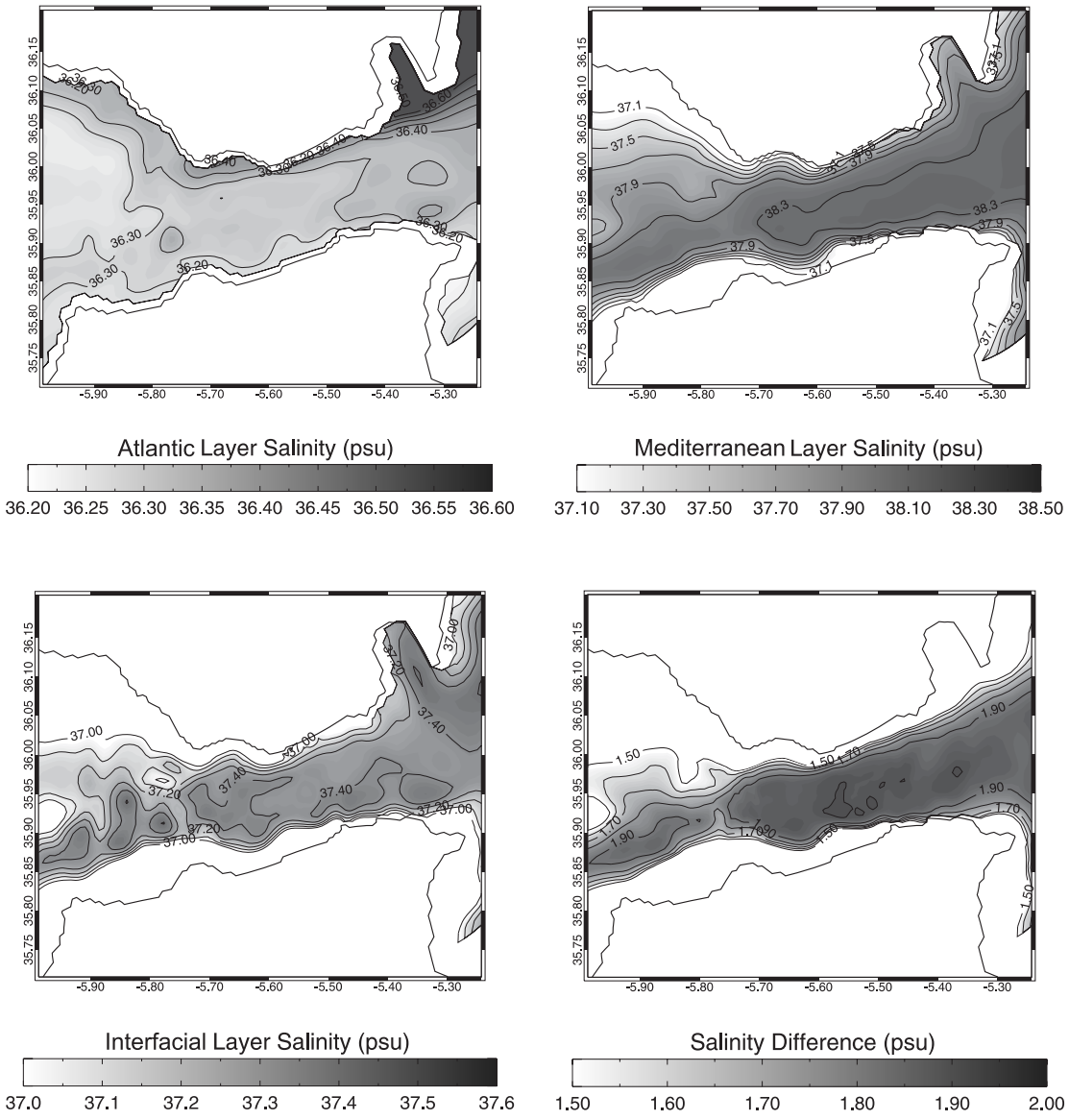

Figure 5.5: Time-averaged Atlantic-layer salinity, Mediterranean-layer salinity, interfacial-layer salinity and difference between the time-averaged salinity of the Mediterranean-layer and the time-averaged salinity of the Atlantic-layer.

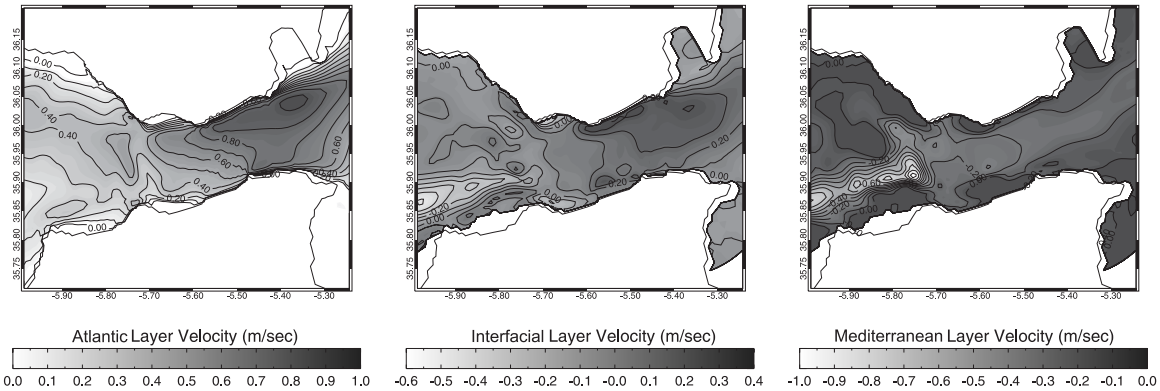

Figure 5.6: Time-averaged Atlantic-layer, interfacial-layer and Mediterranean-layer velocity as simulated by the numerical model.

Camarinal Sill. It is interesting to note that ILT reaches values comparable both with ALT and MLT, contributing to transport mixed Atlantic-Mediterranean water alternatively in both directions. Moreover, the interfacial layer transport exhibits a large along-strait variability, since its range increases, during spring tide, from about 1.5 Sv at Gibraltar to 4 Sv at Camarinal. The Atlantic layer carries water principally toward east, with a small fraction of the transport cyclically directed in the opposite direction. On the contrary, the MLT is directed toward west at Camarinal Sill while at Tarifa and Gibraltar it represents the principal contribution both westward and eastward.

The time-averaged along-strait transports for the three layers exhibit other interesting features (Figure 5.8). A substantial fraction of the total transport occurs in the interfacial layer, in particular in the eastern part of the strait the transport in the interfacial layer is 0.2 Sv higher than that in the Atlantic layer, and contributes to carry water toward east. At the western end, the time-averaged transport in the interfacial layer is directed toward west contributing only for about 0.1 Sv. The transition occurs at the sill, where the net interfacial layer transport reduces to zero, reflecting the velocity behaviour (Figure 5.6). Within the Atlantic layer, the eastward transport monotonically decreases toward the east end of the strait, almost halving its initial value of 0.65 Sv. The MLT is

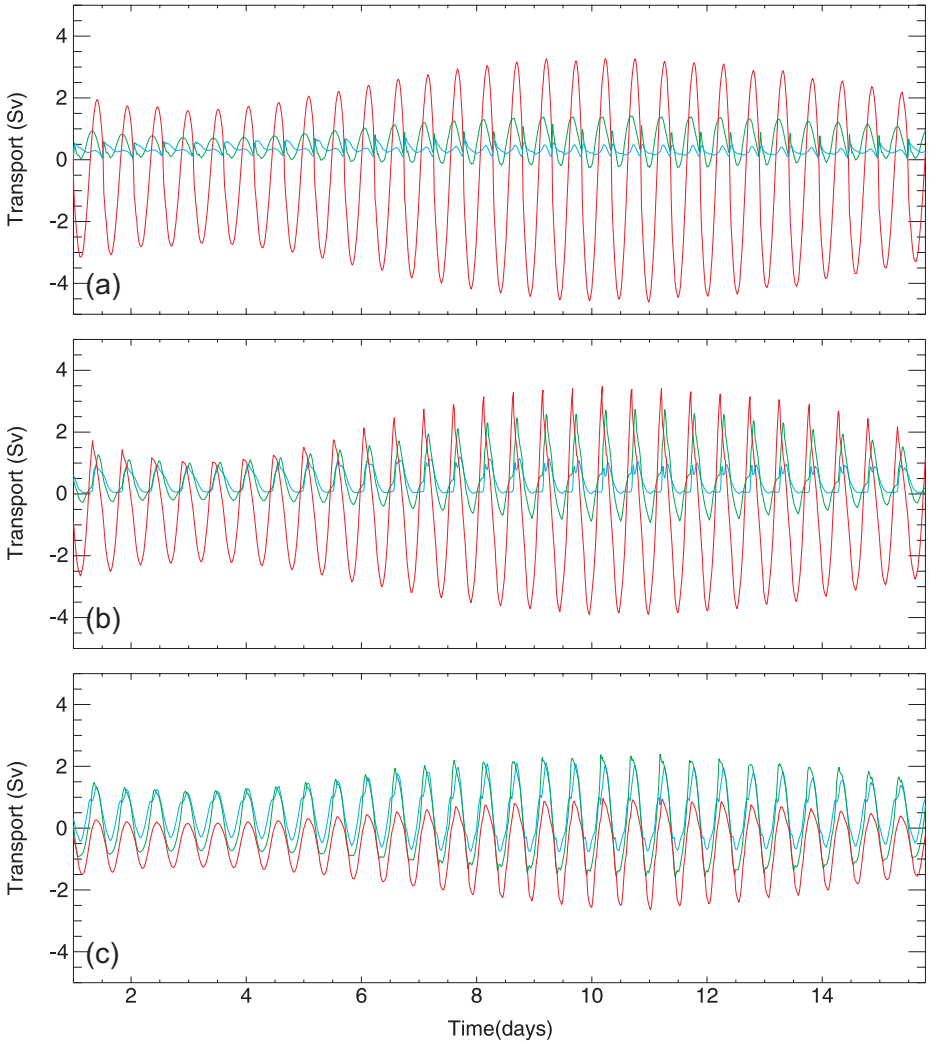

Figure 5.7: Time dependent Atlantic-layer (blue line), interfacial-layer (green line), and Mediterranean-layer (red line) transports at (a) Gibraltar, (b) Tarifa and (c) Camarinal Sill computed for the three-layer case.

always directed toward west, loosing about 30% of its initial value of 0.75 Sv going from the eastern to the western end of the strait; in this case the transport undergoes a sudden decrease in the sill region, coincident with the sudden increase of the interfacial layer transport. The general behaviour of the transport in the three layers is comparable with that shown in the analogous figure by Bray *et al.* (1995), even if the magnitudes are slightly less.

In order to estimate the along-strait time-averaged two-way transports the algebraic sum of the three instantaneous transports has been evaluated (Figure 5.9). The eastward transport decreases from 0.62 Sv at the western end of the strait to its minimum of 0.52 Sv near Camarinal Sill, and then increases, reaching a value of 0.8 Sv at Tarifa, that remains practically constant till the eastern end of the strait. The westward transport shows the same behaviour but with slightly smaller values, determining a constant net eastward transport of about 0.1 Sv throughout the strait. This net transport is equivalent to an excess of evaporation, averaged over the entire Mediterranean Sea, of about 0.69 m yr-1. This value is in good agreement with the experimental estimates of 0.55 m yr-1 and 1 m yr-1 by Bryden & Kinder (1991) and Bethoux (1979) respectively.

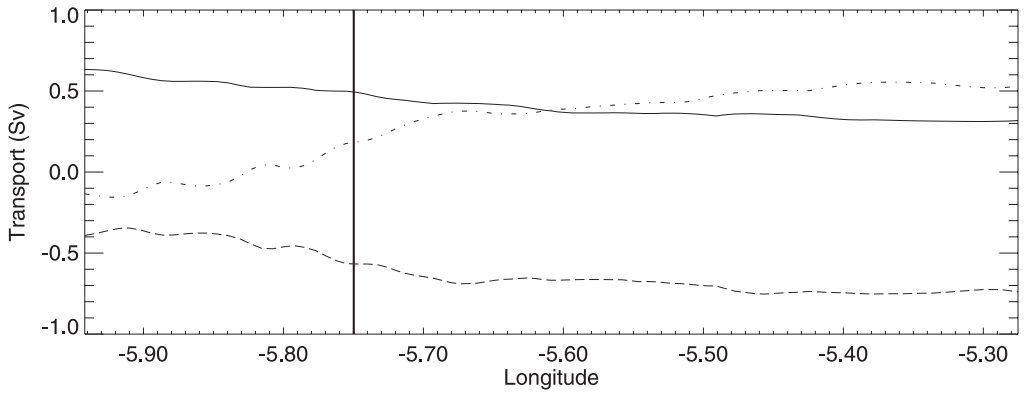

Figure 5.8: Along-strait time-averaged Atlantic-layer (solid line), interfacial-layer (dashed-dotted line), Mediterranean-layer (dashed line) transports. The location of Camarinal Sill is marked by the vertical solid line.

In Figure 5.8, it has been shown that the time-averaged transport in the interfacial layer increases from the Atlantic to the Mediterranean Sea. This large

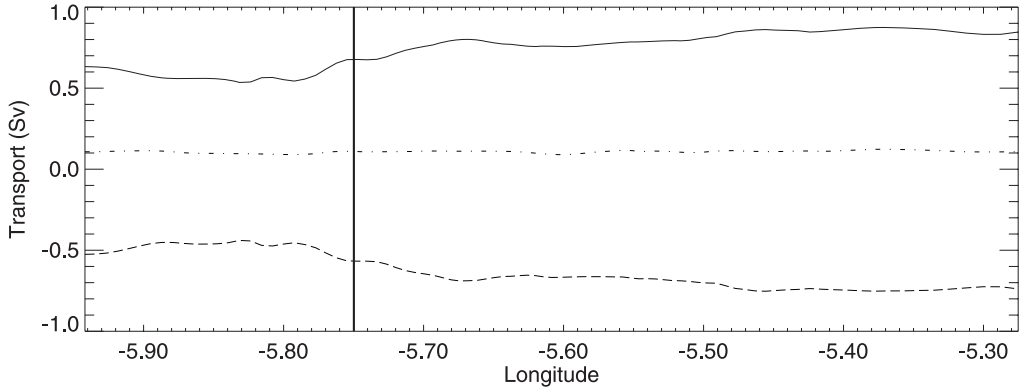

Figure 5.9: Along-strait time-averaged eastward (solid line), westward (dashed line), and net (dashed-dotted line) transports computed for the three-layer case. The location of Camarinal Sill is marked by the vertical solid line.

variation in the horizontal transport can be interpreted in terms of vertical exchanges between layers. Temporal variations of the along-strait vertical exchange between Atlantic layer and interfacial layer, and between interfacial layer and Mediterranean layer, during spring tide, are shown in Figure 5.10 (note that negative values represent downward fluxes while positive values represent upward fluxes). These fluxes have been computed as the instantaneous differences of the horizontal transports between two adjacent model cross-sections. The vertical exchange between Atlantic layer and interfacial layer shows two distinct behaviours east and west of Camarinal Sill. From the Sill to the western end of the strait the exchange oscillates regularly between positive and negative values reaching 0.15 and -0.25 Sv respectively; on the contrary, to the east of Camarinal Sill is present a downward flux propagating toward east within Tarifa Narrow, in accordance with the internal eastward propagating bore. At the eastern end of the strait the downward flux reaches 0.45 Sv, while the upward flux reduces to 0.05 Sv. The vertical exchange between the interfacial layer and the Mediterranean layer exhibits a similar behaviour, with generally higher values of the upward and downward fluxes (the upward flux reaches values up to 0.7 Sv at the eastern end of the strait). The instantaneous unbalance of the magnitude of the vertical exchange between the interfacial layer and the two other layers can be used to explain the time variability of the interfacial thickness shown in Figure 5.4b,

where it has been observed a maximum of about 200 m generated over Camarinal Sill and propagating toward east. The previous vertical exchange description is also valid during neap tide, but in this case the vertical exchanges are reduced by almost a factor of two.

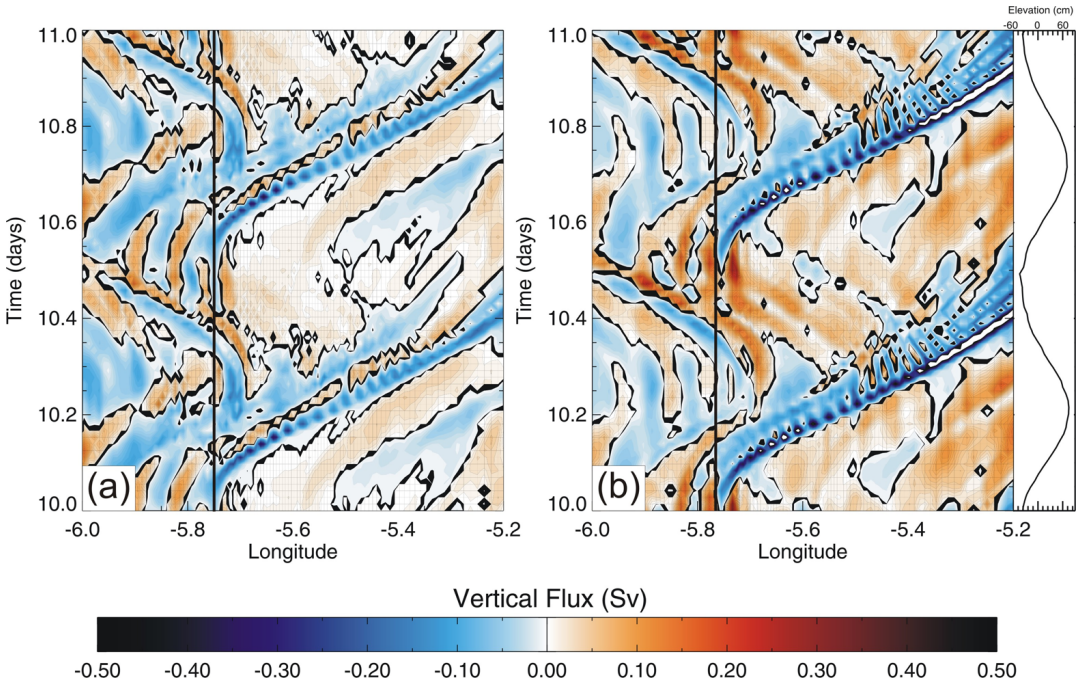

Figure 5.10: Exchange between (a) Atlantic-layer and interfacial-layer and between (b) interfacial-layer and Mediterranean-layer as a function of longitude and time during an entire day corresponding to spring tide (day 10). Negative values represent downward fluxes while positive values represent upward fluxes. Simultaneous tidal elevation at Camarinal Sill is also shown. The location of Camarinal Sill is marked by the vertical solid line.

Since the downward flux from the Atlantic layer and the upward flux from the Mediterranean layer are not instantaneously balanced, the interfacial layer does not behave as a simple permeable layer, but as an active layer that is able to horizontally transport the water masses coming from Atlantic layer and Mediterranean layer.

In order to describe in detail the flow transfer between layers, a schematic representation of the horizontal and vertical transports along the strait is shown

in Figure 5.11. Here the horizontal transport in each layer is presented together with the vertical flux from the Atlantic layer and the Mediterranean layer (depth of the upper and lower bounds of the interfacial layer along section E are also shown). Times are chosen to describe the semidiurnal cycle during spring tide. At low water at Tarifa, transports in the three layers are all eastward directed. A strong downward flux from the interfacial layer to the Mediterranean layer is present to the east of the sill so that, in the subsequent hours, the interfacial layer becomes thinner; on the western side of the sill, instead, during the rising tidal phase, the interfaces between the layers increase their slope, with an evident growth of the Atlantic layer thickness. Six hours before high water, the flow in the Mediterranean layer veers toward west while the transport in the two other layers is decreasing. At high water, the Atlantic layer east of the sill is very thin, and almost all the horizontal transports are westward directed. The decreasing tidal phase is characterized in the Atlantic layer by a bore that starting from Camarinal Sill propagates toward east along Tarifa Narrow.

5.3 Hydraulic Control

In this Section the time evolution of the hydraulic control in the three-layer framework is explored. In particular the three-layer hydraulic theory proposed by Smeed (2000) to study the hydraulic control variability in the strait of Bab al Mandab is applied. In the theory proposed by Smeed the fluid is assumed to be Boussinesq, hydrostatic, inviscid, steady and each layer is characterized by a uniform density and velocity (similar assumptions were used for the developing of the two-layer hydraulic theory). In a three-layer flow with a rigid lid there are two possible internal wave modes and each of them can be subcritical, critical, or supercritical. Each internal mode has two phase speeds; if they have opposite signs the wave can propagate both upstream and downstream and the mode is said to be subcritical, while if they have the same sign, or one of them is zero, the wave can only propagate in one direction and the mode is said to be supercritical. The first internal mode is characterized by displacements of the two interfaces that are in phase and it corresponds, in first approximation, to the mode that

Figure 5.11: Schematic representation of the horizontal and vertical transports for the three-layer system in a longitudinal view during the semidiurnal cycle of the spring tide. The two lines represent the vertical position of the upper and lower bounds of the along-strait interfacial layer following section E. Arrows show the magnitude and direction of the transports. Horizontal and vertical magnitudes have been normalized by the maximum horizontal and vertical transport of all panels respectively. Time interval between each panels is two hours. The times of the individual snapshots are marked on the tidal elevation at Tarifa (lower panel).

would arise in a two-layer system, while the second internal mode is characterized by 180 ° out of phase displacements of the interfaces (Pratt *et al.* (1999)).

According to the three-layer hydraulic theory proposed by Smeed (2000) the condition for the flow to be critical with respect to one or both of the modes is:

$$\det(\mathbf{M}) = h^2 \left[F_2^4 - \left(r - F_1^2 - F_2^2\right)\left(1 - r - F_2^2 - F_3^2\right)\right] = 0, \tag{5.5}$$

where $F_i^2 = u_i^2/g'h_i$ is the Froude number for the i-th layer with $i = 1, 2, 3$ (1 for the Atlantic layer, 2 for the interfacial layer, and 3 for the Mediterranean layer), $r = (\rho_2 - \rho_1)/(\rho_3 - \rho_1)$, and h is the total depth. Here u_i, ρ_i are the vertically averaged along-strait velocity and density for the i-th layer, h_i is the depth of the i-th layer, and $g' = g_1' + g_2'$ with $g_i' = g\,(\rho_{i+1} - \rho_i)/\bar{\rho}$, where $\bar{\rho}$ represent the mean density. Moreover, it has been shown by Lane-Serff *et al.* (2000) that at a control it is the first mode to be critical if $F_1^2 + F_2^2 > r$ while the second mode appears to be critical if $F_1^2 + F_2^2 < r$.

In Figure 5.12, maps of the frequency of occurrence, over the fortnight period, of the two supercritical modes are presented. Regions where the first internal mode is supercritical are confined along the Tarifa Narrow, starting from Camarinal Sill, and in some scattered areas close to the northern coast west of Camarinal. Along the Tarifa Narrow the frequency increases in the north-east direction reaching its maximum value of 100%, corresponding to a permanent supercritical region, only in a small region around Gibraltar. At Camarinal Sill the supercritical region does not extend over the whole width of the strait and appears only for 20% of the total time, corresponding to about three days over the entire fortnight period. The second internal mode is supercritical in a small region over Camarinal Sill, that does not extend over the whole width of the strait. The maximum frequency of 20% is reached over the shallower part of the sill. A second supercritical region is present over Spartel Sill where, however, the frequency is limited to only 10%. Finally both modes are simultaneously supercritical, in the same position, only in some scattered regions limited to the western side of the strait, and in particular close to the north and south coast near Camarinal. Here the maximum frequency reached is of about 20%.

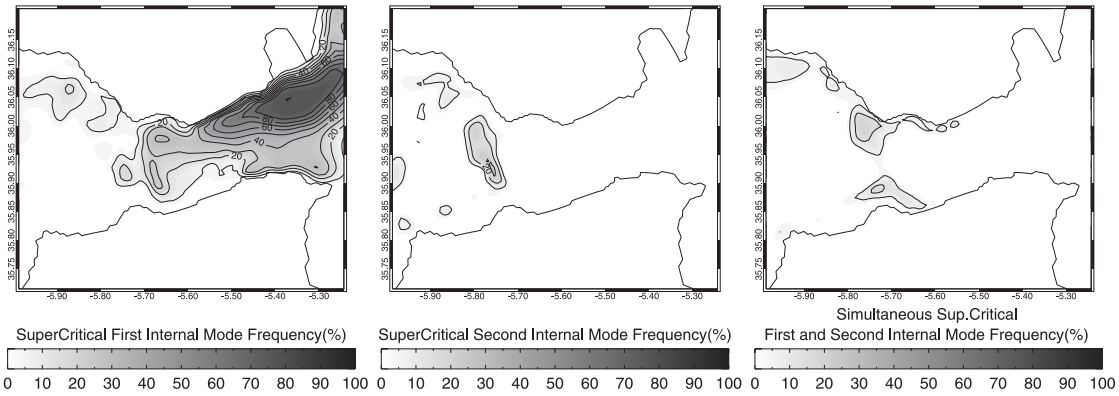

Figure 5.12: Frequency of occurrence of supercritical first mode, second mode, and simultaneous first and second internal modes over the fortnight period.

The model reproduces most of the features found by Armi & Farmer (1985) and Armi & Farmer (1988). It predicts the presence of episodic controlled regions over Spartel and Camarinal Sill, but, in contrast with them, our model does not predict the existence of controls to the west of Spartel Sill, as well as of a permanent control within Tarifa Narrow. In fact, as shown in Figure 5.12, the model predicts a permanent control, due to the first internal mode, only in a limited region close to Gibraltar and not in the whole cross section. In the rest of Tarifa Narrow the hydraulic control has the characteristics of a moving hydraulic control that is locked in phase with the eastward bore propagation. It reaches its minimum extension during high tide at Tarifa and its maximum extension during low tide. At Camarinal Sill the model reproduces the tidally-induced periodic loss and subsequent renewal of the control that occurs two times for each semidiurnal cycle (Figure 5.13). During rising water at Tarifa the control at Camarinal, due to both the first and second internal modes, is well developed over the entire cross-section; during the subsequent descending phase the control is initially lost and then recovered, mainly due to the contribution of the first internal mode, and lost again at low tide.

While the previous description is useful in identifying the regions within the strait where the flow is controlled, a complete understanding of the hydraulic

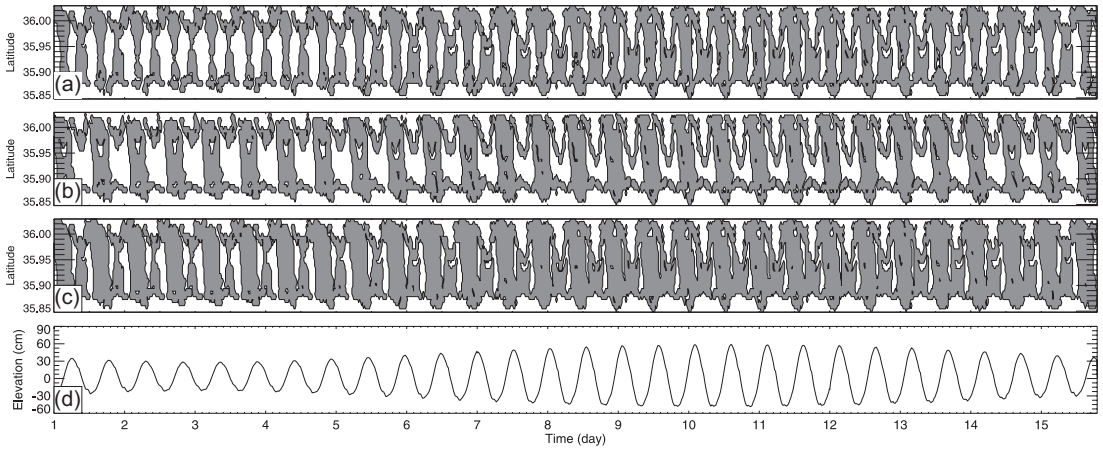

Figure 5.13: Variation of the supercritical region over a fortnight period and in the across-strait direction at Camarinal Sill due to (a) the first internal mode, (b) the second internal mode and (c) both the internal modes. The regions where the flow is supercritical are shaded. In the lower panel (d) the tidal elevation at Tarifa is plotted.

regimes, in terms of maximal or submaximal exchange, can only be achieved by exploring the simultaneous presence of supercritical flow regions through the strait. This is done in Figure 5.14, where in the light of the previous findings, analysis is restricted to the region over Camarinal Sill and the region of Tarifa Narrow. Bars in panels 5.14a and 5.14b of the figure indicate the presence of supercritical regions, covering the whole cross-section of the strait, in Tarifa Narrow and over Camarinal Sill, respectively. Comparison of Figure 5.14a and Figure 5.14b shows that the flow exchange exhibits intermittent maximal regimes (see black bars in Figure 5.14c). Maximal exchange is achieved intermittently during the entire fortnight period. Its frequency increases from 2 times per day during neap tide to 6 times per day during spring tide. Adding all the maximal exchange periods we find that the flow through the strait is in a maximal exchange regime for about 20% of the total fortnight period.

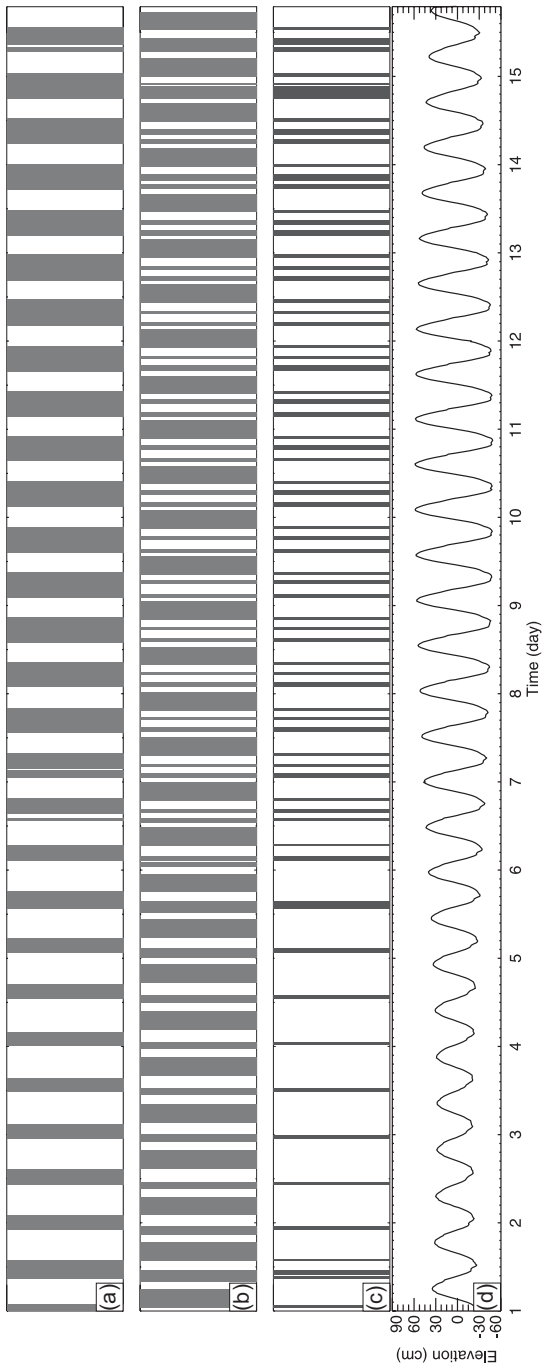

Figure 5.14: Bars indicating the presence of a supercritical region, extending on the whole cross-section of the strait within (a) Tarifa Narrows and over (b) Camarinal Sill. Black bars in panel (c) indicate the simultaneous presence of supercritical regions within Tarifa Narrows and Camarinal Sill. In the lower panel (d) the tidal elevation at Tarifa is plotted.

5.4 Three-layer vs Two-layer approximation

The first difference emerging by comparing the three-layer and the two-layer approximation is that the two-layer system, as it is divided by a single salinity surface, produces a time-averaged upper layer salinity substantially higher and a lower layer salinity substantially lower than that obtained for the same layer in the three-layer system. In fact, salinity differences between the upper and lower layers do not exceed 1.6 for the two-layer case (Figure 4.2), while for the three-layer case a value of about 2.0 is reached (Figure 5.6).

About transports, Figure 4.4 in Section 4.2 can be compared with Figure 5.9 that has been evaluated in the three-layer framework. As expected, the net transport is unchanged in the two calculations. The transports at the eastern end of the strait are almost the same for the two approximations, while it is evident the difference in both the eastward and westward transports over the region around Camarinal Sill. In particular the minimum eastward transport west of the sill increases from 0.52 Sv to more than 0.70 Sv in the two-layer approximation, furthermore the transport increases rapidly toward the western end of the strait reaching the value of about 0.8 Sv, instead of 0.62 Sv that is the value obtained for the three-layer case.

These large differences in the along-strait horizontal transport in the western part of the strait, and in particular over Camarinal Sill, is due to the fact that in the three-layer approximation the net transport of the intermediate layer does not contribute to the total two-way transports, while in the two-layer approximation the fraction of instantaneous transport of the intermediate layer is almost equally distributed in both the upper and lower layers.

It has been shown in Section 4.3 that over Camarinal Sill, for the two-layer approximation, the control is achieved two times for each semidiurnal period: the flow is controlled during the rising water at Tarifa then the control is lost and recovered again during the subsequent descending tidal phase (Figure 4.6). A similar general behaviour has been found also for the three-layer approximation (Figure 5.13) even if some significant differences come forth: for the two-layer case the control extends cyclically over the whole cross section only for about 8 days, from day 7 to day 15, while for the three-layer case the control extends

through the entire cross-section cyclically over the entire period, moreover, for the two-layer case the control holds over Camarinal Sill for a time interval that is always less than the corresponding time-interval found in the three-layer case.

Always in Section 4.3 it has been pointed out the complete absence of a supercritical region extending over any entire cross-section within Tarifa Narrow, for the two-layer case. Control variability within Tarifa Narrow found in the three layer approximation is completely different, in fact in this case a permanent supercritical region is present near the northern coast at Gibraltar extending cyclically over the entire cross-strait section. Furthermore, looking at the simultaneous presence of controlled regions both at Camarinal Sill and Tarifa Narrow for the three-layer case, our results reveal that the exchange through the strait of Gibraltar switches cyclically between maximal and submaximal, with a frequency increasing from 2 times per day during neap tide to 6 times per day during spring tide.

Chapter 6

Conclusions and Discussion

The two-layer approximation is generally used to describe both the exchange and hydraulics within the Strait of Gibraltar. However, analyzing experimental data from the *Gibraltar Experiments*, Bray *et al.* (1995) have shown the presence of an active interfacial layer suggesting, in the final remarks, the use of a model that incorporates an interfacial layer of finite thickness between the Atlantic and Mediterranean layers. One of the aims of this Thesis has been the developing of a three-dimensional numerical model ables to reproduce this interfacial layer, in order to investigate the effect of tidal forcing on the hydrological and physical properties of this layer. Moreover this Thesis has been devoted to evaluate the differences on both the hydraulics and transports of the exchange flow when the 'classical' two-layer or the three-layer approximation, that takes in to account the interfacial layer, are applied.

The three-dimensional model used in this Thesis can be considered as the natural improvement of the three-dimensional models developed by Wang (1989, 1993). It is the parallel version (Sannino *et al.* (2005)) of the Princeton Ocean Model (POM) developed by Blumberg & Mellor (1987) in the configuration implemented by Sannino *et al.* (2004). The model grid has a non uniform horizontal spacing; horizontal resolution is maximum in the strait, where it is less than 500 m, while at the eastern end (Alboran Sea) and western end (Gulf of Cadiz) it reaches 10-20 km and 8-15 km, respectively. The vertical grid is made of 32 sigma levels, logarithmically distributed at the surface and at the bottom. Initial temperature and salinity fields are derived from climatological data sets for

the spring period: MODB for the Mediterranean side of the model domain and Levitus (1982) for the Gulf of Cadiz. A significant aspect of this model is that it takes into account the effect of entrainment and mixing since it resolves the vertical sub-grid scale turbulence by prognostic equations for the turbulence velocity and length scale (Ezer (2005)). The model is forced at the two open boundaries through the specification of the surface elevation that is characterized by the two principal semidiurnal harmonics: M_2 and S_2. The main experiment analyzed in this work simulates an entire tidal fortnight period.

The validity of this numerical model has been tested by comparing the observed and simulated amplitude and phase of the two semidiurnal tidal component, both for the tidal elevation and the semimajor tidal ellipse for the currents. It has been shown that model results are in good agreement with the observed tidal elevation amplitudes and phases. The model reproduces all the known features of the spatial structure of both the M_2 and S_2 tidal components: a decrease of more than 50% in amplitudes and slight variations in phases along the strait, a prevailing propagation of phases southwestward, and nearly constant amplitude ratios and phase differences between the M_2 and S_2 tidal elevations throughout the strait. At the same time the model has revealed a distribution of amplitude and phase in the region of Camarinal Sill (both for the M_2 and S_2) that is different from the empirical cotidal chart presented by Candela *et al.* (1990). The predicted semimajor axis as well as amplitude and phase of the along-strait velocities are quantitatively and qualitatively in good agreement with all available observed data. The simulated eastward and westward internal bores are also in agreement with available data as well as the internal bore speeds in different sections of the strait coincide with those estimated by Izquierdo *et al.* (2001) who used a completely different model.

In this Thesis it has been shown that the model implemented is also able to reproduce an interfacial layer with time-averaged characteristics substantially similar to that found by Bray *et al.* (1995). The thickness (Figure 5.2) is characterized by an almost constant value of about 120 m throughout Tarifa Narrow as far as Camarinal Sill and about 160 m along Tangier Basin. A maximum of about 200 m is present just west of Camarinal Sill. The depth of the midpoint of the interfacial layer presents a north-south gradient throughout the entire strait

that is more intense east of Camarinal Sill. Here the values range from about 180 m in Tangier Basin to 40 m on the north coast, while in Tarifa Narrow the values range from about 120 m on the south to 40 m on the north. Model results also show that the interface layer thickness is strongly affected by tide, with an increase of the time-averaged value of about 50 m in the tidal experiment respect to the non-tidal one. The maximum tidal variability is confined in Tarifa Narrow, where a maximum of about 200 m propagates towards east, starting from Camarinal Sill, in accordance with the eastward propagating bore (Figure 5.4).

Model results have confirmed that the interfacial layer has to be considered an active layer since it is able to carry a substantial fraction of the total transport. Figure 6.1 summarizes the time-averaged transport both in the horizontal and vertical direction. Here the time-averaged upper and lower bounds of the interfacial layer for the along-strait section E (see Figure 2.4) are plotted. While the Atlantic layer is characterized everywhere by an inflow and the Mediterranean layer by an outflow, the interfacial layer is split in two parts with an inflow in the eastern part of the strait and an outflow in the western part of the strait. Over Camarinal Sill there is no transport in the interfacial layer. On the west end of the strait most of the total transport is carried by the Mediterranean layer with a value of about 0.4 Sv, while the interfacial layer contributes for only 0.1 Sv. On the eastern end the interfacial layer transport is about 0.2 Sv higher than the Atlantic layer. The large differences in horizontal transports along the strait evident in Figure 6.1 can be interpreted as due to vertical exchanges between layers. Everywhere along the strait the exchange is directed into the interfacial layer. The exchange between the Mediterranean layer and the interfacial layer shows a maximum over Camarinal Sill, while it decreases both in the western and the eastern part. The exchange between the Atlantic layer and the interfacial layer slowly decreases from the western to the eastern end.

From the model results it also emerges also that the transports at the eastern end of the strait are almost the same for the two approximations, while it is evident the difference in both the eastward and westward transports over the region from Camarinal Sill toward west. In fact, in the three-layer approximation, the minimum over the sill is deeper and extends till the western end of the strait. The large differences in the along-strait horizontal transport in the western part of the

strait, is due to the fact that in the three-layer approximation the net transport of the intermediate layer does not contribute to the total two-way transports, while in the two-layer approximation the fraction of instantaneous transport of the intermediate layer is almost equally distributed in both the upper and lower layers.

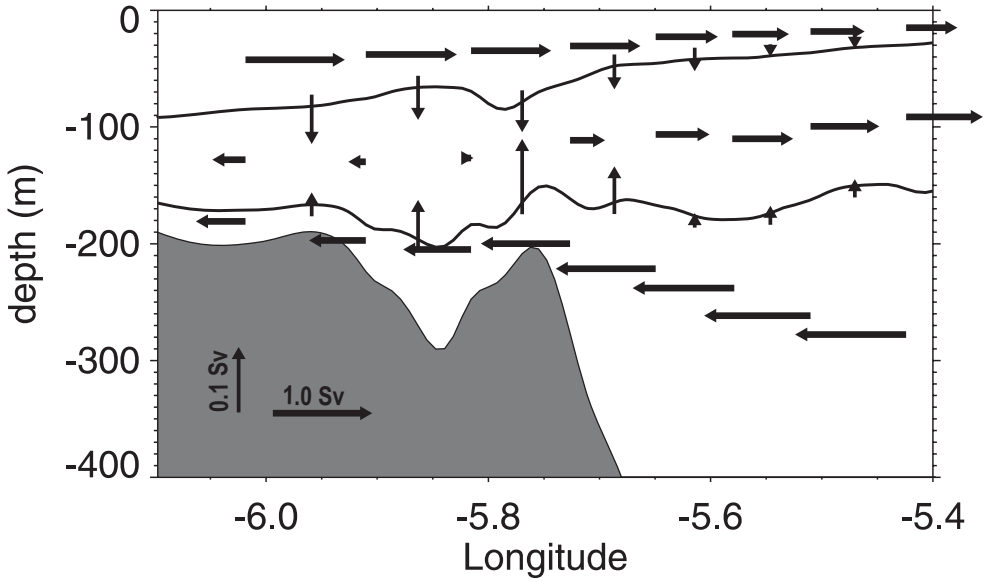

Figure 6.1: Time-averaged along-strait (sec. E in Figure 2.4) variations in transports and interface structure. Solid lines outline the time-averaged upper and lower bounds of the interfacial layer. Horizontal arrows are scaled to indicate the magnitude of the transport in each layer at the various sections along the strait. Vertical arrows are scaled to indicate the magnitude of the vertical transport between the interfacial layer and the Atlantic and Mediterranean layers.

The time evolution of the hydraulic control, using the three-layer hydraulic theory proposed by Smeed (2000), has been presented and compared with results from the two-layer hydraulic theory. In the three-layer approximation, the model predicts a permanent supercritical region, due to the first internal mode, in a limited region close to Gibraltar (Figure 5.12) and regions in Tarifa Narrow controlled only cyclically. Moreover at Camarinal Sill the three-layer approximation predicts a tidally-induced periodic loss and subsequent renewal of the control that occurs two times for each semidiurnal cycle. In this approximation the flow in

the strait is in a maximal exchange regime on about 20% of the total fortnight period. Despite the two-layer approximation predicts a control over Camarinal Sill with a general behaviour similar to the three-layer approximation, it does not predict any controlled region extending over the whole cross section in Tarifa Narrow, and, as a consequence, it predicts always a submaximal exchange for the strait. These conclusions could appear in contrast with previous experimental studies (see for example Armi & Farmer (1985); Armi & Farmer (1988)); in fact, using a two-layer approach, they predicted a control variability more similar to that found in this study using the three-layer approximation than that found with the two-layer approximation. This apparent inconsistency is essentially due to the fact that the previous studies did not take into account the vertical, and in some case also horizontal, variation of the hydrological and physical properties in computing the composite Froude Number. For example, in the experimental study by Armi & Farmer (1988) they used, for the western part of the strait, $2\sigma_\theta$ units of density as pycnocline step and as velocity the nearby current meter value within the layer of interest, while at the eastern end they used as interface $\sigma_\theta = 28$ and as velocity the value present at mid-depth of each layer. In both cases the velocity used to compute the Froude numbers cannot be properly considered as representative of two homogeneous layers, implying a general overestimation of the layer velocity and consequently an overestimation of the Froude numbers.

For continuously stratified flows, Pratt *et al.* (2000) suggested that a necessary condition for a flow to be supercritical is to reach a Richardson number less than 0.25 somewhere in the water column. Applying this criterion to the model results we have identified regions where the Richardson number, defined as:

$$Ri = -\frac{g}{\rho}\frac{\partial \rho}{\partial z}\left(\frac{du}{dz}\right)^{-2}, \tag{6.1}$$

satisfies this condition (Figure 6.2). In agreement with the results obtained from the three-layer hydraulic theory, the Richardson number is less than 0.25 not only in the region of CS but also in TN. Moreover from Figure 6.2 appears clear that in TN the critical Richardson number moves together with the eastward propagating bore with critical Richardson number also in the wake of the

bore. Even if this criterion is not sufficient to prove that the flow is supercritical it represents, however, a further indication on the validity of the three-layer hydraulic theory.

Nevertheless it is necessary to stress that for a complete understanding of the hydraulic regime within the Strait of Gibraltar a new hydraulic theory, accounting for the continuously stratified properties of the flow, friction, departure from hydrostatics, rotation, time dependence, mixing and entrainment, should be developed.

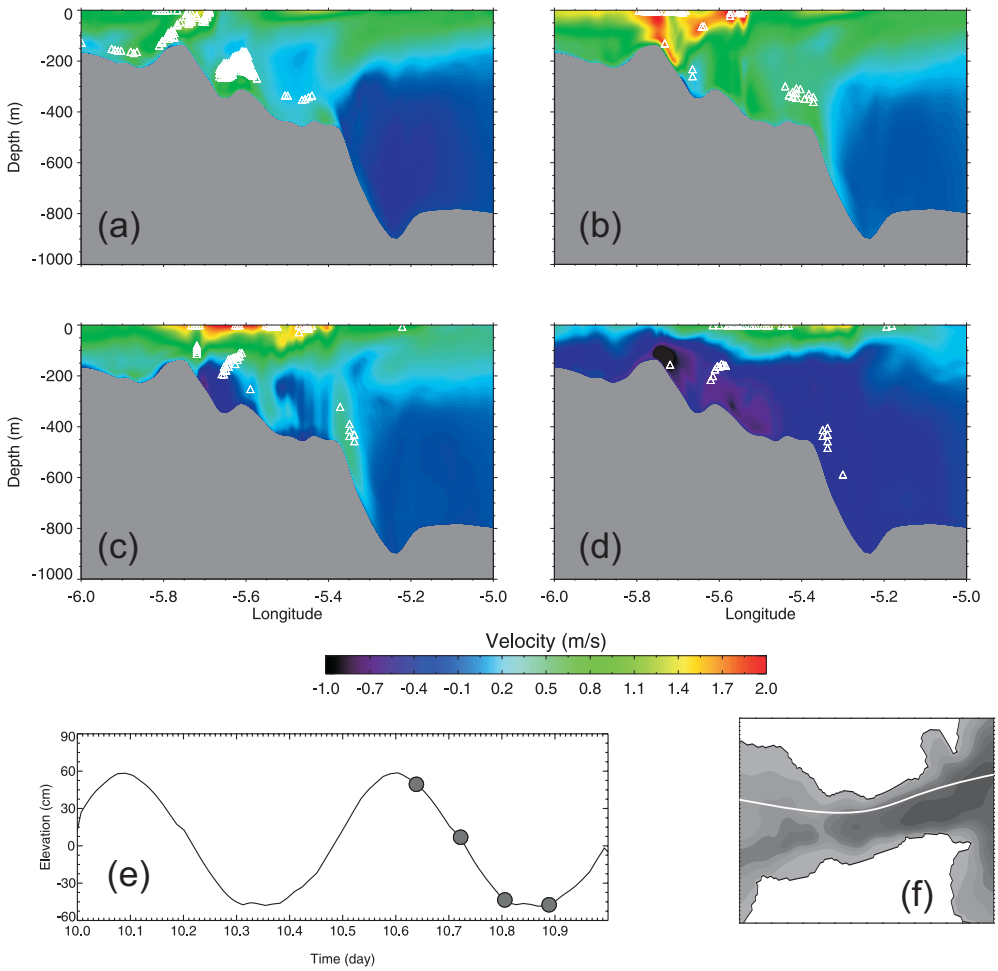

Figure 6.2: (a)-(d) Four velocity fields along the longitudinal section (f) during spring tide. Triangles mark the position where the flow reaches a Richardson number less than 0.25. The times of the individual snapshots are marked on the tidal elevation at Tarifa (panel (e)).

References

Arakawa, A. & Lamb, V. (1977). Computational design of the basic dynamical processes of the ucla general circulation model. *Methods in Computational Physics*, **17**, 174–267. 20

Armi, L. (1986). The hydraulics of two flowing layers with different densities. *J. Fluid Mech.*, **163**, 27–58. 10, 11

Armi, L. & Farmer, D. (1986). Maximal two layer exchange through a contraction with barotropic net flow. *J. Fluid Mech.*, **164**, 27–51. 10

Armi, L. & Farmer, D. (1987). A generalization of the concept of maximal exchange in a strait. *J. Phys. Oceanogr.*, **92 (C13)**, 1467914680. 10

Armi, L. & Farmer, D.M. (1985). The internal hydraulics of the strait of gibraltar and associated sill and narrows. *Oceanol. Acta*, **8**, 37–46. 71, 81

Armi, L. & Farmer, D.M. (1988). The flow of mediterranean water through the strait of gibraltar. *Progrss in Oceanography*, **21**, 1–105. viii, 5, 12, 44, 45, 71, 81

Artale, V. & Levi, D. (1990). Nonlinear surface and internal waves in stratified shear flow. *Geophys. Astrophys. Fluid Dynamics*, **54**, 35–48. 45

Artale, V., Levi, D., Marullo, S. & Santoleri, R. (1990). Analysis of nonlinear internal waves observed by landsat-tm. *J. of Geophysical Research*, **95 (C9)**, 16065–16074. 45

Baschek, B., Send, U., García-Lafuente, J. & Candela, J. (2001). Transport estimates in the strait of gibraltar with a tidal inverse model. *J. Geophysic. Research*, **106 (C12)**, 31033–31044. 7, 9, 39, 48, 49, 50

Bethoux, J. (1979). Budgets of the mediterranean sea. their dependence on the local climate and on the characteristics of the atlantic waters. *Oceanol. Acta*, **2 (2)**, 157–163. 66

Bills, P. & Noye, J. (1987). *Numerical Modelling: Applications to Marine Systems*, chap. An investigation of open boundary conditions for tidal models of shallow seas. Elsevier Science Publishers. 28

Blumberg, A.F. & Mellor, G.L. (1987). *A description of a three-dimensional coastal ocean circulation model*. Washington D.C: American Geophysical Union, n.s. heaps edn. iv, 19, 77

Bormans, M. & Garrett, C. (1989a). The effect of nonrectangular cross section, friction, and barotropic fluctuations on the exchange through the strait of gibraltar. *J. Phys. Oceanogr.*, **19**, 1543–1557. 11

Bormans, M. & Garrett, C. (1989b). The effect of rotation on the surface inflow through the strait of gibraltar. *J. Phys. Oceanogr.*, **19**, 1535–1542. 11

Brandt, P., Alpers, W. & Backhaus, J. (1996a). Study of the generation and propagation of internal waves in the strait of gibraltar using a numerical model and synthetic aperture radar images of the european ers 1 satellite. *J. Geophysic. Research*, **101 (C6)**, 14237–14252. 45

Brandt, P., Alpers, W. & Backhaus, J.O. (1996b). Study of the generation and propagation of internal waves in the strait of gibraltar using a numerical model and synthetic aperture radar images of the european ers1 satellite. *J. Geophys. Res.*, **11**, 14237–14252. 13, 15

Brandt, P., Rubino, A., Sein, D.V., Dmitry, V., Baschek, B., Izquierdo, A. & Backhaus, J.O. (2004). Sea level variations in the western mediterranean studied by a numerical tidal model of the strait of gibraltar. *J. Phys. Oceanography*, **34**, 433–443. 17, 53

Bray, N., Ochoa, J. & Kinder, T.H. (1995). The role of the interface in exchange through the strait of gibraltar. *J. of Geophysical Research C: Oceans*, **100**, 10755–10776. viii, 13, 14, 17, 56, 57, 66, 77, 78

Bruno, M., Mananes, R., Alonso, J., Izquierdo, A., Tejedor, L. & Kagan, B. (2000). Vertical structure of the semidiurnal tidal currents at camarinal sill, the strait of gibraltar. *Oceanol. Acta*, **23**, 15–24. 8

Bryden, H. & Kinder, T. (1991). Steady two-layer exchange through the strait of gibraltar. *Deep-Sea Res*, **38 (SUPPL. 1)**, S445–S463. 66

Bryden, H. & Stommel, H. (1984). Limiting processes that determine basic features of the circulation in the mediterranean sea. *Oceanol. Acta*, **7 (3)**, 289–296. 7, 9, 11

Bryden, H., Candela, J. & Kinder, T. (1994). Exchange through the strait of gibraltar. *Progress in Oceanography*, **33 (3)**, 201–248. xv, 7, 8, 48, 49, 50

Candela, J. (2001). *Ocean Circulation and Climate: Observing and Modeling the Global Ocean.*, chap. Mediterranean water and global circulation. Academic Press, Amsterdam. 7

Candela, J., Winant, C. & Bryden, H.L. (1989). Meteorologically forced subinertial flows through the strait of gibraltar. *J. Geophys. Res.*, **94**, 12667–12674. 8, 48, 49

Candela, J., Winant, C. & Ruiz, A. (1990). Tides in the strait of gibraltar. *J. Geophys. Res.*, **95**, 7313–7335. ix, 8, 15, 32, 33, 34, 35, 37, 38, 50, 78

Castro, M., Garcia-Rodriguez, J., Gonzalez-Vida, J., Macias, J., Pares, C. & Vazquez-Cendon, M. (2004). Snumerical simulation of two-layer shallow water flows through channels with irregular geometry. *J. Computational Physics*, **195**, 202235. 13, 15

Dalziel, S. (1990). *The Physical Oceanography of Sea Straits*, chap. Rotating two-layer sill flows. Kluwer Acad., Norwell, Mass. 10, 11

Ezer, T. (2005). Entrainment, diapycnal mixing and transport in three-dimensional bottom gravity current simulations using the mellor-yamada turbulence scheme. *Ocean Modelling*, **9**, 151–168. 20, 78

Farmer, D.M. & Armi, L. (1986). Maximal two-layer exchange over a sill and through the combination of a sill and contraction with barotropic flow. *J. Fluid Mech.*, **164**, 53–76. 11, 12

García-Lafuente, J. (1986). *Variabilidad del nivel del mar en el Estrecho de Gibraltar: Mareas y oscilaciones residuales*. Ph.D. thesis, Inst. Esp. de Oceanogr., Fuengirola, Malaga, Spain. 33, 34, 38

García-Lafuente, J., Vargas, J., Plaza, F., Sarhan, T., Candela, J. & Bascheck, B. (2000). Tide at the eastern section of the strait of gibraltar. *J. Geophysic. Research*, **105 (C6)**, 14197–14213. ix, 7, 8, 35, 37

García-Lafuente, J., Alvarez-Fanjul, E., Vargas, J. & Ratsimandresy, A. (2002a). Subinertial variability through the strait of gibraltar. *J. Geophys. Res.*, **107 (C10)**, 3168. 8

García-Lafuente, J., Delgado, J. & Criado, F. (2002b). Inflow interruption by meteorological forcing in the strait of gibraltar. *Geophy. Res. Lett.*, **29 (19)**. 8

Garrett, C., Bormans, M. & Thompson, K. (1990). *The Physical Oceanography of Sea Straits*, chap. Is the exchange through the Strait of Gibraltar maximal or submaximal? Kluwer Acad., Norwell, Mass. 8

Govett, M., Hart, L., Henderson, T., Middlecoff, J. & Schaffer, D. (2003). The scalable modeling system: Directive-based code parallelization for distributed and shared memory computers. *J. of Parallel Computing*, **129**, 995. iv, 23

Haney, R. (1991). On the pressure gradient force over steep topography in sigma coordinate ocean models. *J. Phys. Oceanogr*, **21 (4)**, 610–619. 27

Helfrich, K. (1995). Time-dependent two-layer hydraulic exchange flows. *J. Phys. Oceanogr*, **25 (3)**, 359–373. 11, 12

Horatius (23 B.C.). *Ode 3 - Book III*. 3

Hsü, K., Ryan, W. & Cita, M. (1973). Late miocene dessication of the mediterranean. *Nature*, **242**, 240244. 1

Izquierdo, A., Tejedor, L., Sein, D.V., Backhaus, J.O., Brandt, P., Rubino, A. & Kagan, B.A. (2001). Control variability and internal bore evolution in the strait of gibraltar: a 2-d two-layer model study. *Estuarine, Coastal and Shelf Science*, **53**, 637–651. 12, 13, 16, 17, 44, 53, 78

Kantha, L. (1995). Barotropic tides in the global oceans from a nonlinear tidal model assimilating altimetric tides. part 1: Model description and results. *J. Geophys. Res.*, **100**, 25283–25308. 31

Kantha, L., Desai, S., Lopez, J., Tierney, C., Parke, M. & Drexler, L. (1995). Barotropic tides in the global oceans from a nonlinear tidal model assimilating altimetric tides. part 2: Altimetric and geophysical implications. *J. Geophys. Res.*, **100**, 25309–25317. 31

Kinder, T. & Bryden, H. (1987). 1985-1986 gibraltar experiment: Data collection and preliminary results. *EOS*, **68**, 786–787. 8

Kinder, T. & Bryden, H. (1988). Gibraltar experiment: Summary of the field program and initialresults of the gibraltar experiment. Tech. Rep. Whoi-88-30, Woods Hole Oceanographic Institution. 8

Knudsen, M. (1899). De hydrografiske forhold i de danske farvande indefor skagen i 1894-98. *Komm. Vidensk. Unders. Dan. Farvande*, **2(2)**, 19–79. 7, 9

Lacombe, H. & Richez, C. (1982). *Hydrodynamics of Semi-Enclosed Seas*, chap. The regime of the Strait of Gibraltar. Elsevier, Amsterdam. xv, 7

Lane-Serff, G., Smeed, D. & Postlethwaite, C. (2000). Multi-layer hydraulic exchange flows. *J. Fluid Mech.*, **416**, 269–296. 71

Lawrence, G. (1990). *The Physical Oceanography of Sea Straits*, chap. Can mixing in exchange flows be predicted using internal hydraulics? Kluwer Acad., Norwell, Mass. 10

Levitus, S. (1982). *Climatological Atlas of the World Ocean*. 29, 78

Longo, A., Manzo, M. & Pierini, S. (1992). A model for the generation of nonlinear internal tides in the strait of gibraltar. *Oceanologica Acta*, **15**, 233–243. 13, 15

Mellor, G. (1991). An equation of state for numerical models of oceans and estuaries. *J. Atmosph. and Oceanic Tech.*, **8 (4)**, 609–611. 19

Mellor, G. (2006). *User's Guide for a Three-dimensional, Primitive Equation, Numerical Ocean Model*. http://www.aos.princeton.edu/WWWPUBLIC/htdocs.pom/PubOnLine/POL.html. 21

Mellor, G. & Yamada, T. (1982). Development of a turbulence closure model for geophysical fluid problems. *Reviews of Geophysics and Space Physics*, **20 (4)**, 851–875. 20

Mellor, G., Ezer, T. & Oey, L. (1994). The pressure gradient conundrum of sigma coordinate ocean models. *J. of Atmospheric and Oceanic Technology*, **11 (4 part 2)**, 1126–1134. 27

Morozov, E.G., Trulsen, K., Velarde, M. & Vlasenko, V. (2002). Internal tides in the strait of gibraltar. *J. Phys. Oceanogr.*, **32**, 3193–3206. 13, 15

Nielsen, J. (1912). Hydrography of the mediterranean and adjacent waters. Tech. Rep. 1, Danish Oceanographical Expedition 1908-1910, Copenhagen. xv, 7

Orlanski, I. (1976). A simple boundary condition for unbounded hyperbolic flows. *J. of Computational Physics*, **21**, 251–269. 28

Parrilla, G., Neuer, S., Le Traon, P. & Fernandez, E. (2002). Topical studies in oceanography: Canary islands azores gibraltar observations (canigo). *Deep Sea Res. II*, **49**, 3951–3955. 8

Pierini, S. (1989). A model for the alboran sea internal solitary waves. *J. Phys. Oceanogr*, **19**, 755–772. 15, 45

Pratt, L., Johns, W., Murray, S.P. & Katsumata, K. (1999). Hydraulic interpretation of direct velocity measurements in the bab al mandab. *Journal of Physical Oceanography*, **29**, 2769–2784. 69

Pratt, L., Deese, H., Murray, S. & Johns, W. (2000). Continuous dynamical modes in straits having arbitrary cross sections, with applications to the bab al mandab. *Journal of Physical Oceanography*, **30 (10)**, 25152534. 81

Richez, C. (1994). Airborne synthetic aperture radar tracking of internal waves in the strait of gibraltar. *Prog. in Oceanogr.*, **33**, 93–159. 8

Sannino, G., Artale, V. & Lanucara, P. (2001). An hybrid openmp/mpi parallelization of the princeton ocean model. *Parallel Computying Advances and Current Issues: Proceedings of the International Conference ParCo2001*, **129**. 23

Sannino, G., Bargagli, A. & Artale, V. (2002). Numerical modeling of the mean exchange through the strait of gibraltar. *J. of Geophysical Research*, **107 (8)**, 9 1–24. iv, 12, 13, 16, 17, 39

Sannino, G., Bargagli, A. & Artale, V. (2004). Numerical modeling of the semidiurnal tidal exchange through the strait of gibraltar. *J. of Geophysical Research*, **109**, C05011, doi:10.1029/2003JC002057. 13, 17, 48, 77

Sannino, G., Carillo, A., Artale, V., Ruggiero, V. & Lanucara, P. (2005). Flow regimes study within the strait of gibraltar using a high-performance numerical model. *Nuovo Cimento*, **28, Issue 2,DOI: 10.1393/ncc/i2005-10177-2**, 97–104. iv, 23, 77

Sannino, G., Carillo, A. & Artale, V. (2006). Three-layer view of transports and hydraulics in the strait of gibraltar: a 3d model study. *Accepted on J. of Geophysical Research*. 13, 17

Smagorinsky, J. (1963). General circulation experiments with primitive equations. i: the basic experiment. *Mon. Weather Rev.*, **91**, 99–164. 20

Smeed, D. (2000). Hydraulic control of three-layer exchange flows: application to the bab al mandab. *Journal of Physical Oceanography*, **30 (10)**, 2574–2588. 69, 71, 80

Smolarkiewicz, P. (1984). A fully multidimensional positive definite advection transport algorithm with small implicit diffusion. *J. Comput. Phys.*, **54**, 325–362. iv, 22

Stommel, H. & Farmer, H. (1953). Control of salinity in an estuary by a transition. *J. Mar. Res.*, **12**, 13–20. 6, 9

Tejedor, L., Izquierdo, A., Kagan, B. & Sein, D. (1999). Simulation of the semidiurnal tides in the strait of gibraltar. *J. of Geophysical Research*, **104 (C6)**, 13541–13557. 13, 15

Tsimplis, M. (2000). Vertical structure of tidal currents over the camarinal sill at the strait of gibraltar. *J. of Geophysical Research*, **105 (C8)**, 19709–19728. 9

Tsimplis, M. & Bryden, H. (2000). Estimation of the transports through the strait of gibraltar. *Deep-Sea Research Part I*, **47 (12)**, 2219–2242. 7, 8, 9, 50

Tsimplis, M., Proctor, R. & Flather, R. (1995). A two-dimensional tidal model for the mediterranean sea. *J. of Geophysical Research*, **100 (C8)**, 16223–16239. 33, 34

URL: MODB (2006). http://modb.oce.ulg.ac.be/modb/welcome.html. 29

URL: POM (2006). http://www.aos.princeton.edu/htdocs.pom/. 19

URL: POM papers (2006). http://www.aos.princeton.edu/htdocs.pom/. 19

URL: SMS (2006). http://www-ad.fsl.noaa.gov/ac/SMS_UsersGuide_v2.8.pdf. 23

Vargas, J. (2004). *Fluctuaciones Subinerciales y Estado Hidraulico del Intercambio a traves del Estrecho de Gibraltar*. Ph.D. thesis, Universidad de Sevilla. xv, 7

Wang, D. (1989). Model of mean and tidal flows in the strait of gibraltar. *Deep-Sea Res.*, **36**, 1535–1548. 13, 16, 22, 77

Wang, D. (1993). The strait of gibraltar model: internal tide, diurnal inequality and fortnightly modulation. *Deep-Sea Research. Part I*, **40 (6)**, 1187–1203. 13, 16, 22, 77

Wesson, J. & Gregg, M. (1988). Turbulent dissipation in the strait of gibraltar and assiciated mixing. In C. Nihoul & B. Jamart, eds., *Small-Scale Turbulence and Mixing in the Ocean*, 201–212, 19th International Liege Colloquium on Ocean Hydrodynamics, Elsevier. 11

Wesson, J. & Gregg, M. (1994). Mixing at camarinal sill in the strait of gibraltar. *J. Geophys. Res.*, **99 (C5)**, 9847–9878. 13, 62